The Role of CYLD in Dendritic Cell Function

Dissertation

to achieve the degree
"Doktor der Naturwissenschaften"

in the Faculty of Biology
at the Johannes Gutenberg-Universität Mainz

Cathy Cecilia Srokowski

Mainz, November 2008

This thesis is dedicated to my mother

Acknowledgements:

Thank you to all the members of the laboratory for their scientific advice and friendship.

TABLE OF CONTENTS

List of Figures and Table

Abbreviations Used

Listed in Alphabetical Order

A20 is also known as TNAIP3 tumor necrosis alpha induced protein 3

Ac acetylation

Ag antigen

BCL-10 B-cell lymphoma 10

Bcl-3 B-cell lymphoma 3

BMDC bone marrow derived dendritic cells

bp basepair

CC1/2 coil coil domain

CD cluster of differentiation

cDNA complementary DNA

CLIP class II associated invariant chain peptide

CpG cytosine and guanine separated by a phosphate

CYLD cylindromatosis protein

DALIS dendritic cell aggresome- like induced structures

DC dendritic cell

DD death domain

DNA deoxyribonucleic acid

dsRNA double stranded RNA

DUB deubiquitinating enzyme

ERK extracellular signal regulated kinase

FL-CYLD full CYLD

G- gram negative

G+ gram positive

GMCSF granulocyte macrophage colony-stimulating factor

GPI glycophosphoinositol

GRR glycine rich domain

GST glutathione S-transferase

HLH helix loop helix

HPLC high performance liquid chromatography

IFN interferon

Ii invariant chain

IKB I kappa B

IKK I kappa kinase

IL interleukin

i.p. intraperitoneal

IRAK interleukin-1 receptor associated kinase

i.v. intravenously

JAMM JAB1/MPN/Mov34 metalloenzyme

K48 lysine 48

K63 lysine 63

KDa kilodalton

ko knockout

LBP LPS binding protein

LFA lymphocyte function-associated antigen

LN lymph node

LRR leucine rich repeats

LZ leucine zipper

MAGUK membrane-associated guanylate kinase homologue

MALT mucosal-associated lymphoid tissue

MAP mitogen-activated protein

MAPK mitogen-activated protein kinase

MFI mean fluorescence intensity

MHC major histocompatibility complex

MJD Maschado-Joseph disease protein domain

MKK mitogen-activated protein kinase kinase

MOD/UBD minimal oligomerization domain and ubiquitin binding domain

mRNA messenger RNA

MyD88 myeloid differentiation primary response gene 88

NBD NEMO binding domain

NEMO, IKKγ NF-kappaB essential modulator

NF-κB NF-kappaB

NLS nuclear localization signal

OTU ovarian tumor proteases

OVA ovalbumin

P phosphorylation

p65/RelA protein 65

PAMPs pathogen-associated molecular patterns

PCR polymerase chain reaction

PolyUb polyubiquitination

RIP receptor interacting protein

RNA ribonucleic acid

RTPCR realtime polymerase chain reaction

sc subcutaneous

sCYLD short CYLD

TAB1/2 transforming growth factor β activated protein kinase 1/2 binding protein

TAK1 transforming growth factor β activated kinase 1

TAP transporter of antigen processing

TCR T cell receptor

TGF transforming growth factor β

TIR toll/interleukin-1 receptor-like domain

TIRAP toll-interleukin receptor adapter protein

TLR toll-like receptor

TNF tumor necrosis Factor

TRAF tumor necrosis receptor associated factor

TRIF TIR-domain-containing adapter-inducing interferon-β

Ub ubiquitin

UCH ubiquitin C-terminal hydrolases

USP ubiquitin-specific proteases

Vis. visceral

WT wildtype

Abstract

Deubiquitination of NF-κB members by CYLD is crucial in controlling the magnitude and nature of cell activation. The naturally occurring CYLD splice variant, devoid of exons 7 and 8, lacks TRAF2 and NEMO binding sites. The role of this splice variant in dendritic cell (DC) function was analyzed using $CYLD^{ex7/8}$ mice, which lack the full-length CYLD (FL-CYLD) transcript and over-express the short splice variant (sCYLD). Bone marrow derived DCs (BMDC) from $CYLD^{ex7/8}$ mice display a hyper-reactive phenotype *in vitro* and *in vivo* and have a defect in establishing tolerance using DEC"205-mediated antigen targeting to resting DCs. This phenotype was accompanied by an increased nuclear translocation of the IκB molecule Bcl-3, and increased degradation of cytoplasmic p105 in $CYLD^{ex7/8}$ BMDCs after stimulation. This suggests that in contrast to FL-CYLD, sCYLD is a positive regulator of NF-κB activity and its over-expression induces a hyper-reactive phenotype in DCs.

1. Introduction

Dendritic cells (DCs) extensively use ubiquitination to influence the initiation and regulation of antigen specific immune responses through cell surface receptors linked to the NF-κB pathway. Therefore, deubiquitination of NF-κB members is crucial in controlling the magnitude and nature of DC activation. CYLD is a deubiquitinating enzyme fundamental to the regulation of the NF-κB signaling pathway. To date, the role of CYLD and CYLD splice variants, which are known to be endogenously expressed in different circumstances, has not been evaluated in DCs. One of the naturally occuring CYLD splice variants is devoid of exons 7 and 8, and thus lacks TRAF2 and NEMO binding sites. The role of this splice variant in DC function was analyzed using $CYLD^{ex7/8}$ mice which are characterized by the loss of the full-length CYLD transcript and the over-expression of the splice variant.

1.1. Dendritic Cells

Dendritic cells (DCs) are a sparsely distributed population of migratory bone-marrow-derived leukocytes specialized for the uptake, transport, processing and presentation of antigens to T cells[1-3]. There are two categories of DCs: plasmacytoid DCs and conventional DCs. Plasmacytoid DCs circulate through the blood and lymphoid tissues and only acquire the typical DC morphology after activation and subsequently release type I interferons (IFN). The conventional DCs are present in the thymus, spleen and lymph nodes and can be subdivided into 5 different populations based on the pattern of expression of markers. **Table 1** outlines the conventional DCs subsets, including localization, marker expression, functional features in the steady state and the *in vitro* equivalent produced by culture conditions.

Table 1: Mouse dendritic cell subsets (conventional)

Features	Lymphoid-organ-resident DC subsets			Migratory DC subsets		Monocyte derived
	CD4+DCs	CD8+DCs	DN DCs	Interstitial DCs	Langerhans cells	
Location						
Spleen	Yes	Yes	Yes	No	No	Sites of inflammation
Sc LN	Yes	Yes	Yes	Yes	Yes	
Vis. LN	Yes	Yes	Yes	Yes	No	
Thymus	Yes	Yes	Yes	No	Yes	
Surface Markers						
CD11c	+++	+++	+++	+++	+++	+++
CD4	+	-	-	-	-	-
CD8	-	++	-	-	-/+	-
CD205	-	++	-/+	+	+++	-/+
CD11b	++	-	++	++	++	++
Langerin	-	+	-	-	+++	-
CD24	+	++	+	ND	ND	ND
Functional features in the steady state						
Maturity	Immature	Immature	Immature	Mature	Mature	N/A
Antigen processing and presentation	+++	+++	+++	+/-	+/-	N/A
MHC II	++	++	++	+++	+++	N/A
In vitro equivalent						
	Bone-marrow precursors + FLT3L	Bone-marrow precursors + FLT3L	Bone-marrow precursors + FLT3L	Bone-marrow precursors + GM-CSF, TNF + TGFβ	Bone-marrow precursors + GM-CSF, TNF + TGFβ	Bone-marrow, spleen or blood precursors plus GM-CSF

Adapted from Villadangos et al., Intrinsic and cooperative antigen-presenting functions of dendritic-cell subsets in vivo. Nature Reviews Immunology (2007) vol. 7 pp 543-555.[4] Table created with Canvas software. Sc = subcutaneous, Vis = visceral, LN= lymph node

In this thesis, whenever DCs are discussed in an *in vitro* setting (except for the analysis of endogenous spleen, lymph node or bone marrow derived DC populations, section 3.9) this denotes the culturing of bone marrow precursors in medium that is supplemented with granulocyte/macrophage-colony stimulating factor (GM-CSF), without interleukin-4 (IL-4). The DCs generated by this method resemble monocyte-derived DCs, which do not correspond with any of the lymphoid-organ resident DCs subsets found *in vivo*. It is believed that the monocyte-derived DCs (in the *in vivo* setting) resemble pre-cursors of migratory DCs capable of migrating to sites of inflammation[5, 6].

1.1.1. The role of dendritic cells in the immune system: immunity and tolerance

In the "immature" stage of development, DCs act as guards in peripheral tissues, repeatedly scanning and sampling the antigenic environment. Immature DCs express a variety of receptors including those for pathogen-associated molecular patterns (PAMPs), as well as for secondary inflammatory compounds such as Toll-like receptors (TLRs), nucleotide-binding oligomerization domain (NOD) proteins, RIG-I-like receptors, C-type lectin receptors, cytokine receptors and chemokine receptors[7, 8]. When these receptors are triggered, DCs migrate towards the secondary lymphoid organs from nonlymphoid tissues via the afferent lymph or the blood stream to the T-dependent areas of lymphoid organs. Upon reaching these organs, DCs develop into a mature state, which is characterized by high levels of expression of MHC and T-cell co-stimulatory molecules and the ability to present antigen captured in the periphery to T cells. The step towards the mature state, termed "maturation" is currently defined as the phenotypic changes involved in this process rather than the ability of DCs to initiate immunity as DCs that undergo these phenotypic changes are also able to induce tolerance[4]. Maturation is a process characterized by reduced Ag-capture capacity and increased surface expression of MHC and co-stimulatory molecules. However, the maturation of DCs is completed only upon interaction with T cells (whether it is to induce immunity or mediate tolerance). It is characterized by loss of phagocytic capacity and expression of many other accessory molecules that interact with receptors on T cells to enhance adhesion and signaling (co-stimulation) including: LFA-3/CD58, ICAM-1/CD54, B7-1/CD80, B7-2/CD86 and CD83 [9, 10]. Expression of one or both of the co-stimulatory molecules B7-1 (CD80) and B7-2 (CD86) on the DCs is essential for the effective activation of T lymphocytes and for IL-2 production. These co-stimulatory molecules bind the CD28 molecules on T lymphocytes. Some of the most powerful DC-mediated T cell immunity *in vivo* involves mediating responses in contact allergy (initate

inflammatory response) and transplantation (rejection of transplant), not to mention viral clearance and other pathogen exposure. However, the principal function of DCs is not only to initiate T cell-mediated immunity but also to maintain/develop tolerance.

DCs are pivotal in mediating peripheral tolerance. Peripheral tolerance is defined as the immunological tolerance developed after T and B cells mature and enter the periphery. This is in contrast to central tolerance which occurs during lymphocyte development and operates in the thymus and bone marrow. It appears that self-specific T cells are tolerized in the periphery by two mechanisms. The first is the absence of inflammatory pathogens when T cells recognize antigen presented by quiescent DCs which express lower levels of co-stimulatory molecules, or secrete cytokines which cause T cell tolerance or express receptors such as Fas which promote the deletion of T cells through this death receptor[11]. The second critical factor that defines "self" and drives tolerance through anergy, deletion or suppression is the persistence of antigen[12]. Figure 1 illustrates the two outcomes of DC-T cell interactions: priming/immunity or tolerance induction.

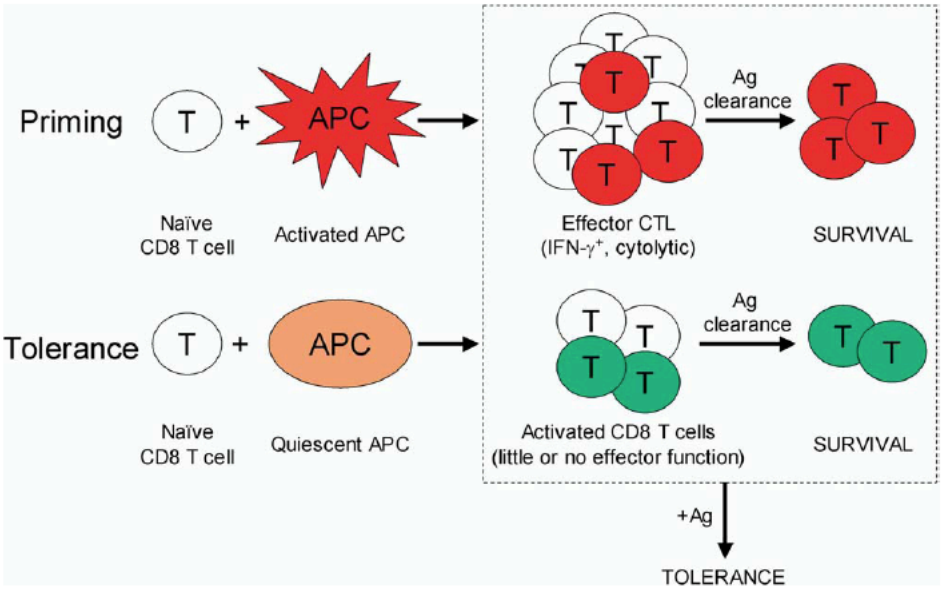

Figure 1. Outcomes from DC and T cell interactions.

Activated DCs expressing high levels of co-stimulatory molecules promote the proliferation and differentiation of CD8 T cells into effectors. Alternatively, activation of CD8 T cells by quiescent DCs leads to an abbreviated proliferative response and upon additional exposure to Ag, the end result is tolerance.

Taken from Redmond and Sherman (2005). Peripheral Tolerance of CD8 T Lymphocytes, Immunity vol.22, pp275-284[12].

In this thesis, to study the effects of tolerance in an *in vivo* model, the anti-DEC-205 antibody was used to specifically target DC with an antigen in a steady state, in other words, with no inflammatory or "danger" signals present.

DEC-205 is a C-type lectin receptor, homologous to the macrophage mannose receptor and is related to receptors which bind carbohydrates and mediate endocytosis[13]. The characterization of DEC-205 as a potent antigen receptor *exclusively* expressed on DCs opened up the opportunity to specifically load antigens onto DCs through antibody targeting and to study the presentation of antigen on MHC class I and II receptors. When model antigens such as ovalbumin (OVA) are covalently linked to anti-DEC-205 antibodies and injected into mice, this results in antigen loading of the DCs in lymph nodes and presentation of these antigens to OVA-specific T cells by immature DCs [14-16]. Anti-DEC-205:OVA delivers endocytosed protein in the absence of infection (therefore no inflammatory response present) to MHC class I peptide loading[15]. DEC-205 targeting with OVA showed induction of tolerance mediated by the disappearance of antigen-specific T cells and the induction of T regulatory cells (Treg) upon re-challenged with OVA protein[14, 15]. It is hypothesized that Treg induction is an early response to dampen activation of T cells followed by deletion as a final means to abolish antigen-specific T cells and ensure long-lasting unresponsiveness towards the respective antigen.

1.1.2. Antigen Processing: the choice between two pathways

If there is one functional feature of DCs that sets them apart from other immune cells, it is their high capacity to capture, process and present antigens. DCs efficiently present peptide antigens on their MHC class I and II molecules. When mature, DCs express high levels of MHC class I and II molecules. The peptides presented by MHC class I molecules are derived from proteins degraded mainly in the cytosol by the proteasome, whereas MHC class II molecules present peptides that are derived from proteins degraded in endosomal compartments by the cathepsins and other hydrolytic enzymes[17].

Exogeneous antigens are first endocytosed by pinocytosis, phagocytosis or receptor-mediated endocytosis. The internalized Ags then become accessible to endosomal proteases and can be presented by MHC class II molecules. During maturation of MHC class II molecules, ingested antigens are prevented from binding to endogenous antigens in the ER by the association of the invariant chain (Ii). The invariant chain moves from the golgi to another compartment where it is degraded to the class II associated invariant chain peptide (CLIP). CLIP is then replaced by the antigenic peptide (Figure 2a). For

MHC class I-restricted responses, which are generally thought to target antigens that are synthesized within the cell presenting the antigen, the DCs could themselves be infected with the pathogen, thus allowing MHC class I-restricted presentation of pathogen-derived antigens. The antigens that are synthesized inside the DC are degraded into peptides by the proteasome and then transported through the transporters of antigen processing (TAP) molecules into the endoplasmic reticulum for loading onto MHC class I (Figure 2b). However, not all pathogens are known to infect DCs and pathogen infected DCs are often functionally compromised[17, 18]. Furthermore, DCs are the main cell type capable of an important process called "cross-presentation"(Figure 2c). Cross-presentation involves the uptake and processing of exogenous antigens within the MHC class I pathway and is attributed to be important for the generation of cytotoxic T cell immunity and to the development of tolerance[19]. The ability of DCs to endocytose antigens from other cells and then cross-present them to CD8+ T lymphocytes is believed to be TAP-dependent[20] which suggests that there is a diversion of the ingested exogenous cellular antigen into the conventional MHC class I pathway. Figure 2 displays a simplified model of MHC class I and II antigen processing pathways as well the cross-presentation process.

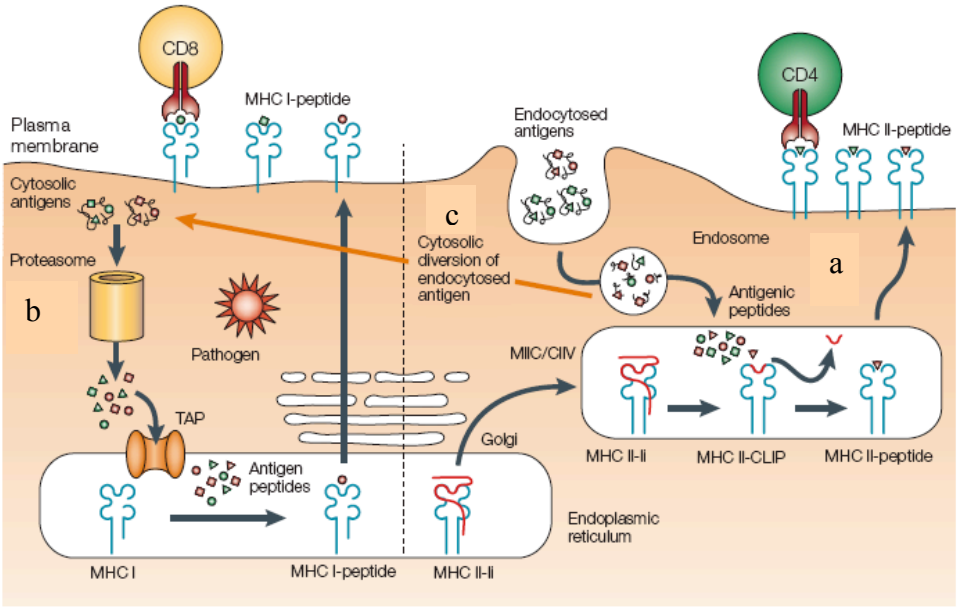

Figure 2. MHC class I and II antigen processing pathways.

a) MHC class I b) MHC class II c) Cross presentation
Figure taken from Heath and Carbone (2001) Cross-presentation in viral immunity and self-tolerance. Nature Reviews Immunology, vol 1 (2) pp.126-34[18].

1.1.3. Toll like receptors on dendritic cells

It is now well established that the activation of adaptive responses requires direction from the innate immune system[21] of which Toll like receptos (TLRs) play a crucial role. The mammalian TLRs compromise a family of germline-encoded transmembrane receptors which are characterized by an extracellular leucine-rich repeat (LRR) domain and an intracellular Toll/IL-1 receptor (TIR) domain[22]. TLRs recognize conserved microbial structures called PAMPs, which are invariant within a class of microorganisms. TLRs control multiple DC functions and activate signals that are critically involved in the initiation of the adaptive immune responses.

In mice, 9 distinct TLRs have been identified. In addition to ligand specificity, the functions of individual TLRs differ in their expression patterns and the signal transduction pathways they activate. TLR ligands are quite diverse in structure and origin. However, several common themes have emerged- most ligands are conserved microbial products (PAMPs) that signal the presence of infection, many TLRs can recognize several, structurally unrelated ligands and some TLRs require accessory proteins to recognize their ligands[22].

Mouse splenic DCs subsets express TLRs 1,2,4,6,8,and 9[23]. In this thesis, LPS a ligand for TLR4 stimulation was predominantly used for stimulation conditions. In comparison to freshly isolated splenic DCs which do not respond well to LPS stimulation, the CD11c+ DCs used in this thesis which were derived from bone marrow precursors in the presence of GM-CSF, have high expression of TLR4 and are able to respond to LPS[7].

Recognition of LPS by TLR4 is complex and requires several accessory molecules. LPS is first bound to a serum protein, LPS-binding protein (LBP), which functions by transferring LPS monomers to CD14[24], a high affinity receptor that is either secreted into serum or expressed on the surface of cells. MD-2 is another component that is crucial for the recognition of LPS on TLR4[25]. MD-2 is a small protein expressed on the cell surface in association with the ectodomain of TLR4. Figure 3 illustrates the ligand specificites of the 9 TLRs present in the murine system.

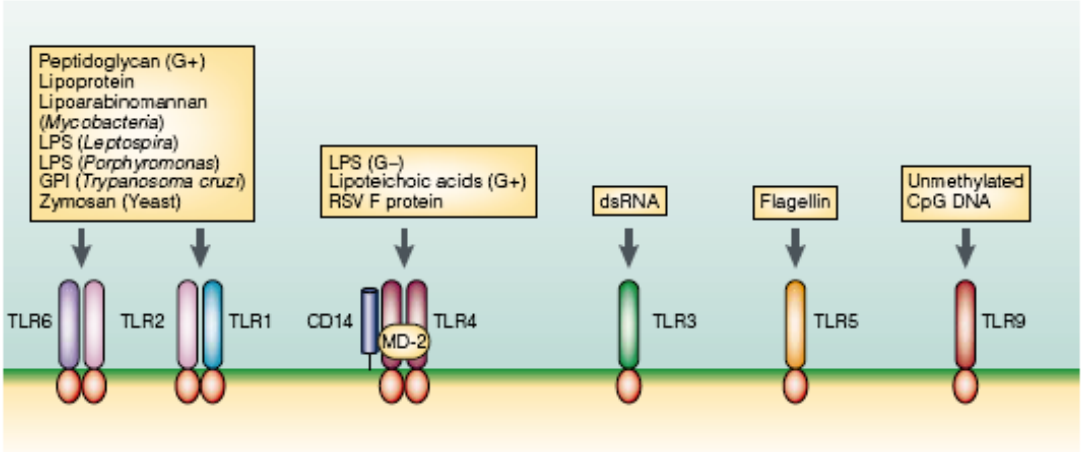

Figure 3. Ligand specificities of TLR 1-9

Toll-like receptors 1-9 recognize a unique assortment of pathogen-associated molecular patterns (PAMPs). Ligation of LPS on TLR4 is aided by 2 accessory proteins:CD14 and MD-2. TLR2 recognizes a broad range of structurally different ligands and functions in combination with some other TLRs (1 and 6). TLR3 is involved in recognition of double-stranded (dsRNA). TLR5 is specific for bacterial flagellin, while TLR9 is the receptor for unmethylated CpG motifs which are abundant in bacterial DNA. G+, gram-positive, G-, gram negative, GPI, glycophosphoinositol, RSV, respiratory syncytial virus
Figure taken from Medzhitov R. (2001), Toll-like receptors and innate immunity. Nature Reviews Immunology vol. 1. pp 135-145 [22].

Stimulation of TLR4 on DCs induces cytokine secretion and enhances surface expression of co-stimulatory molecules such as CD40, CD80 and CD86 and thus TLR signaling is thought to promote "maturation" of the DC. Induction of the co-stimulatory molecules CD80 and CD86 on the DC surface is an important step in the initiation of adaptive immunity which involves the coupling of microbial recognition with the induction of the co-stimulators that allows activation of pathogen specific T cells.

All TLRs are thought to signal through a MyD88-IRAK-TRAF6 pathway to induce the signaling cascades NF-κB and MAP kinases, with some TLRs (such as TLR4) also having independent MyD88 signaling capabilities albeit with delayed kinetics[26, 27]. Figure 4 illustrates the MyD88 dependent signaling cascade through TLR4. MyD88 contains two protein interacting domains, TIR domain and an amino terminal death domain. MyD88 interacts with the TLR through the TIR domain and its death domain interacts with the IL-1R-associated kinase (IRAK) thus forming a receptor complex upon which IRAK is autophosphorylated and associates with TRAF6[28]. TRAF6 induces activation of TGF-B-activated kinase (TAK1) and MAP kinase kinase 6 (MKK6), which, in turn activate NK-KB, c-Jun N-terminal kinase (JNK) and p38 MAP kinase, respectively[22].

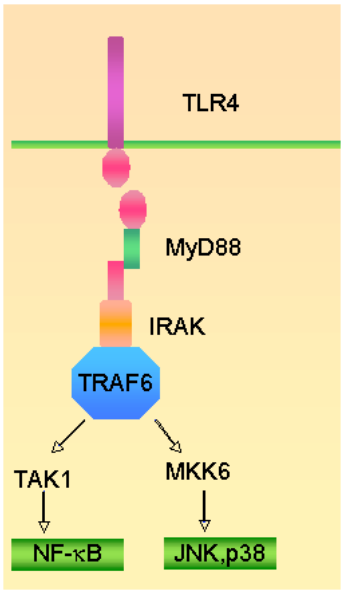

Figure 4. MyD88 dependent TRL4 signaling pathway

Signaling cascade of TLR4 upon LPS ligation initiates MyD88 recruitment and IRAK to form a receptor complex which then activates TRAF6. TRAF6 initiates signaling either by TGF activated kinase 1 (TAK1) or mitogen-activated protein kinase kinase 6 (MKK6) which leads either to NF-κB or JNK,p38 activation, respectively.
Figure created with Canvas software.

1.1.4. Dendritic cells and DALIS: ubiquitin aggregates with DRiPs

As mentioned above, DC maturation and antigen processing are intricately involved. One way in which these two DC functions are coordinated is through a modification process called ubiquitination which allows coordinated maturation and Ag presentation in DCs. When DCs are LPS-matured, they transiently accumulate newly synthesized ubiquitinated protein in an aggregated form in the cytosol. The protein aggregates are defined as DC aggresome-like-induced structures (DALIS)[29]. Newly synthesized proteins are ubiquitinated and most often degraded because of the errors that occur in protein synthesis[30]. These errors are termed "defective ribosomal products" (DRiPs) and the proteins that are synthesized are unable to attain native structure. However, their storage in DALIS delays their degradation. By delaying the degradation of newly synthesized misfolded proteins, DCs have the time to secrete proinflammatory cytokines and begin to initiate the expression of co-stimulatory molecules[31]. This process most likely prevents the DC from acquiring a tolerance-like state. Hence, ubiquitination plays an important role in synchronizing the co-stimulatory receptors needed on the DC cell surface with peptide MHC expression. Without ubiquitination, there would not be a delay in the presentation of peptide MHC expression and DCs would not be able prime T cell mediate immunity.

1.2. Ubiquitination

Ubiquitin (Ub) is a highly conserved protein composed of 76 amino acids (aa) that can be covalently attached to lysine (K) residues of target proteins. Three classes of enzyme are involved in the ubiquitination reaction: Ub-activating enzymes (E1), Ub-conjugating enzymes (E2) and Ub-protein ligases (E3). E1 adenylates the C terminus of Ub and then forms thioesters with E2, which acts as mobile carriers of activated Ub. E3 ligases are responsible for the specificity of Ub attachment to the target protein through the recruitment of both an E2 thioester and a specific substrate[32]. Deubiquitination of the substrate is performed by deubiquitinating enzymes (DUB) which recycle the Ub for further usage. Figure 5 illustrates the reversible process of ubiquitination by DUBs. Protein-attached Ub is a substrate for the attachment of further Ub residues, which leads to the formation of a polyubiquitin (polyUb) chain, in which the Ub molecules are linked through the C-terminal glycine residue of each Ub unit and a specific internal K of the previously attached Ub. Classically, polyUb was found to be a signal that directs proteins to the proteasome for degradation[33]. However, polyUb also remodels the surface of substrate proteins and thereby affects its properties such as stability and activity, drives interactions with other proteins and plays roles in subcellular localization[34].

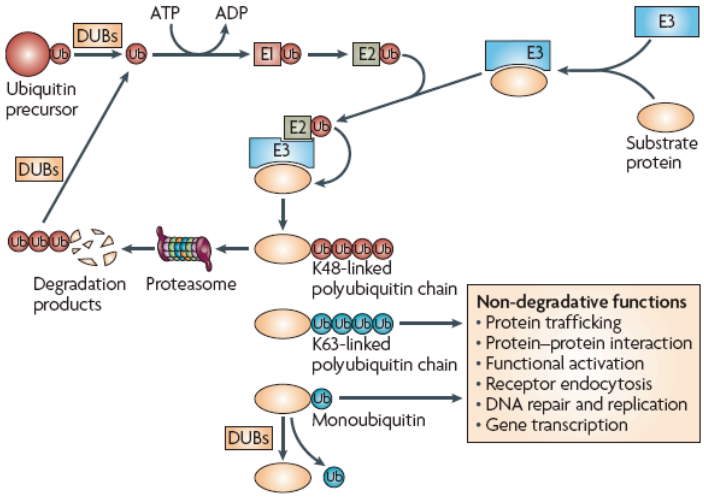

Figure 5. Protein ubiquitination and deubiquitination

Substrate proteins are covalently mono- or polyubiquitinated with the aid of energy expenditure and E1,E2 and E3 enzymes . The two most common internal lysine linkages in polyubiquitin chains are K^{48} and K^{63}. K^{48} linked ubiquitin chains generally mark the substrate for proteasomal degradation, while K^{63} linked ubiquitin chains and mono-ubiquitin mediate various non-degradative functions. DUB can deconjugate the ubiquitin chains from ubiquitinated proteins and proteasomal degradation products and in turn, reverse the ubiquitination process and regenerate free ubiquitin.

Image taken from Sun (2008) Deubiquitylation and regulation of the immune response. Nature Reviews Immunology,vol.8, pp.501-11.[35]

In polyubiquitination there are at least seven different possible linkages between ubiquitins because there are seven internal lysines in the Ub molecule (Figure 6a). Of these seven possible polyUb linkages, linkage through K^{48} (Ub^{K48}) targets substrates to the proteasome while K^{63} (Ub^{K63}) linkages seem to play important roles in directing cellular signaling events. As illustrated in Figure 6b and confirmed by crystallization, polyubiquitin chain K^{48} and K^{63} linkages differ in their structures with K^{48} polyubiquitin chains acquiring a more closed conformation and K^{63} polyubiquitin chains displaying a more open conformation[36-39].

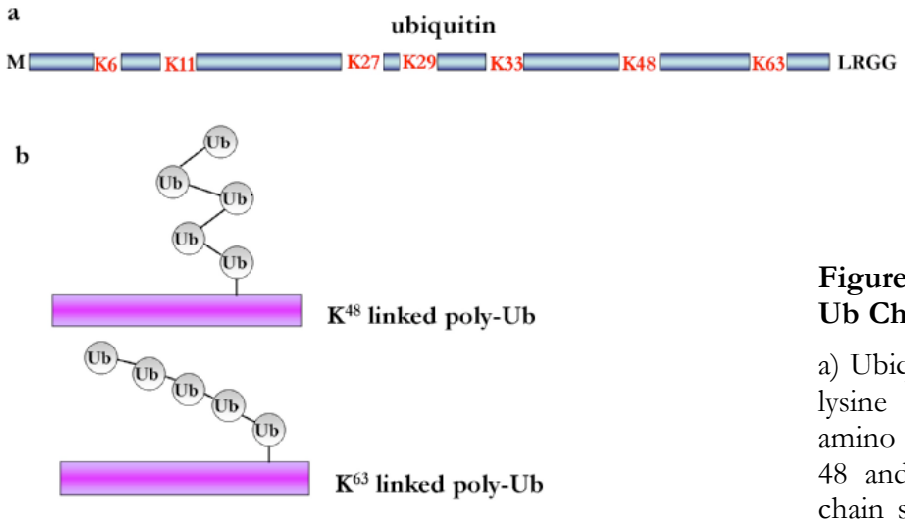

Figure 6. Ubiquitin and Poly-Ub Chain Structures

a) Ubiquitin protein consists of 7 lysine residues indicated by amino acid sites in red. b) Lysine 48 and Lysine 63 polyubiquitin chain structure. Figure created with Canvas software.

1.3. NF-κB

Nuclear factor-kappaB (NF-κB) is a protein complex that is a transcription factor. In the context of the immune system, NF-κB is involved in cellular responses to stimuli such as stress, cytokine, bacterial or viral antigens and is key in regulating the immune response to infection. Consistent with this role, incorrect regulation of NF-κB is linked to cancer, inflammatory and autoimmune diseases, septic shock, viral infection and improper immune development[40]. NF-κB belongs to a category of "rapid-acting" primary transcription factors. The speed of response is based on its independence from new protein synthesis since the transcription factors are already present in the cell but in an inactive state. In unstimulated cells, NF-κB dimers are sequestered in the cytoplasm by a family of inhibitors called inhibitor of κB (IκBs)[41]. These proteins contain multiple copies of a sequence called ankyrin repeats. Through these ankyrin repeats IκB proteins are able to mask the nuclear localization signals (NLS) of NF-κB proteins and keep them sequestered in an inactive state in the cytoplasm.

1.3.1. NF-κB signaling pathways

Activation of the NF-κB pathway is initiated by the signal-induced degradation of IκB proteins. This occurs primarily via activation of a kinase called the IκB kinase (IKK). IKK is composed of a heterodimer of the catalytic IKK alpha and IKK beta subunits and a "master" regulatory protein termed NEMO (NF-κB essential modulator) or IKK gamma. The IKK complex is a converging point for the activation of NF-κB by a large number of stimuli. When activated by signals, usually coming from the outside of the cell, the IκB kinase phosphorylates two serine residues located in an IκB regulatory domain. When phosphorylated on serines 32 and 36, the IκB inhibitor molecules are modified by a process called ubiquitination at positions K^{21} and K^{22} by an E3 ligase[42], which then leads them to be degraded by a cell structure called the 26S proteasome, thereby releasing NF-κB dimers from the cytoplasmic NF-κB-IκB complex and allowing them to translocate to the nucleus. Ubiquitination plays a central role not only in degrading IκB inhibitor but also in the processing of NF-κB precursors p100 and p105 into p52 and p50 respectively[43]. In addition, ubiquitination plays a role in activating NF-κB members such as tumor necrosis factor 6 (TRAF6) via lysine 63 polyubiquitin linkages which act as a platform for the further recruitment of NF-κB signaling members[44]. The basic scheme for NF-κB activation can be summarized as consisting of stimuli which triggers IKK activation leading to phosphorylation, ubiquitination and degradation of Iκβ proteins[45] (figure 7). NF-κB activity is stimulated by many pathways, including and not limited to; LPS, TNF and TCR. Figure 6 depicts the NF-κB activation pathways stimulated either through a) LPS b) TNF or c) TCR ligation. As can be seen in the figure, all pathways converge on the degradation of IKBα so that NF-κB dimers such as p65/p50 (or other dimer pairs) can translocate to the nucleus to activate NF-κB target gene transcription. In this thesis, NF-κB activation was investigated primarily through LPS stimulation.

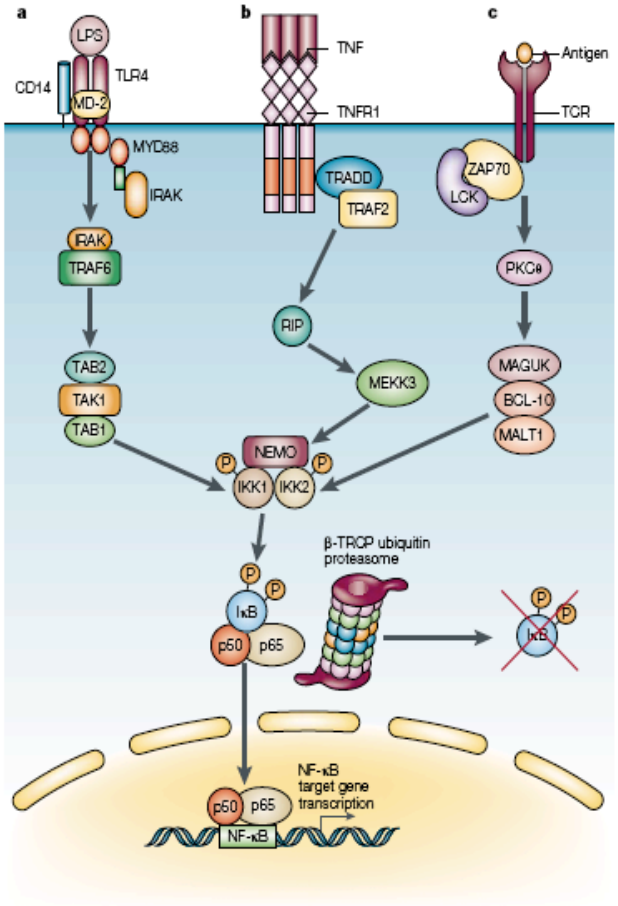

Figure 7. NF-κB activation pathways

a) LPS binding to TLR4-CD14-MD2 activates a signaling cascade which recruits MyD88 and IRAK. Activation of IRAK results in the activation of TRAF6 which relays signals through the TAK1-TAB1-TAB2 complex to IKK complexes which then activate NF-KB pathway. b) TNF engagement of the TNFR1 results in receptor trimerization and recruitment of the adaptor protein TNF receptor associated via death domain (TRADD) along with TRAF2 which then subsequently promotes the activation of various mitogen-activated proteins (MAP) and extracellular signal-regulated kinase (ERK) kinases through the receptor interacting protein (RIP) which links the signaling transduction to IKK activation. c) In T cell stimulation, the protein kinase is rapidly translocated to the plasma memberane and through components such as the membrane-associated guanylate kinase homologue (MAGUK), the mucosal-associated lymphoid tissue (MALT) associated protein BCL-10 and MALT1, IKK is activated.
Taken from Li and Verma (2002). NF-κB regulation in the immune system. Nature Reviews Immunology. Vol 2(10) pp.725-34[43].

1.3.2. NF-KB, IκB and IKK protein families

The NF-κB family of transcription factors consists of five members: p50, p52, p65 (RelA), c-Rel, and RelB, encoded by *NFκB1, NFκB2, RELA, REL, and RELB,* respectively[45]. These 5 members all share an N-terminal Rel homology domain (RHD) which aids in the binding of DNA as well as facilitating homo- and heterodimerization

between the family members (figure 8). Only p65, c-Rel and RelB have the capacity to bind to κB within the promoters/enhancers of target genes and regulate transcription since they contain the transcription activation domain (TAD) necessary for positive regulation of gene expression[46]. p50 and p52 lack TADs and unless associated with a TAD-containing NF-κB family member (such as p65, Rel or c-Rel) or other proteins capable of positive gene regulation, they most likely repress transcription themselves[45].

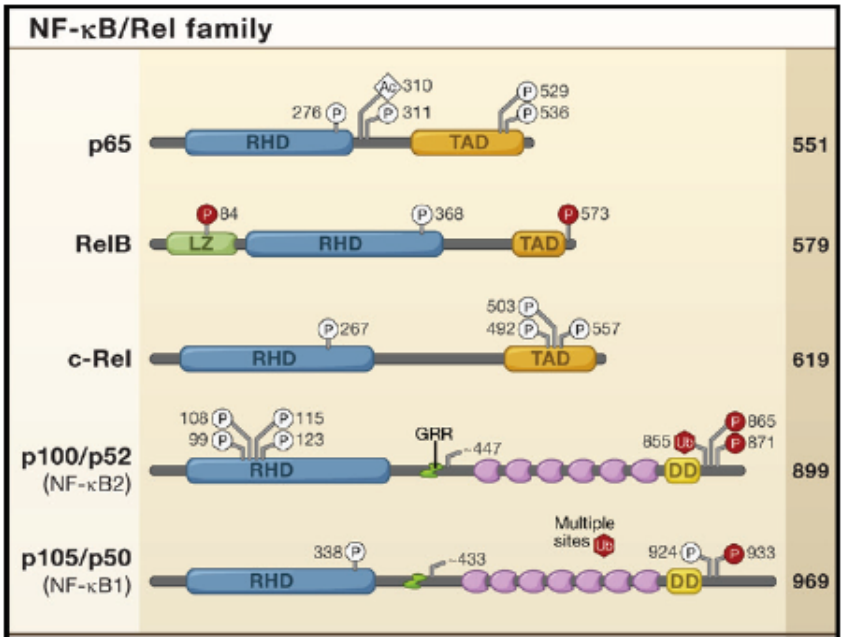

Figure 8. NF-κB/Rel family members

Protein members are depicted from human sequence. Amino acid length is indicated on the right. Protein modifications that can occur in each member include phosphorylation (P), acetylation (Ac) and ubiquitination (Ub). p100 and p105 are able to undergo proteasomal processing and the breakdown to p52 and p50, respectively, is shown by a green line in the protein. LZ stands for leucine zipper domain, GRR for glycine-rich domain, TAD is the transactivation domain and DD is the death domain. Purple boxes on protein structures depict ankyrin repeat domains.
Taken from Hayden and Ghosh, (2008) Shared Principles in NF-κB signaling. Cell vol. 132 pp344-362[45].

In the inactive state NF-κB dimers are associated with one of the IκB family members (or as precursors p100 or p105). IκB family members consist of IκBα, IκBβ, IκBε, IκBγ, Bcl-3 and IκBζ. The three typical IκB proteins, IκBα, IκBβ, IκBε are responsible for maintaining NF-κB in the cytoplasm. Bcl-3 and IκBγ are inducibly expressed and function differently in the regulation of NF-κB (Bcl-3 is discussed in next section). To date, there is no defined role for IκBζ.

All IκBs are characterized by the presence of multiple ankyrin repeat domains (figure 9). It should be noted that IκBα degradation and p105 processing into p50 is responsible for activating the canonical/classical NF-κB signaling cascade. p100 processing on the otherhand, which is independent of IκBα, is dependent on the proteasomal processing of p100 into p52 and signals the noncanonical/alternative NF-κB signaling cascade. The two NF-κB signaling cascades function to regulate distinct sets of genes through distinct sets of receptors.

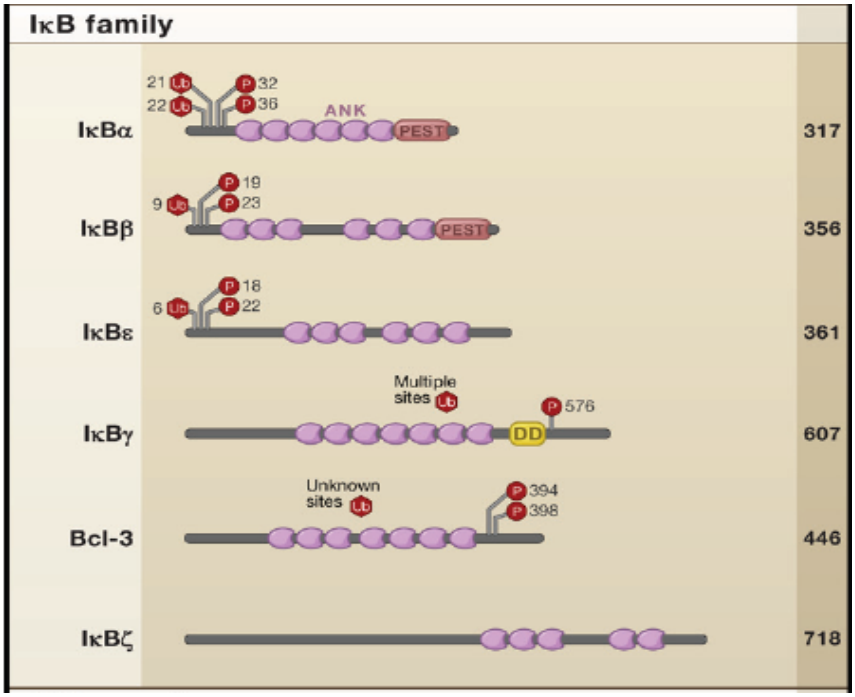

Figure 9. IκB family

Protein members are depicted from human sequence. Amino acid length is indicated on the right. Protein modifications that can occur in each member include phosphorylation (P) and ubiquitination (Ub). Ankyrin repeat domains are depicted by purple boxes. DD indicates death domain.
Taken from Hayden and Ghosh, (2008) Shared Principles in NF-κB signaling. Cell vol. 132 pp344-362[45].

Degradation of IκBα is mediated by IKK. The IKK complex consists of two highly homologous kinase units, IKK1(IKKα) and IKK2 (IKKβ) and a regulatory subunit NF-κB essential modulator (NEMO/IKKγ)[47](Figure 10). In the canonical pathway, IKK1 mediates the phosphorylation of IκBα (which then promotes its ubiquitination and subsequent degradation) while in the noncanonical pathway, IKK1 phosphorylates p100 causing the inducible processing to p52. Phosphorylation of the conserved serine

residues (DS*GXXS*) in IκB proteins results in their K^{48}-linked polyubiquitination by an E3 ligase.

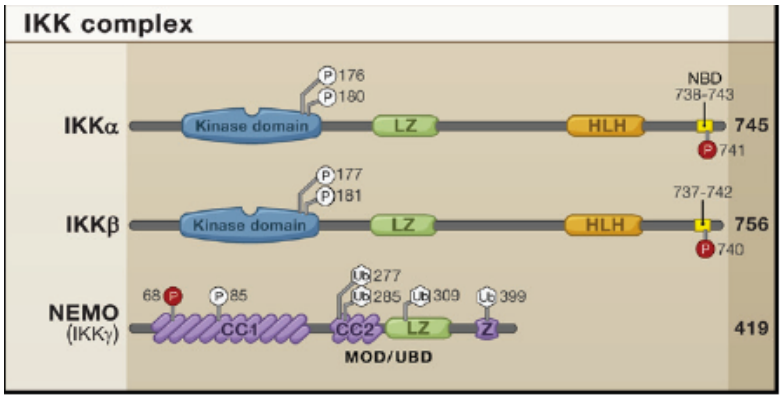

Figure 10. IKK complex

Protein members are depicted from human sequence. Amino acid length is indicated on the right. Protein modification that can occur in each member include phosphorylation (P) and ubiquitination (Ub). CC1/2 are coiled-coil domains, NBD stands for NEMO-binding domain, MOD/UBD for minimal oligomerization domain and ubiquitin-binding domain. LZ depicts the leucine zipper domain. HLH indicates helix loop helix.
Taken from Hayden and Ghosh, (2008) Shared Principles in NF-κB signaling. Cell vol. 132 pp344-362[45].

1.3.3. Bcl-3

Although homodimers of p50 and p52 are, in general, repressors of κB site transcription, both p50 and p52 participate in target gene transactivation by forming heterodimers with RelA, RelB, or c-Rel[43]. In addition, p50 and p52 homodimers also bind to the nuclear protein Bcl-3, which is induced by NF-κB forming what is hypothesized to be an autoregulatory loop that controls the nuclear residence of p50/p52, and such complexes may in some experimental setups function as transcriptional activators[48-50]. Bcl-3 is a unique member of the IκB family because in addition to the ankyrin repeat domain characteristic of the inhibitory IκB proteins, it also contains a domain for transcriptional activation predominant in Rel proteins [48, 51, 52]. Because of the two domains, the function of Bcl-3 is notoriously known for producing contradictory results. For example, in a recent report, it was shown that Bcl-3 is an essential negative regulator of TLR signaling[53]. Bcl-3 blocks the ubiquitination of p50 and thereby stabilizes this transcription factor since ubiquitination (presumably K^{48} linked ubiquitin) would signal for the degradation of p50. This negative regulatory function of Bcl-3 is in contrast to other reports. Bcl-3 was originally discovered by its translocation into the immunoglobulin alpha-locus in B cell leukemia as well as its significantly high expression in the breast tissue of cancer patients[54, 55]. Its over-expression causes cells to initiate G1 transition into the cell cycle[56] and a multitude of reports suggest that Bcl-3

expression correlates with increased survival and cell proliferation[57-64]. Bcl-3 transgenic mice for instance, have an expansion of B cells[65] and an overall hyper-responsive immune response. Bcl-3^{ko} mice have impaired T cell responses in addition to disordered germinal centers and altered secondary lymphoid organ structures, including partial loss of B cells[66]. What appears to cause the most confusion is the role of Bcl-3 with p50 or p52. It is unclear whether Bcl-3 binding to p50 or p52 promotes transcriptional activation or prevents p50 from binding to a NF-κB dimer such as p65 to then promote NF-κB activation. However, new Bcl-3 binding partners have been discovered and this may shed some light not only on the relationship between p50 and Bcl-3 but also how Bcl-3 is regulated. The deubiquitinating enzyme CYLD has recently been identified as a target of Bcl-3. It is believed that CYLD blocks Bcl-3-dependent NF-κB signaling since absence of CYLD causes increased Bcl-3 localization in the nucleus of CYLD^{ko} keratinocytes[67]. Specifically, the results from this study suggest that CYLD binds and deubiquitinates Bcl-3 thereby preventing nuclear accumulation of Bcl-3 and subsequent Bcl-3 binding to p50 or p52 to mediate NF-κB activation. However, it is unclear if Bcl-3 binding to p50 promotes the dimer p50 to associate with a dimer like p65 with a TAD or whether the stabilization of p50 by Bcl-3 has other effects. Further investigations are needed to answer how Bcl-3 functions physiologically and what factors regulate its expression, localization and function. Figure 11 illustrates the binding of Bcl-3 with p50 and p65. The question mark indicates the uncertainty of whether this binding causes activation or inhibition. Bcl-3 interaction with CYLD appears to regulate its localization and how exactly this regulation occurs still remains unanswered. However, what is clear is that NF-κB activation is a complex signaling pathway with many regulators and sophisticated means of controlling responses. Control in NF-κB activation is a must since aberrant activation would cause unnecessary and hazardous inflammatory responses.

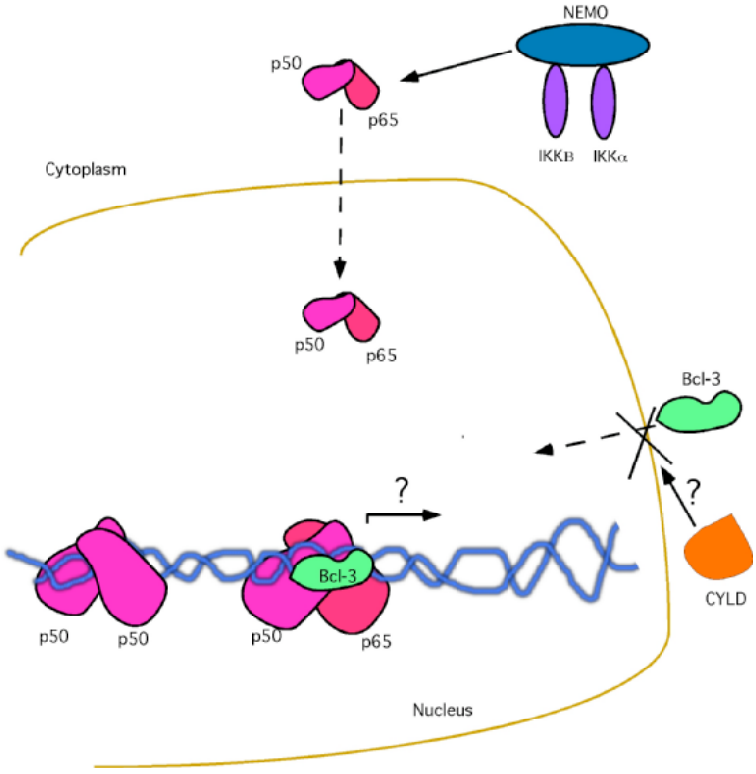

Figure 11. Bcl-3 in NF-κB activation

Bcl-3 binds to p50 dimer in the NF-κB pathway. It is unclear however, if Bcl-3 association with p50 promotes then binding to p65 dimer and subsequent DNA transcription or if Bcl-3 somehow inhibits these dimer pairs. Bcl-3 appears to be regulated by CYLD, a DUB which appears to control the localization of Bcl-3.
Image created with Canvas software.

1.4. DUB

Deubiquitinating enzymes (DUB) belong to the family of proteases. Of the five classes of proteases (aspartic, metallo, serine, threonine, and cysteine), only cysteine and metallo proteases contain deubiquitinating activity and can be classified as DUBs. DUBs can be further subdivided according to the five different catalytic domains. These include ubiquitin C-terminal hydrolases (UCHs), ubiquitin-specific proteases (USPs), Maschado-Joseph disease protein domain proteases (MJDs), ovarian tumor proteases (OTUs) and JAB1/MPN/Mov34 metalloenzyme (JAMM) motif proteases. In order for a DUB to remove ubiquitin moieties from a substrate, it must first recognize this substrate and then perform the hydrolysis of Ub from its substrate. Substrate specificity is complex and confounded by the fact that not only are there different substrates to be recognized by the DUB enzymes, but also 7 different lysine residues in the Ub molecule that can form different types of polyUb chains, of which K^{48} and K^{63} conjugation seems to be the most frequently found and certainly the most frequently studied. It is well acknowledged that there must be a combinatorial mechanism relying on recognition of both the target and

the attached moiety. In addition, there are most likely further mechanisms such as protein localization and interactions with binding partners that may contribute to specificity[68]. Ub polymers are able to determine the substrate specificity of DUB, in a way that is not yet well characterized. As described above, protein ubiquitination comes in many different forms that serve distinct functions[69]. Interstingly, K^{63} linked Ub molecules differ structurally from K^{48} chains as depicted in figure 6 above. Apparently, the K^{63} Ub linked chain is characterized by an extended conformation with no direct interaction with hydrophobic residues and thus confers an open conformation[37]. In contrast, the K^{48} Ub linked chain is distinguished by its closed conformation wherein the hydrophobic residues of Ub form an interdomain interface[36]. This interesting finding indicates that different DUBs may act on specific Ub branches. Indeed this is exactly so, as exemplified by the yeast DUB Ubp2, which prefers K^{63} over K^{48} linked Ub chains as a substrate [70]. Furthermore, there are other examples of DUBs (ie. USP8 and USP14)[71] cleaving only K^{48} linkages but not K^{63} linked Ub polymers.

CYLD is an example of a DUB that has substrate specificity for mediators involved in the NF-κB pathway (NEMO and TRAF2) and is supposedly specific for only K^{63} [72-74], although some other studies suggest also the deubiquitination of K^{48} Ub linkages by CYLD[75]. The NF-κB pathway not only utilizes CYLD but another DUB called A20. A20 is a cytoplasmic protein that inhibits TNF-induced NF-κB activity[76]. It is intriguing to note that both CYLD and A20 interact with TRAF2 and NEMO to deubiquitinate K^{63} linked Ub chains. Their relationship and function whether cooperative, altruistic or redundant is of great interest in understanding the role of DUB in NF-κB signaling.

1.4.1. CYLD

CYLD was identified as a tumor suppressor gene that is mutated in patients with familial cylindromatosis, an autosomal dominant predisposition to benign tumors of the skin appendages[77]. Afterwards, in a precedent discovery, three distinct research groups simultaneously identified CYLD as DUB enzyme important in down-regulating NF-κB activity by targeting the deubiquitination of targets such as TRAF2/6 and NEMO[72-74]. CYLD belongs to the USP subclass of DUBs which are characterized by the presence of cysteine and histidine boxes[77]. These cysteine and histidine boxes contain the deubiquitinating activity of the USP DUBs[78, 79]. Some cylindromatosis patients have a deletion in the histidine box of CYLD, suggesting a link between deubiquitination and signals propagating to cancer. Furthermore, the importance of the deubiquitinating

domain of CYLD has recently been shown in patients who have the missense mutation D681G, which renders the CYLD protein incapable of deubiquitinating target proteins such as TRAF2 and ultimately leads to hyper-activation of NF-κB signaling pathway[80]. As shown in figure 12, the CYLD protein encompasses 956 aa harboring a NEMO binding site located between aa 570 and 674 and a TRAF2 binding site located between CYLD aa 394 and 470. The CYLD gene also encodes 3 cytoskeletal-associated-protein-glycine (CAP-Gly) conserved domains found in other proteins to coordinate the attachment to microtubules indicating a possible role for CYLD in cytoskeletal formation. In comparison, the naturally occurring short splice variant of CYLD (sCYLD) is devoid of TRAF2 and NEMO binding sites while the Bcl-3 binding site is still intact.

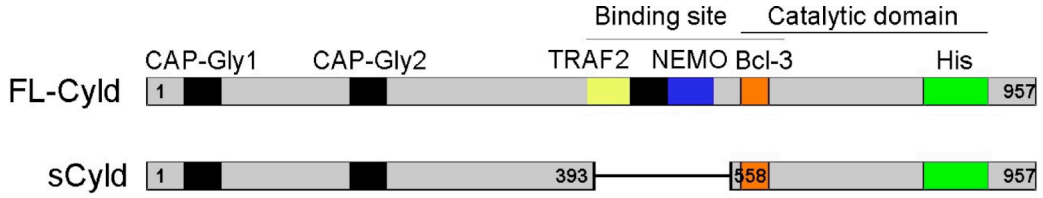

Figure 12. The protein structure of FL-CYLD and sCYLD

Comparison between full length CYLD (FL-CYLD) and short CYLD (sCYLD) shows that both proteins retain their catalytic domain at the C-terminus, but sCYLD lacks the TRAF2 and NEMO binding sites while retaining the Bcl-3 binding site. The CAP-Gly domains are depicted by black boxes.
Taken from Hövelmeyer et al. (2007) Regulation of B cell homeostasis and activation by the tumor suppressor gene *CYLD*. Journal of Experimental Medicine. vol. 11 pp.2615-27. [81]

The naturally occurring splice variant of CYLD is missing exons 7 and 8 and is naturally found in murine cells in addition to full length CYLD (FL-CYLD)[81]. Interestingly, the naturally occurring splice variant appears to play an important role in B cell homeostasis as the B cell population is significantly increased in the mice expressing exclusively this short splice variant, $CYLD^{ex7/8}$, and not in mice lacking the complete *cyld* gene [81]. The relationship of this naturally occurring short CYLD splice variant to full length CYLD in terms of deubiquitinating activity, target proteins and significance to immunologically relevant signaling cascades is of importance in understanding the manifestations exhibited in the different CYLD mutated mouse models.

1.4.2. CYLD mouse models

To date, 3 different complete $CYLD^{ko}$ mice have been generated using different gene-targeting methods[82-84] in addition to the sCYLD over-expressing mouse[85]. From

these mouse models, several interesting new functions of CYLD have been discovered ranging from roles in host defence against infections, immune-cell development, activation and inflammation, cell survival, cell proliferation and tumorigenesis, microtubule assembly and cell migration, mitotic cell entry, calcium-channel function, spermatogenesis and osteoclatogenesis[35]. The 2 CYLD mouse models used in this thesis were the $CYLD^{ko}$ mouse made by Ramin Massoumi in Reinhard Fässler's group and the sCYLD over-expressing mouse ($CYLD^{ex7/8}$) made by Nadine Hövelmeyer in Ari Waisman's lab. These two mice models are interesting to examine for several reasons including the fact that they differ in their B cell phenotype. $CYLD^{ko}$ mice for example, do not exhibit the increased B cell survival and expansion of B cells in their secondary lymphoid organs like $CYLD^{ex7/8}$ mice. This is in apparent contrast to the $CYLD^{ko}$ mice made by the Sun group (using a different gene targeting approach) where an obvious B cell hyperplasia along with enlarged lymphoid organs and B cell surface markers indicative of spontaneous activation and hyper-proliferation was found[86]. This observation certainly raises a flag when comparing mouse models to one another and may be indicative of different penetrance of gene targeting approaches. However, the availability of the $CYLD^{ko}$ mice from the Fässler group has allowed us to explore and identify differences between this $CYLD^{ko}$ mouse and the $CYLD^{ex7/8}$ mouse. Comparison and investigations using these two mouse models will hopefully shed some light on the functions of FL-CYLD and sCYLD in the *in vivo* environment.

1.4.3. A20

A20 is another DUB important in circumstances similar to CYLD. A20 is an inducible ubiquitin-editing enzyme that restricts both TLR-and TNF-induced responses by regulating the ubiquitination of key signaling proteins[76, 87]. The N-terminal region of A20 contains an OTU domain which has DUB activity towards several NF-κB signaling factors, including TRAF2/6, RIP1, RIP2 and IKKγ [76, 88-91] which are important in the TNF induced TNFR1 NF-κB signaling pathway (see figure 7). A very unique feature of A20 is its ability to function both as a DUB as well as an E3 ligase. A20 catalyzes the K^{48}-linked ubiquitination of RIP1 through its carboxy-terminal zinc-finger domain, so that RIP1 is destined for proteasomal degradation. Simultaneously, A20 removes K^{63}-linked ubiquitin chains from RIP1 which serves to inactivate the signaling function of RIP1 and possibly facilitates its K^{48}-linked ubiquitination by A20. Not only does A20 have overlapping function with CYLD in terms of deubiquitinating similar substrates (TRAF2 and NEMO/ IKKγ), mouse models of A20 and CYLD show similarities as

well. A20-/- mice experience severe inflammation as well as upregulated NF-κB activity. CYLD$^{ex7/8}$ mice have increased B cell survival in addition to an activated NF-κB activity while CYLD^{ko} mice have keratinocytes which exhibit increased cyclin D1 and increased NF-κB family member, Bcl-3. All 3 mouse models mentioned draw parallels to one another due the disturbance in NF-κB signaling members leading to elevated NF-κB activation.

1.5. Goals of this Thesis

1. **Examine the effect of sCYLD over-expression on DC cell function**
2. **Propose a mechanism for the hyper-reactive phenotype of CYLD$^{ex7/8}$ DCs**
3. **Investigate the involvement of NF-κB members**
4. **Utilize an *in vivo* model of viral challenge or tolerance induction to investigate *in vivo* DC function in CYLD$^{ex7/8}$ mice**
5. **Understand the expression pattern of sCYLD in WT setting**

1. Examine the effects of sCYLD over-expression on DC cell function

As the B cell population was remarkably affected by the over-expression of sCYLD *in vivo*, we decided to investigate the effect of sCYLD on DCs. In our laboratory we have setup a reproducible and reliable system of culturing bone marrow derived dendritic cells. With this established assay the DCs from CYLD^{ko} and CYLD$^{ex7/8}$ were compared in terms of DC cell surface markers, cytokine secretion, *in vivo* capacity to stimulate T cells, and the ability to phagocytose, process and present Ag.

2. Propose a mechanism for the hyper-reactive phenotype of CYLD$^{ex7/8}$ DCs

Several hypotheses were generated to explain the hyper-reactive phenotype in CYLD$^{ex7/8}$ DCs and these included analysis of ubiquitination levels, DALIS formation and ubiquitination state of TRAF2, a target of CYLD. It is believed that the differences in phenotype between the CYLD^{ko} and CYLD$^{ex7/8}$ DCs lies in the different ubiquitin targets of FL-CYLD and sCYLD.

3. Investigate the involvement of NF-κB members

It was obvious to investigate NF-κB members as CYLD plays a crucial role in deubiquitinating NF-κB members and downregulating NF-κB activity. Several approaches were used including analyzing TRAF2, Bcl-3, p105 in whole cell lysates in

Western blot analysis. TRAF2 and Bcl-3 localization was visualized by confocal microscopy in the DCs of CYLD^{ko}, CYLD$^{ex7/8}$ and compared to WT counterparts. In addition, the nuclear accumulation of the TAD containing NF-κB Rel member, p65 (RelA) was investigated using Western blot analysis. Furthermore, NF-κB luciferase assays were conducted in transfected BMDCs to analyze NF-κB activity. To begin to understand the differences in phenotypes between the CYLD mutant mice, a model where A20 may compensate for the lack of FL-CYLD was investigated by observing the levels of A20 induction in DCs. Figure 13 illustrates the targets which were the focus of this thesis. CYLD targets: TRAF2, and Bcl-3 were intensely investigated throughout the duration of the thesis. In addition, A20 which has substrate specificity similar to CYLD was evaluated to determine if A20 levels are upregulated in the absence of CYLD or in the presence of over-expressed sCYLD. It was thought that if A20 is upregulated in the CYLD^{ko} background this might explain the lack of any phenotype in the DCs of CYLD^{ko} mice.

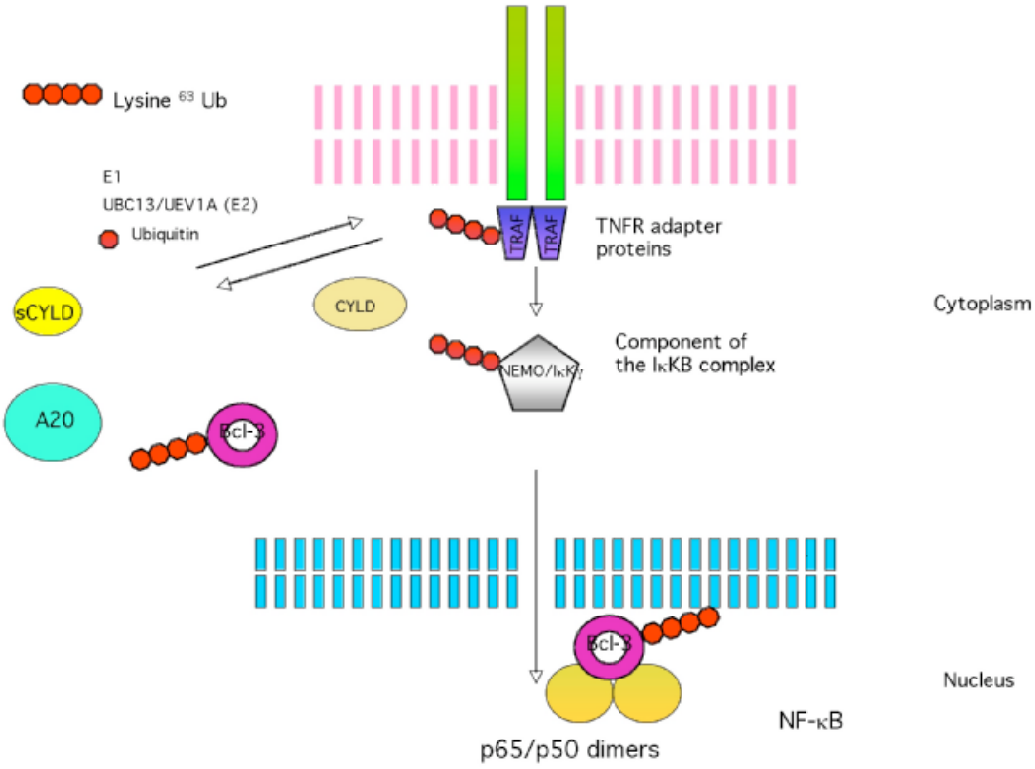

Figure 13. CYLD targets considered

CYLD targets considered in this thesis: TRAF2, Bcl-3, p50 (from p105) and p65. The relationship with A20 was also investigated.
Figure created with PowerPoint software.

4. Utilize an *in vivo* model of viral challenge or tolerance induction to investigate *in vivo* DC function in CYLD$^{ex7/8}$ mice

In vivo DC functions of CYLD$^{ex7/8}$ mice were tested with LCMV infection to observe how well the mice respond to viral exposure. Since LCMV is a virus that is heavily dependent on an intact DC function this appeared to be a good model of choice. However, the strength of LCMV infectivity could not decipher any differences between the mouse models. Therefore, we looked at the other *in vivo* DC function with T cells, that is, the induction of tolerance. We used a model of anti-DEC-205:OVA mediated tolerance to observe the ability of CYLD$^{ex7/8}$ *in vivo* DCs to mediate tolerance and found that tolerance induction is altered in these mice and not in CYLD^{ko} or WT counterparts.

5. Understand the expression pattern of sCYLD in WT setting

Understanding the expression pattern of sCYLD and when it is induced or upregulated in the dendritic cells could provide insight as to what it could be doing differently compared to FL-CYLD. Therefore, we compared the levels of sCYLD and FL-CYLD through several timepoints during stimulation. The anti-CYLD antibody in western blot applications is not optimal and therefore we had to resort to designing specific primers for sCYLD and FL-CYLD to use in real-time PCR analysis. The expression patterns were monitored through a realtime PCR to quantitate the levels of mRNA expression during LPS stimulation in WT BMDCs.

2. MATERIALS & METHODS

2.1. Cell lines, Antibodies and Reagents

IL-2 was made from mouse myeloma X63Ag8-653 (ATCC) in our laboratory. The GM-CSF was made in our laboratory from an over-expressing GM-CSF stable cell line (X63). Agonistic rat anti-mouse CD40 was made from FGK115 cell line. Culture media IMDM was supplemented with 5% FCS, glutamine, penicillin/streptomycin, and 50uM 2-ME (Sigma Aldrich). TLR2 agonist Palmitoyl-3-Cys-Ser-(Lys)4 (Pam3Cys: EMC Microcollection, Tubingen, Germany) and TLR3 agonist Poly-I:C (Amersham, Freiburg, Germany) and TLR4 agonist, LPS (Salmonella typhimurium: Sigma, Deisenhofen, Germany) was used where indicated.

2.2. Mice

C57BL/6 wildtype (WT) mice were bred in our Animal Facility (Johannes Gutenberg Mainz Universität) according to the guidelines of the Central Animal Facility Institute. $CYLD^{ex7/8}$ mice were generated by Nadine Hövelmeyer in the laboratory of Dr.Ari Waisman. This mouse strain is completely devoid of the full CYLD protein whereas the splice variant of CYLD is over-expressed compared to control mice. LoxP sites flanking exon 7 of the *cyld* gene were introduced into the *cyld* locus. Upon Cre-mediated recombination *in vitro* the $CYLD^{ex7/8}$ mice were generated by blastocyst injection of the mutant embryonic stem cells. $CYLD^{ex7/8fl/fl}$x CD11c-Cre which express sCYLD in CD11c+ cells and full CYLD in the other cell types was bred by crossing $CYLD^{ex7/8fl/fl}$ mice with CD11c-Cre in Dr. Ari Waismans's lab. $CYLD^{ko}$ were obtained from Dr.Ramin Massoumi & Dr. Fässler from Mansfried Germany and generated by the insertion of LacZ reporter gene into the ATG encoding exon 4. OT-I and OT-II mice were obtained from Dr. Christian Kurts (Bonn, Germany). St42 transgenic mice were generated in the laboratory of Martin Kast (Maywood, IL).

2.2.1. Genotyping $CYLD^{ex7/8}$ mice

Since $CYLD^{ex7/8}$ homozygous males are sterile, heterozygous males are bred with homozygous $CYLD^{ex7/8}$ females and offspring need to be genotyped with the following primers:

$CYLD^{ex7/8}$ primers:

Primer 1 Sense: GAAGAAGAGAAACAAGGACAGACG

Primer 2 Anti-sense: GGAATGGCAAAGGGTGAATG

Primer 3 Anti-sense spanning exons 7 and 8: AGAAGAGATGGGCAAGGGTG

1+2: 749bp WT band, 201bp $CYLD^{ex7/8}$,

1+3: 427bp WT band (specific only to WT)

Therefore, if $CYLD^{ex7/8}$ are homozygous for the deletion of exons 7 and 8, the result from the triple primer combination would result in only a 201bp band.

The following PCR mix was used:

10x PCR buffer	5.0ul
25 mM dNTPs	0.3ul
50mM $MgCl_2$	0.3ul
Primer 1(stock 20pmol/ul)	0.5ul
Primer 2	0.5ul
Primer 3	0.5ul
H_20	25.5ul
Taq polymerase 1unit	0.25ul
DNA stock 100ng/ul	0.5ul
total	30ul

After the hot start (5 min at 94°C), samples were amplified for 35 cycles; 45s at 94°C, 30s at 56°C, and 1 min at 72°C followed by a 10 min extension at 72°C.

2.3. Mouse bone marrow derived dendritic cells

Mouse immature DCs were generated according to standard protocols. Bone marrow was extracted from the tibia and femur of mice using 2%FCS in PBS with a 22 gauge needle. Bone marrow was resuspended into single cell suspension by gentle pipetting. Blood cells were lysed with red blood cell lysis buffer (155 mM NH_4Cl,12 mM $NaHCO_3$, 0.1 mM EDTA) and remaining cells were cultured in 6 well plates (Greiner Bio One) at $3.0x10^6$/well. On day 2 and 4 culture medium containing GM-CSF (200units/mL) was replaced along with the removal of non adherent cells. Culture media IMDM was supplemented with 5% FCS, glutamine, penicillin/streptomycin, and 50uM 2-ME. On day 6 the immature DCs were activated with TLR ligands or TNFR agonist or left untreated. The following TLR stimuli were used: TLR2 agonist Palmitoyl-3-Cys-Ser-$(Lys)_4$ (Pam3Cys: EMC Microcollection, Tubingen, Germany) and TLR3 agonist Poly-I:C (Amersham, Freiburg, Germany). TLR4 was stimulated with LPS (Salmonella typhimurium: Sigma, Deisenhofen, Germany). Agonist CD40 was made from clone FGK115.

2.3.1. BMDC cytokine release measurement with ELISA or CBA-Flex

After at least 20 hours (40 hours in stimulus-removal experiments) of stimulation, culture supernatants were collected and frozen at -80°C for subsequent analysis. Cytokines were analyzed by standard enzyme-linked immunosorbent assay (ELISA) protocols. All ELISA antibodies and recombinant standards were from BD Pharmingen (Heidelberg, Germany) and used according to the manufacturer's instructions. For detection, 3.3', 5,5' TMB liquid substrate (Sigma) was used. The optical density at 450 nm after adding 2M H_2S0_4 was analyzed using a SpectraFlourPlus reader from Tecan (Creilsheim, Germany). Where indicated, cytokine detection in BMDC culture supernatants was detected also with anti-IL-6, IL-10 and TNF-α antibodies from BD Cytometric Bead Array Flex system (CBA-Flex) and analyzed with FCAP Array Software™ according to manufacturer's instructions.

2.3.2 BMDC immunizations

For immunizations with bone marrow-derived DC (BMDC), differentiated day06 BMDCs were stimulated overnight with 100ng/mL LPS pulsed with SGPSNTPPEI (SGP) peptide (10 nM) for 1hr at 37°C and 1 x 10^5 BMDCs were injected i.p. into recipient mice. Synthetic peptide SGPSNTPPEI derived from Ad5 E1a was kindly provided by Dr. S. Stevanovic (Tübingen, Germany).

2.4. Endogenous DC purification from mouse organs

Collagenase D (Boehringer Mannheim) was used for the digestion of organs. 1mL of Colleganase D was diluted 1:10 to 10mL for 400U/mL. Collagenase was filtered and kept on ice. Spleens, lymph nodes and bone marrow were harvested in Hank's Buffered Salt Solution (HBSS). Using a 22-gauge needle on a 10 mL syringe, organs were fused (except bone marrow) with 100U/ml collagenase D in HBSS. Spleen and lymph nodes were then torn apart into tiny pieces and resuspended using a 5mL plastic pipette. Resuspended cells were placed in a dish and into the incubator for 30 minutes. After the incubation, 10mM of EDTA was added to stop the collagenase digestion. Cell suspensions were collected and passed through a cell strainer (BD Biosciences). Cells were washed 2x with 10mM EDTA/PBS. Cell populations were then stained with the following antibodies: PE channel was a "dump" channel with B220-PE (eBioscience), CD3-PE (eBioscience) markers which would exclude B cells and T cells. Cells were then stained with CD11c (eBioscience), CD11b (eBioscience), Gr-1 (eBioscience), MHC II

(BD Pharmingen), CD86 (eBioscience), Ly6-C/G (eBioscience) using the FACS Canto and FlowJo software® (Treestar).

2.5. RNA isolation and cDNA preparation

Differentiated BMDCs at various stimulation timepoints were harvested and collected in a 15mL Falcon tube and pelleted. Pellets were washed 2x with PBS to get rid of media remnants. Supernatant was discarded and the cell pellet was resuspended (8-10x) with 1ml TRI reagent (Invitrogen) and incubated at room temperature for 5 minutes. 200ul of chloroform was added to the eppendorf and vortexed. After a 10 minute incubation time, eppendorfs were spun for 15 minutes at 11500 rpm in a 4°C microcentrifuge. The aqueous phase, approx. 500ul, was transferred to a new eppendorf tube. 1.5ul of 20ug/mL glycogen stock (Invitrogen) was added to the aqueous layer and vortexed. After a 5 minute incubation period at room temperature, 500ul of isopropanol was added and mixed to the aqueous phase solution followed by another incubation period of 10 minutes at room temperature. The eppendorf tubes were then spun down for 10 minutes (11500rpm) at 4°C and the supernatant was discarded so that only the RNA pellet remained. The RNA pellet was mixed with 1mL 75% cold ethanol (stored in -20°C). This mixture was spun down for 10 minutes at 9200 rpm at room temperature, supernatant was discarded and the pellet was mixed again with 1mL 75% cold ethanol. The pellet with the ethanol was frozen at -20°C overnight. To make cDNA from the RNA pellet, the RNA pellet with ethanol was spun down for 10 min (9200 rpm) at room temperature, supernatant was discarded, pellet was air-dried until it became transparent. 19ul of ***Master Mix*** (see recipe below) was added to each pellet

Master Mix

DEPC water	11ul
M-MuLV-RT buffer	4ul
dNTP mix (10nM)	2ul
oligo(dT)-primer	1ul
N6-primer	1ul
	19ul total

The master mix with RNA pellet was incubated in the water bath at 55°C for 5 minutes to dissolve the pellet. 1ul (20 units) of M-MuLV reverse transcriptase was added to each sample and incubated in the water bath at 42°C for 1 hour.

2.6. Realtime PCR

Each sample condition was repeated three times for target of interest mRNA expression (ie. full length CYLD) in the realtime PCR. The following reaction mix for target of interest/housekeeping gene was used:

SyBr green dye (2x) (Applied Bioscience)	40ul
Primers 20pmol stock(both sense and anti-sense)	3.2ul
cDNA (from 500ng RNA)	8.0ul
H_20 (autoclaved)	28.8ul

In each 96 well, 25ul of reaction mix was allocated. iCycler Program (Biorad) was used to perform the realtime PCR. The mRNA levels of interest targets were normalized by HPRT levels and expressed as fold change relative to selected control as indicated in figures.

2.6.1. Real-time Primer List

Bcl-3
SP: TGCCCATTTACTCTACCCCGACGA
AS: CAGCGATGTGGAGAGGCGTGTC
Annealing temperature: 58.5˚C

sCYLD

SP: CTATTGGCAACTGGGATGGAAGG
AS: CACTTAAATAGCCCCCAAATGCTTC
Annealing temperature: 58.4˚C

FL-CYLD

SP: AGTCCACCCTTGCCCATCTCTT
AS: CATTCATCTTCCAGTTCCAGTCCA
Annealing temperature: 57.2˚C

A20

SP: AGTATCCCTGCCTCCTGTCACCA
AS: GCTGTTCTTCCGTTCTTCTTGCTT
Annealing temperature: 57.5˚C

HPRT

SP: TTAAGCAGTACAGCCCCAAAATG
AS: CAAACTTGTCTGGAACAAATCC
Annealing temperature: 57˚C

All primers listed were ordered from Invitrogen, desalted and the scale of synthesis was 25nmol. Sense and anti-sense primers were diluted together to a stock concentration of 20pmol/ul.

2.7. FACS staining

FACS staining was performed on the FACS Canto (BD Pharmingen) and analyzed with FlowJo software® (Treestar). In general, cells were stained with fluorescently labeled antibodies in FACS buffer (PBS/2% FCS 0.01% sodium azide) for at least 20 minutes and washed 2x with FACS buffer and then subjected to FACS analysis. The following antibodies were used where indicated in the results section:
CD11c PE-Cy7 (eBioscience), CD86 APC (eBioscience), MHC II FITC (BD Pharmingen), Ox40L PE (eBioscience), CD45.1 APC/PE (eBioscience), CD8 PE/APC (eBioscience), IFN-γ APC (eBioscience), PDL-2 FITC (eBioscience), Valpha TCR PE (eBioscience), CD90.1 APC/PE (eBioscience), Gp33 PE and NP396 PE tetramers were made in our laboratory by Dr. Hans-Christian Probst. In addition, CD3-PE (eBioscience), B220 PE (eBioscience), CD11b FITC (eBioscience), Gr-1 APC (eBioscience), Ly6-C/G APC (eBioscience) antibodies were used.

2.8. LCMV infection

WT, $CYLD^{ko}$, $CYLD^{ex7/8}$, $CYLD^{ex7/8fl/fl}$ x CD11c-Cre, were challenged i.v. with 100 Pfu of LCMV-WE. After 8 days, spleens were harvested and single cell suspensions were made. Cell were stained with GP33 tetramer-PE and CD8 APC or NP396 tetramer-PE and CD8 APC. Intracellular staining for IFN-γ cytokine was performed using 3 different immunodominant LCMV peptides, GP33, GP297, NP396 provided by Dr. Hans-Christian Probst in our laboratory.

2.9. DEC-205:OVA mediated tolerance

Recipient mice were given 10^6 adoptively transferred OT-I cells (CD45.1 congenic) and immunized with 20ug DEC-205:OVA (kindly provided by Dr. Karsten Mahnke, Heidelberg, Germany) in the footpad one day later. After 12 days, recipient mice were boosted with 50ug OVA protein (Sigma) resuspended in complete Freund's adjuvant (CFA) (Difco) subcutaneously and presence of OT-I cells in the spleen 3 days later was measured using Valpha PE and CD45.1 APC (both eBioscience).

2.10. T cell isolation

T cells from spleen and lymph nodes were isolated using MACS Pan T cell isolation Kit (Miltenyi Biotec, Germany) according to provided protocol instructions. Purified T cells

were always checked for purity by FACS analysis and only used when a greater than 85% purity was achieved. When purified T cells were used for *in vitro* purposes, IL-2 (mouse myeloma X63Ag8-653) was added to the culture media at 100ng/mL final concentration.

2.10.1. Treg culture

Tregs were isolated from the spleens of 5 WT mice and purified with the MACS Treg Kit (Miltenyi Biotech, Germany) according to manufacturer's instructions. Purified Tregs were cultured on 24-well plates pre-coated with 3ug/ml α-CD3 mAb (145-2C11) and 10ug/mL α-CD28 prior to cell plating. Cells were plated at $1.0x10^6$ cells/well in media in the presence of 200ng/mL IL-2 (mouse myeloma X63Ag8-653). On day 03 of culture, cells were split into new plates without any coated antibodies in media with IL-2. On day 6 of culture, Treg purity was confirmed by the intracellular staining of FoxP3 (BD Bioscience) and cell surface staining of CD4 and CD25 (eBioscience).

2.11. Western Blot

Lysates were run on 10% or 4-12% (gradient) SDS-page gels from NUPAGE® Novex Gel Systems (Invitrogen). The following antibodies were used, anti-Bcl-3 (Santa Cruz), anti-Tubulin (Santa Cruz), anti-p65/RelA (Santa Cruz), anti-CYLD antibodies were prepared by immunization of rabbits with recombinant CYLD fragments, anti-HDAC (Cell Signaling), anti-p105 (AbCam), anti-A20 (Santa Cruz), anti-TRAF2 (Santa Cruz), anti-FK2 (ubiquitin) (Biomol). Secondary HRP conjugated anti-rabbit, anti-mouse, anti-donkey antibodies were purchased from eBiosciences and Sigma Aldrich.

2.11.1. Whole cell lysates (WCL)

Whole cell lysates were prepared as follows: cells were washed 2x with PBS before the addition of lysis buffer:

Lysis Buffer:
Tris-HCl: 50mM pH 7.4 (as the base of the buffer)
NP-40 1%
Na-deoxycholate: 0.25%
EDTA: 1mM
PMSF: 1mM
Aprotinin, leupeptin, pepstatin: 1ug/mL each
Na_3V0_4: 1mM
NaF: 1 mM

Cell pellet was incubated with lysis buffer for 30 minutes with repeated centrifugation steps. After 30 minutes, the samples were spun down in a microcentrifuge at maximum speed and supernatant was kept and frozen at -80˚C. Samples (around 25ul aliquot) were stained with loading dye and 1ul of 1mM DTT stock solution, boiled for 5 minutes at 95˚C and then run on the SDS gel electrophoresis apparatus (Invitrogen). Protein determination was done using the Roti-Nanoquant protocol (Roth) or by using the NanoDrop apparatus (Thermo Scientific). In addition, when samples were not limiting, a separate SDS gel was run and a Coomassie Blue staining was performed to ascertain equal loading of protein.

2.11.2. Isolation of Cytoplasmic and Nuclear Cellular Fractions

Cytoplasmic and nuclear cellular fractions from BMDC preparations were prepared using the Nuclear Extract kit (Active Motif Europe, Belgium) according to manufacturer's instructions. Briefly, cells were lysed with hypotonic buffer, and after the addition of detergent, supernatant was collected after centrifugation and kept as the cytosolic fraction. The remaining pellet was lysed in complete lysis buffer provided by the manufacturer. After lysis of the pellet the supernatant was collected after centrifugation and stored in -80˚C as the nuclear fraction. Protein determination was done using the Roti-Nanoquant protocol (Roth) or by using the NanoDrop apparatus (Thermo Scientific).

2.12. Immunofluorescence

BMDCs differentiated over a period of 6 days as described above were harvested and plated onto Nunc Lab-Tek Chambers and stimulated as indicated in figures for specified timepoints. Samples were fixed with 2% para-formaldehyde (Sigma Aldrich) and stained for anti-Bcl-3 and anti-α-tubulin (Santa Cruz) or in other cases with anti-TRAF2 (Santa Cruz) and anti-FK2 (Biomol) according to standard protocols. Secondary IgG antibodies with fluorescent tags were purchased from Jackson Laboratories. Cells were counterstained with DAPI (Sigma Aldrich) and analyzed by confocal microscopy (Zeiss) with the help of Dr. Denis Strand.

2.13. Antigen Processing/ Antigen Phagocytosis

Differentiated unstimulated day06 BMDCs or 100ng/mL LPS overnight stimulated BMDCs were incubated with 100ug DQ-OVA (Invitrogen) for 10 minutes and washed

thoroughly to remove excess DQ-OVA. Pulse chase experiment of DQ-OVA processing in BMDCs was performed and measured in the FACS Calibur with controls serving as standards to assess fluroscence increase in the pulse chase samples. To determine the rate of phagocytosis, unstimulated differentiated day06 BMDCs were given 10mg/mL TMR dextran (Invitrogen) for 1 hour and the efficiency of phagocytosis was assessed by the fluorescence intensity of TMR in the FACS Calibur.

2.14. CFSE labeling

Purified T cells as described above were washed twice with PBS and resuspended in pre-warmed PBS with 2 uM CFSE and incubated at 37°C for 15 minutes. Cell concentrations were adjusted to 50.0 x 10^6 during the incubation period. After 15 minutes, cold media was added to the PBS solution. Cells were spun once and resuspended in pre-warmed media and incubated at 37°C for 20 min. Cells were then washed and added to culture conditions.

2.15. Intracellular Cytokine Staining

Spleen cell suspensions were restimulated in culture medium (IMDM/10% FCS with antibiotics and 2-ME) for 6hrs at 37°C with 1 uM of Gp33, NP396, or NP276 peptide and Golgi-stop (BD PharMingen, San Diego, CA). Cells were harvested, resuspended in PBS/2% FCS/azide, and surface-stained with PE-anti-CD8 (eBioscience). Following surface-staining, cells were fixed in Cytofix/Cytoperm solution (BD PharMingen) and then stained with APC-conjugated anti-mouse IFN-γ (eBioscience) diluted in 1X perm/wash solution (BD PharMingen). Samples were analyzed using a FACS Canto and FlowJo software® (Treestar).

2.16. BMDC transfection and NF-κB luciferase assay

The NF-κB-Reporter plasmid (pTATA-Luc$^+$; 3 x NFκB) provided by Ralf Marienfeld (Institute of Molecular Pathology, Wurzburg, Germany), comprises three copies of an NF-κB binding site from the murine c-Myb intronic enhancer[92]. BMDC were transfected with 10μg of the pTATA-Luc$^+$ using the Mouse Dendritic Cell Nucleofector Kit™ (VPA-1011; Amaxa, Cologne, Germany) according to the manufacturer´s instructions. To exclude differences in transfection-efficiency, cells were co-transfected with 300 ng of pRL-TK (Promega), which contains the thymidine kinase promoter region upstream of the *Renilla reniformis* luciferase. Cells were lysed after 24 hours, and

luciferase activity was measured by a luminometer (Berthold, Germany) using the dual luciferase reporter assay system from Promega. Data were standardized according to the *Renilla* luciferase activity.

2.17. S5a-GST as a bait to purify poly-ubiquitinated proteins

WT brain homogenates (30mg) were bound to either S5a-GST (provided by Dr. Martin Scheffner) or GST alone (500ug) and rotated overnight at 4°C and eluted either with thrombin, 10mM GSH, or SDS buffer. Eluates from S5a-GST and GST control were run on a SDS gradient gel (12%-4%) and blotted with anti-FK2 antibody. All reagents for GST tagged vectors, purification and isolation of polyUb proteins were used from the Glutathione S-transferase (GST) Gene Fusion System (GE Lifesciences).

2.18. Software Programs Used

FlowJo software® (Treestar)., GraphPad Prism, Cytokine-Flex CBA, Microsoft Word/Powerpoint, Canvas

2.19. Statistical analysis

Values are represented as means $\pm$ SEM analyzed using Student's t-test. Where appropriate some experiments were analyzed by ANOVA (one-way).

3. RESULTS

3.1. CYLD$^{ex7/8}$ BMDCs exhibit a hyper-reactive phenotype in terms of cell surface expression compared to CYLD^{ko} and WT counterparts

The exclusive and sole expression of the naturally occurring short splice variant of CYLD has profound effects on B cell maturation, survival and function[81]. It is clear that when sCYLD is exclusively and excessively over-expressed in B cells, it gives rise to a phenotype that exerts positive effects in B cells. This further points to the hypothesis that the deubiquitinating enzyme CYLD may have positive and negative regulatory capacity based on the expression of CYLD splice variants relative to the full length CYLD expression. In this thesis, the role of sCYLD was explored in the context of dendritic cells. As CYLD is a deubiquitinating enzyme, and DCs themselves heavily depend on the reversible process of ubiquitination and deubiquitination, the role of sCYLD over-expression as well as its complete absence (CYLD^{ko}) was compared in terms of *in vitro* DC functions and in *in vivo* animal models of immunization dependent on intact DC function.

The functions of DCs are complex and multi-faceted, but most importantly, result in the stimulation of antigen specific T cells which are able to recognize foreign antigens processed by DCs. However, in most tissues DCs are present in the so-called "immature" state and thus are unable to stimulate T cells. Although these DCs lack the requisite accessory signals for T cell activation, such as CD40, CD80 and CD86, they are extremely well equipped to capture Ags in peripheral sites. Once they have acquired and processed the foreign Ags, they migrate to the T cell areas of lymph nodes and the spleen, undergo maturation and stimulate an immune response.

An important advance in DC biology has been the ability to propagate *in vitro* large numbers of DCs using defined growth factors and thus allow for in depth studies on DC function without the limitation of DC numbers which would be the case if one studied endogenous DC populations. In this thesis work, bone marrow from CYLD$^{ex7/8}$, CYLD^{ko} and WT mice was obtained and BMDCs from the different mouse types were grown in the presence of GM-CSF as described in Materials and Methods. On day 06 of the differentiation process, BMDCs were subjected to stimulation with a variety of different TLR ligands including LPS, P_3Cys, Poly I:C and the co-stimulatory agonist CD40. CD11c+ cells were analyzed for the B7-2/CD86 cell surface expression and observed to be higher in the CYLD$^{ex7/8}$ BMDCs in all stimulation conditions including media

alone/unstimulated state (Figure 14A). The already higher expression of CD86 in CYLD$^{ex7/8}$ BMDCs in the unstimulated state is about 2 fold higher compared to CYLD^{ko} and WT counterparts. Furthermore, upon stimulation with the aforementioned stimuli, CYLD$^{ex7/8}$ CD11c+ cells further increase their CD86 expression so that ultimately CD86 cell surface expression is 2-4 fold higher than CYLD^{ko} or WT counterparts. Figure 14B shows that not only is the cell surface receptor CD86 expressed higher in CYLD$^{ex7/8}$ CD11c+ cells but also MHC II and Ox40L are higher expressed in the unstimulated state and upon stimulation with the TLR4 ligand LPS. A summary of over 10 BMDC preparations of CYLD$^{ex7/8}$, CYLD^{ko} and WT CD11c+ cells showed that sCYLD's sole and excessive over-expression leads to upregulated CD86, MHC II and Ox40L cell surface expression levels based on the MFI values obtained through FACS analysis (Figure 14C). This summary indicates that CYLD$^{ex7/8}$ BMDCs display a remarkable upregulation of B7, TNFR and MHC II receptors which could result in a hyper-reactive phenotype.

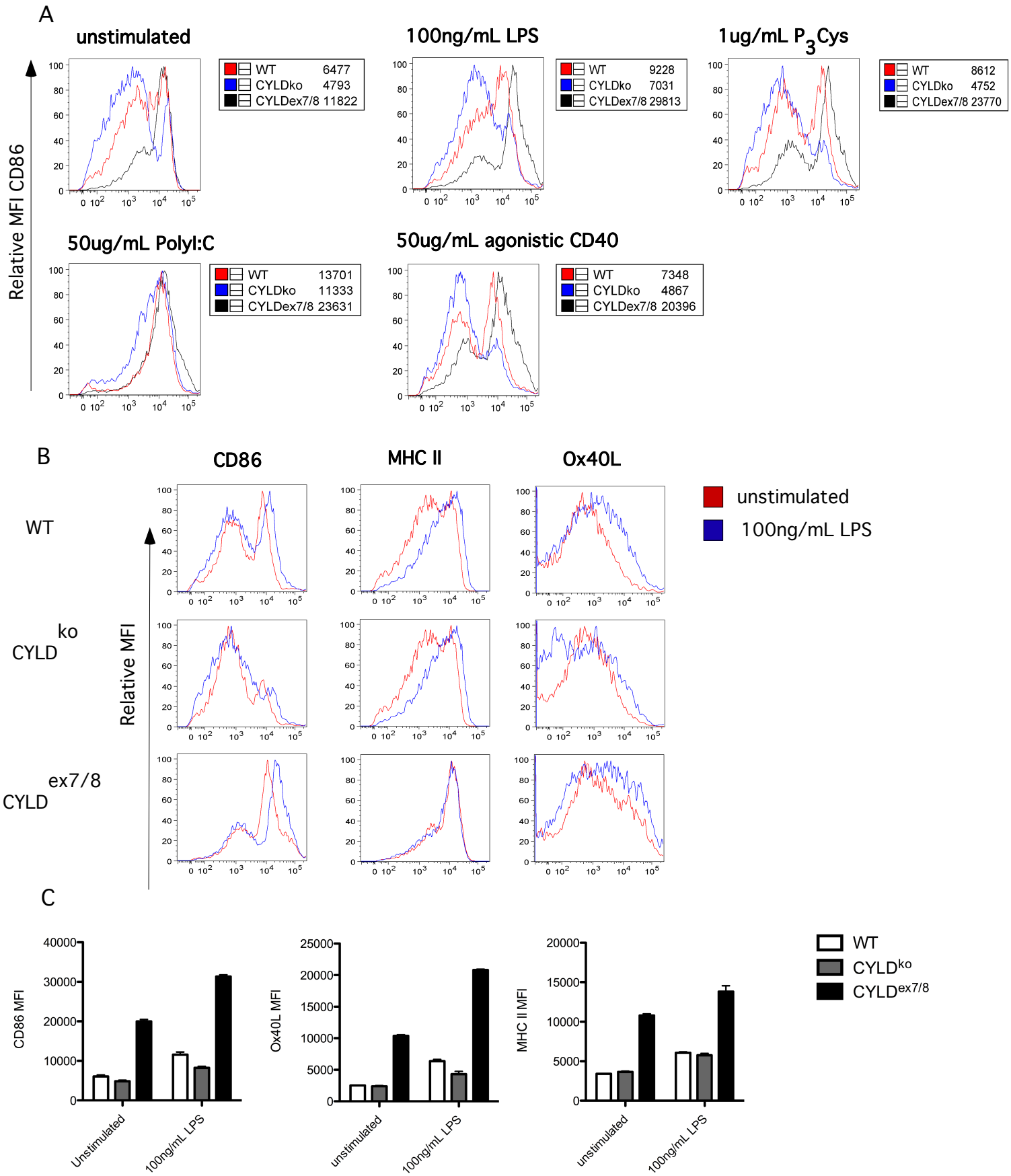

Figure 14. The effect of sCYLD overexpression in BMDCs confers a hyper-reactive phenotype

A) Mean fluorescence intensity values of CD86 cell surface receptor expression of CYLD$^{ex7/8}$ BMDCs compared to CYLD^{ko} and WT BMDCs unstimulated or stimulated with a variety of different TLR ligands. Samples were gated on CD11c+ve cell populations and then displayed for CD86 MFI on histogram. B) Analysis of CD86, MHC II and Ox40L cell surface expression in CYLD$^{ex7/8}$ BMDCs compared to WT and CYLD^{ko} upon stimulation with 100ng/mL LPS or left untreated. Samples were gated on live (PI negative) CD11c+ve cell population and then analyzed for cell surface expression of CD86, MHC II and Ox40L. C) Summary of MFI values of indicated cell surface receptor expression in CYLD$^{ex7/8}$, CYLD^{ko} and WT BMDCs. Representative of at least 10 different BMDCs preparations with triplicates.

3.2. Cytokine secretion in CYLD$^{ex7/8}$ CD11c+ve BMDCs reflects the high expression values of B7, TNF and MHC class II cell surface receptors.

Dendritic cells are a major source of many cytokines, namely, IFN-α, IL-1, IL-6, Il-7, IL-12 and IL-15 and also produce macrophage inflammatory protein (MIP1γ), all of which are important in the elicitation of a primary immune response.

IL-6 is a pleiotropic cytokine involved in immunity, liver regeneration and hemopoiesis. It is produced by macrophages, DCs, T cells, B cells, fibroblasts, endothelial cells, and keratinocytes. IL-6 exerts variable effects in innate and acquired immunity and its secretion is an early response to LPS and TNF-α. It is well documented in the literature that the expression of IL-6 by DCs drives a dominant pro-inflammatory response[93]. After 24hrs stimulation with the TLR4 or TLR2 ligand, LPS or P_3Cys respectively, CYLD$^{ex7/8}$ BMDCs secreted significantly higher amounts of IL-6 (Figure 15A left). Even after the removal of stimulus, in this case washing the stimulus away and replacing it with new fresh media, IL-6 secretion persisted even after 48 hrs in CYLD$^{ex7/8}$ BMDCs but not in WT or CYLD^{ko}(Figure 15A right). Investigation of other cytokines such as TNF-α and IL-10 using the CBA flex bead cytokine system showed that not only is IL-6 secretion also high using this method of detection but TNF-α levels are upregulated while IL-10 appears to be significantly decreased upon stimulation in CYLD$^{ex7/8}$ BMDCs (Figure 15B).

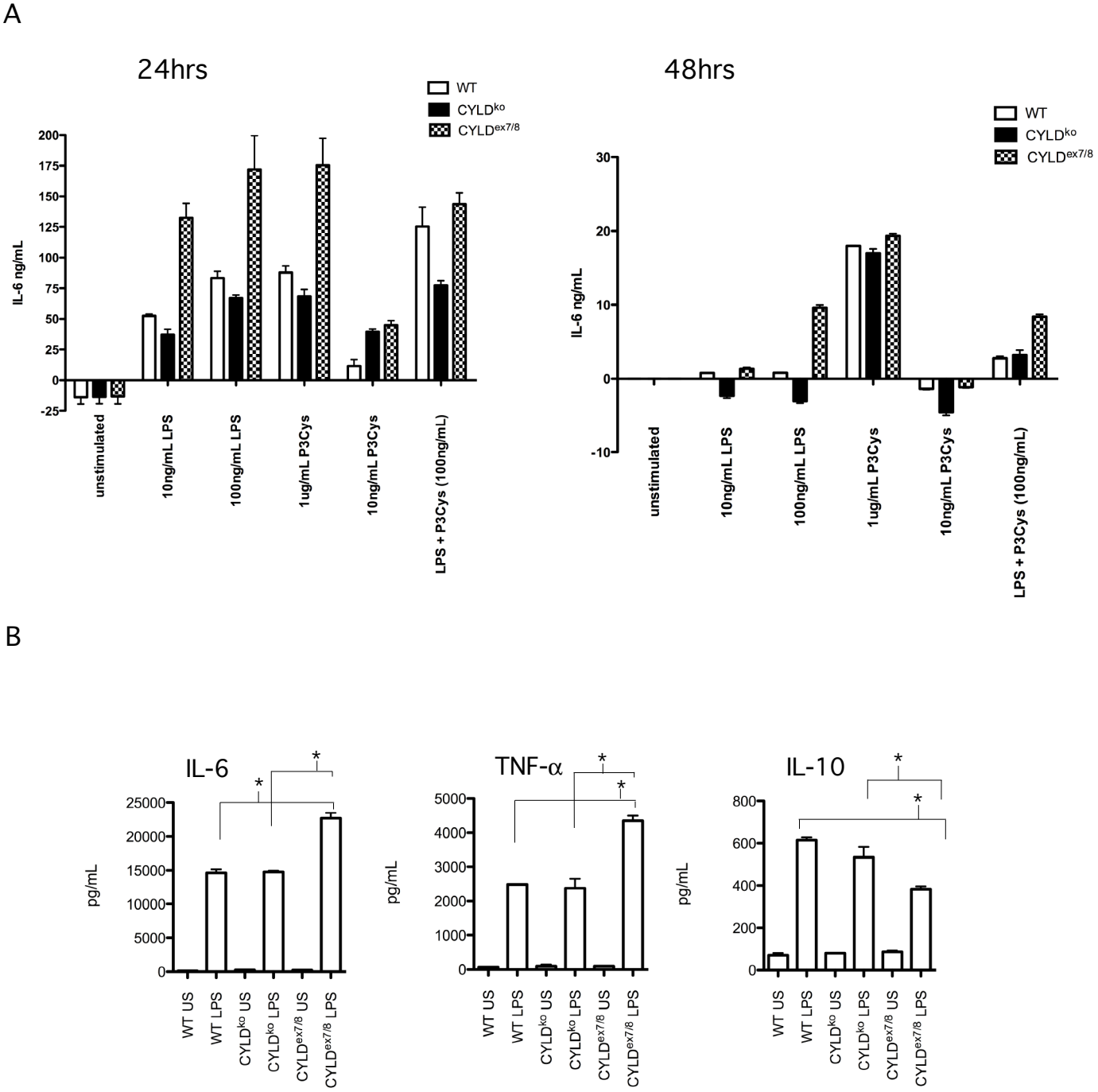

Figure 15. CYLD$^{ex7/8}$ BMDCs secrete significantly higher pro-inflammatory cytokines and lower anti-inflammatory cytokines

A) Left: BMDCs stimulated with LPS and/or P_3Cys overnight. Supernatants were collected and a standard sandwich ELISA for IL-6 was performed. Right: Removal of stimuli after 24hrs and replacement with fresh media. After another 24hrs, supernantant was collected and a standard sandwich ELISA for IL-6 was performed. Graphs are representative of at least 6 ELISA assays with triplicate samples. B) Supernatants from stimulated BMDCs cultures measured for IL-10, TNF-α and IL-6 cytokines with BD CBA Flex Set System after overnight LPS stimulation. * $p<0.05$ using t-test WT compared to CYLD$^{ex7/8}$ and CYLD^{ko} compared to CYLD$^{ex7/8}$ stimulated BMDCs. Values shown are means of triplicates with SEM and representative of 3 experiments with triplicates.

3.3. sCYLD confers a stimulatory phenotype in BMDCs which leads to increased T cell expansion and an enhanced T cell cytotoxicity activity

To understand if the hyper-reactive phenotype observed in $CYLD^{ex7/8}$ BMDCs in terms of cell surface expression (high CD86, MHC II and Ox40L expression) and high inflammatory cytokine secretion (IL-6, TNF-α) and low anti-inflammatory cytokine (IL-10) secretion coincides with *in vivo* BMDC activity, we utilized a model of *in vivo* DC immunization to address this question. The set up of the model (Figure 16A) proposes to address whether the BMDCs over-expressing sCYLD can affect the expansion of adoptively transferred T cells. Naïve St42 TCR specific cells were adoptively transferred to WT recipients and 2 days later overnight LPS stimulated GM-CSF differentiated BMDCs were peptide loaded with SGP peptide and injected i.p. to WT recipients. As illustrated in Figure 16B, T cell expansion in WT recipients stimulated with $CYLD^{ex7/8}$ BMDCs was about 2 fold higher compared to recipients stimulated with either WT or $CYLD^{ko}$ BMDCs. Expansion was highest and peaked at day 03 in the blood followed by subsequent contraction on day 05 (data not shown). The significant increase in T cell expansion prompted us to ask if T cell properties such as IFN-γ secretion differ in mice immunized with $CYLD^{ex7/8}$ BMDCs. Hence, recipient mice were sacrificed and splenocytes were re-stimulated with SGP peptide and intracellular IFN-γ cytokine staining was analyzed. WT recipient mice immunized with $CYLD^{ex7/8}$ BMDCs not only significantly expanded the Ag-specific T cell population but T cells secreted over 30% more IFN-γ cytokine compared to mice immunized with WT or $CYLD^{ko}$ BMDCs (Figure 16C).

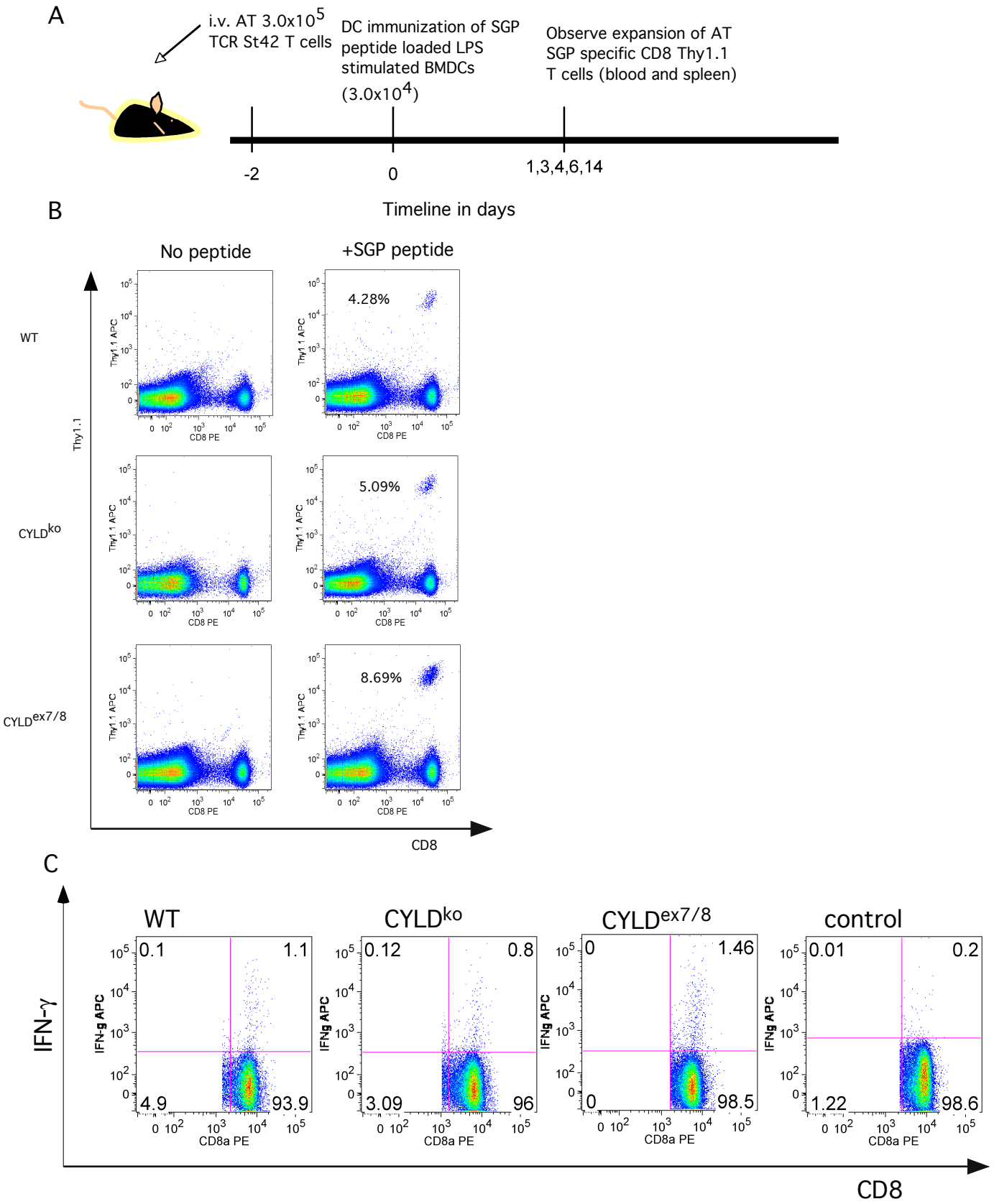

Figure 16. CYLD$^{ex7/8}$ BMDCs accentuate T cell expansion and T cell cytotoxic capacity in vivo

In vivo T cell expansion after DC immunization. A) Representative schematic model of in vivo DC immunization using the St42 transgenic model. B) 3.0x10^6 St42 T cells were transferred into WT recipients on day-2. WT recipients were then immunized with 3.0x10^5 SGP peptide-pulsed BMDCs on day 0 and expansion of T cells in the blood and spleen (not shown) using the congenic marker Thy1.1. B) Day 3 analysis of blood T cell expansion of adoptively transferred TCR tg (St42) donor splenocytes into WT recipient mice immunized with day 6 differentiated and LPS stimulated (WT), CYLD^{ko} or CYLD$^{ex7/8}$ BMDCs SGP peptide loaded and injected i.p. to recipient WT mice. Values are representative of n>4 mice per group and repeated three times. C) IFN-γ expression of splenocytes from WT recipients immunized with WT, CYLD^{ko} or CYLD$^{ex7/8}$ BMDCs. FACS dot plots were gated on Thy1.1 cells and then analyzed for CD8 T cells expressing IFN-γ after SGP peptide stimulation. Control indicates no SGP peptide re-stimulation. FACS plots are representative of 3 independent experiments with triplicates.

3.4. Investigation of DC function in CYLD$^{ex7/8}$ BMDCs

3.4.1. Processing and phagocytic activity in CYLD$^{ex7/8}$ BMDCs

DC main attributes can be simplified into three basic activities:

1. Ingestion
2. Processing
3. Presentation

To examine processing in BMDCs, a reagent called DQ-ovalbumin was used.

DQ-ovalbumin is a fluorogenic substrate for proteases. DQ ovalbumin is a self-quenched conjugate of ovalbumin that exhibits bright green fluorescence upon proteolytic degradation. A strong fluorescence quenching effect is observed when proteins are heavily labeled with BODIPY dyes such as DQ. DQ-ovalbumin is conjugated to the proprietary BODIPY FL dye, which exhibits bright, photostable and pH insensitive fluorescence in a pH range of 3-9. Upon hydrolysis of the DQ ovalbumin to single, dye-labeled peptides by proteases, this quenching is relieved, producing brightly fluorescent products (see figure 17). It is predicted the reagent should be quite efficiently internalized as OVA itself is internalized via the mannose receptor mediated endocytosis pathway. A caveat of DQ-ovalbumin is that experiments must be done quickly, repeated often and controls must be abundant to ensure reliability of results. Figure 17A shows the controls that must accompany experiments using DQ-ovalbumin. Day06 differentiated unstimulated BMDCs were cultured and incubated in the presence or absence of DQ-OVA. Several controls were made including no DQ-OVA, DQ-OVA with immediate cold PBS and a 10 minute incubation of DQ-OVA followed by cold PBS. Cold PBS prevents ingestion of DQ-OVA and stops processing. As can be seen in Figure 17A, all cell types responded similarly in the control phase of the DQ-ovalbumin experiment. Consequently, a pulse chase experiment was initialized after a 10 minute incubation phase of DQ-OVA with BMDCs. This was followed by a thorough washing step to get rid of DQ-OVA that was not ingested. Thereafter, the pulse chase was initialized. BMDCs were left in the incubator for the indicated timepoints followed by immediate FACS analysis to determine processing based on fluorescence (Figure 17B). It can be observed that WT BMDCs process DQ-ovalbumin most efficiently compared to the other BMDCs. CYLD$^{ex7/8}$ BMDCs are poor at processing and appear to get less efficient as time progresses. After overnight LPS stimulation, another pulse chase

experiment with DQ-OVA reveals once more the inadequate processing efficiency in CYLD$^{ex7/8}$ BMDCs (Figure 17C).

Left unstimulated, CYLD$^{ex7/8}$ BMDCs are able to process to some degree, however upon overnight LPS stimulation, the processing capacity is severely diminished. This was also the case with CYLD^{ko} BMDCs but only after LPS stimulation. To assess whether the differences in processing can be attributed to a difference in phagocytosis of antigen, TMR-dextran was used. Dextrans are hydrophilic polysaccharides synthesized by *Leuconostoc* bacteria and are characterized by their high molecular weight, good water solubility, low toxicity and relative inertness. Moreover, their biologically uncommon α-1,6-polyglucose linkages are resistant to cleavage by most endogenous cellular glycosidases and therefore dextran conjugates are ideal markers for the uptake of exogenous materials by phagocytotic and endocytic pathways. However, phagocytotic activity appears to be similar in all BMDC cell types (Figure 17C). WT, CYLD^{ko} and CYLD$^{ex7/8}$ appear to have roughly ingested the same amount of TMR dextran based on the fluorescence observed in the FACS. In fact, CYLD$^{ex7/8}$ BMDCs had a slightly higher TMR dextran ingestion in the FACS analysis but after 3 independent experiments this was determined to be nonsignificant (data not shown). Therefore, unstimulated day06 differentiated BMDCs "ate" TMR dextran to the same degree and as such this finding does not correlate to the differences seen in CYLD$^{ex7/8}$ BMDCs in terms of DQ-OVA processing.

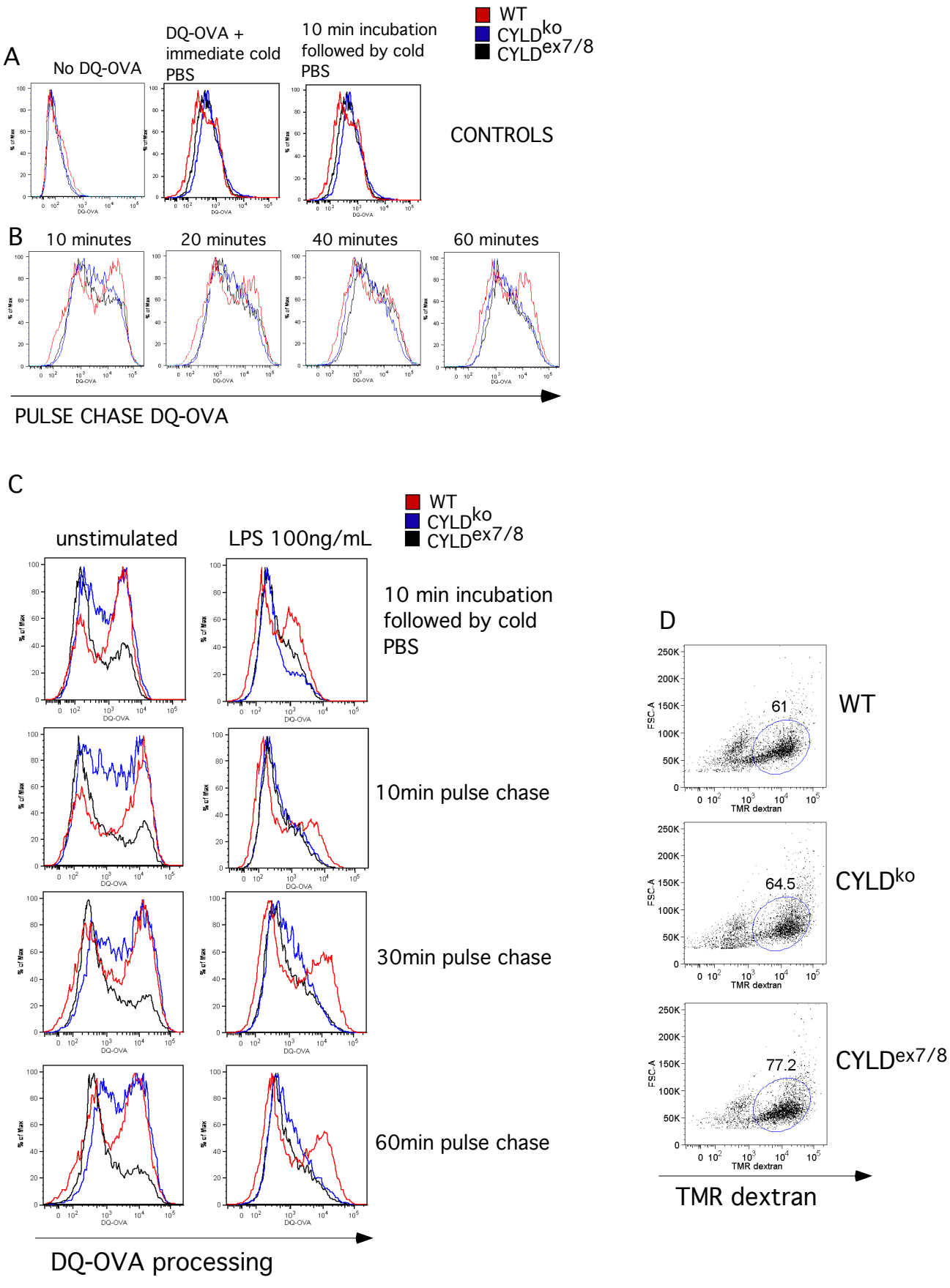

Figure 17. The capacity to process antigen in CYLD$^{ex7/8}$ BMDCs is altered but not the capacity to phagocytose
Fluorescent reagents to visualize processing and phagocytosis. A) Day06 unstimulated differentiated BMDCs are used to control the DQ-OVA fluorescence in the FACS and assess stability of DQ-OVA. BMDCs were incubated together with 100ug DQ-OVA or its absence followed either immediately by cold PBS or an incubation of 10 min followed by cold PBS. B) Differentiated unstimulated day06 BMDCs were incubated with 100ug DQ-OVA for 10 minutes and washed thoroughly to remove excess DQ-OVA. Pulse chase experiment of DQ-OVA processing in BMDCs at indicated timepoints. Processing was measured in the FACS Calibur with controls in (A) serving as standards to assess fluroscence increase. C) Unstimulated day07 or overnight LPS stimulated BMDCs were cultured with 100ug DQ-OVA and processing was determined through a pulse chase analysis at indicated timepoints. D) To determine the rate of phacocytosis, unstimulated differentiated day06 BMDCs were given 10mg/mL TMR dextran for 1 hour and the efficiency of phagocytosis was assessed by the fluorescence intensity of TMR in the FACS Calibur. Representative FACS plots for DQ-OVA processing and phagocytosis are from 3 independent experiments with triplicates.

3.4.2. NH_4Cl and chloroquine markedly inhibited the processing of DQ-OVA in BMDCs

Both NH_4Cl and chloroquine markedly inhibited the processing and presentation of DQ-OVA in BMDCs. NH_4Cl and chloroquine are both lysosomotropic agents, meaning that they inhibit lysosomal function. The acidotropic antigen-processing inhibitor chloroquine is used often to determine whether processing of particular determinants from an antigen requires acidic intracellular compartments. NH_4Cl is reported to inhibit lysosomal movements and phagosome-lysomal fusion [94]. To determine if DQ-OVA processing can be ceased with these lysosomotropic agents, day 06 differentiated but unstimulated BMDCs were incubated with 20mM NH_4Cl + 100μM chloroquine 30 minutes prior to incubation with 100ng/mL DQ-OVA. DQ-OVA was incubated for 10 minutes and thoroughly washed thereafterwards to initiate a pulse chase of ingested DQ-OVA over a time period of 60 minutes. In Figure 18 WT BMDCs process DQ-OVA to the highest efficiency as evidenced by the high fluorescence intensity observed in the histogram plot. Upon prior administration of NH_4Cl + chloroquine, processing of DQ-OVA is reduced. $CYLD^{ex7/8}$ BMDC's DQ-OVA processing is already restricted without any addition of inhibitors. However, upon NH_4Cl + chloroquine administration, DQ-OVA processing is further restrained. This phenomenon is also observed in $CYLD^{ko}$ BMDCs which signifies that changes in CYLD expression or its absence in DCs attenuates antigen processing. WT BMDCs when incubated prior with inhibitors, process DQ-OVA to almost the same extent as $CYLD^{ko}$ and $CYLD^{ex7/8}$ BMDCs that have not been exposed to any inhibitor. This highlights the importance of lysosomal function in DQ-OVA processing and may point to CYLD having a role in an intact lysomosal processing function.

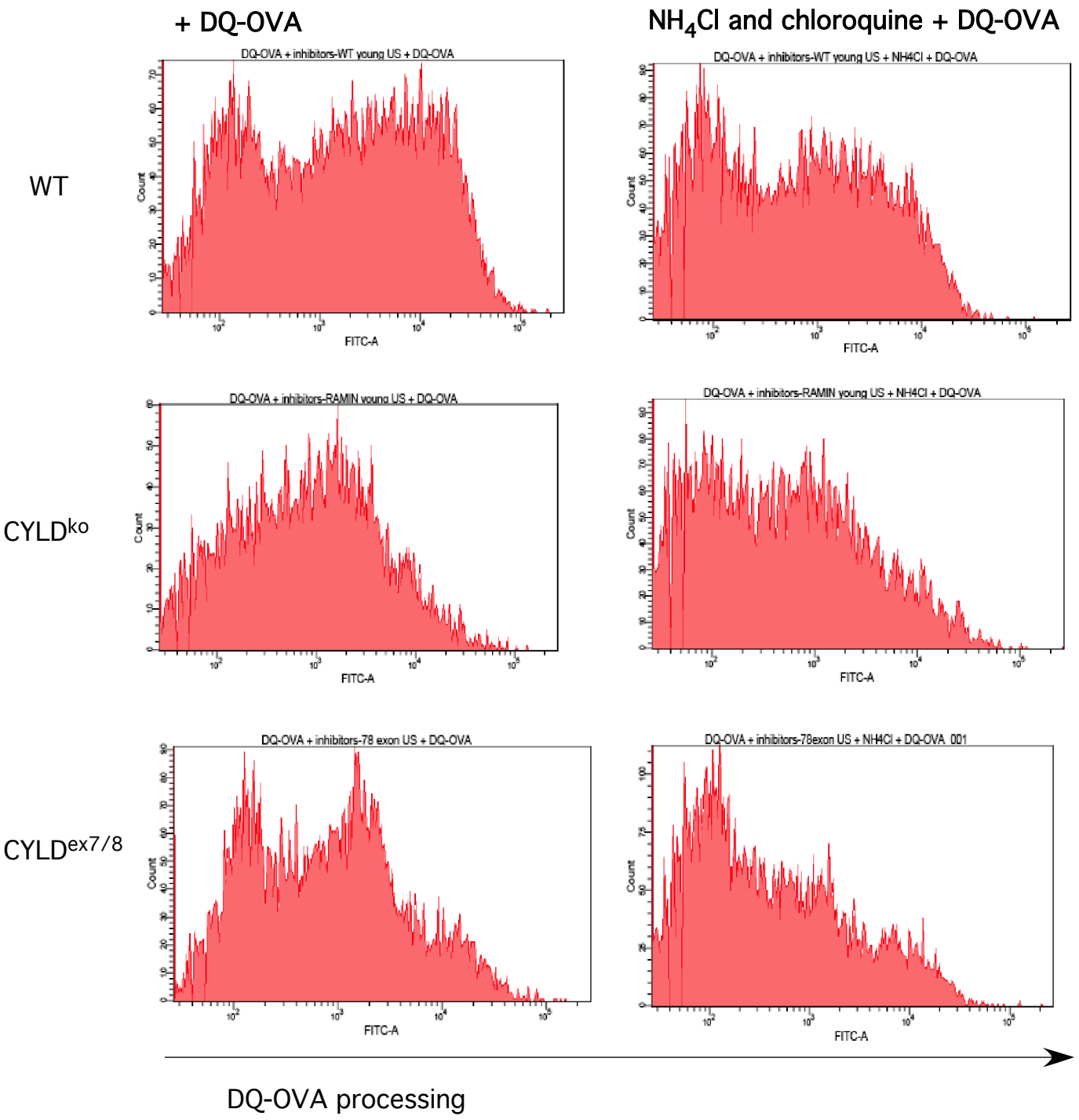

Figure 18. Addition of NH_4Cl + chloroquine, antigen processing inhibitors, attenuates DQ-OVA processing in WT BMDCs to a reduced level similar to $CYLD^{ex7/8}$ BMDC processing

Inhibition of lysosomal function decreases the efficiency of DQ-OVA processing. Differentiated day06 unstimulated BMDCs were incubated with or without the presence of 20mM NH_4Cl and 100uM chloroquine 30 minutes prior to the addition of 100ug of DQ-OVA. DQ-OVA was incubated with BMDCs for 10 minutes, washed thoroughly and a pulse chase to assess processing was performed after 60 minutes. DQ-OVA processing was determined by FACS analysis of DQ fluorescence intensity. FACS plots are representative of 2 independent experiments with triplicates.

3.4.3. Investigating MHC class II presentation efficiency confirms the hyper-reactive phenotye in CYLD$^{ex7/8}$ BMDCs when co-cultured with TCR Ag specific OT-II T cells

The processing of exogenous antigens occurs in the phagosomal/endosomal compartments as a result of the action of proteases that partially digest antigens along the internalization route. The same compartments contain MHC class II molecules. Relatively large antigen fragments (several tens of amino acids) are loaded on MHC class II molecules after degradation of the associated Ii chain. These large fragments are then further processed on the MHC class II molecules into 10-20 amino acid peptides. The peptide-loaded MHC class II molecules are translocated to the cell surface there they are recognized by CD4+ T cells. To understand whether the presentation capacity in CYLD mutated BMDCs is affected, unstimulated day 06 differentiated BMDCs were incubated with DQ-OVA for 1 hour and then co-cultured with CFSE purified OT-II T cells for a duration of up to 7 days. Presentation efficiency was measured by OT-II proliferation and division which was observed by the decrease in relative fluorescence intensity of the CFSE dye by half after each round of cell division. To take the inefficient processing capacity of CYLD mutated BMDCs out of the picture, BMDCs were peptide loaded with $OVA_{323-339}$ class II restricted peptide and co-cultured together with OT-II (class II restricted) CFSE labeled T cells. Figure 19 shows the representative FACS data of OT-II expansion and division when co-cultured with WT, CYLD^{ko} or CYLD$^{ex7/8}$ BMDCs on day 3 (peak of the response). BMDCS were either incubated with DQ-OVA or peptide loaded with $OVA_{323-339}$ peptide. Control indicates incubation with BMDCs and CFSE labeled OT-II T cells only. WT BMDCs efficiently process DQ-OVA and hence present the OVA class II restricted peptide to OT-II cells in culture. Consequently, OT-II T cells expand and divide. As can be seen in Figure 19, OT-II T cells cultured with DQ-OVA-exposed WT BMDCs divide 3 divisions and the percentage of dividing cells is 56.9%. When WT BMDCs do not need to process (ie. when peptide loaded with class II restricted peptide), the division of OT-II T cells appears to be minimally affected with 42.1% OT-II T cells dividing and 2 divisions observed in the CFSE histogram. Co-culture of OT-II T cells with CYLD$^{ex7/8}$ BMDCs appears to promote division. In this experimental setup, the processing of DQ-OVA did not affect the ability of CYLD$^{ex7/8}$ BMDCs to promote the division of OT-II T cells. As can be observed in Figure 19, 66.1% of OT-II T cells divided and up to 3 divisions were observed in the CFSE histogram. When CYLD$^{ex7/8}$ BMDCs do not need to process the antigen and are peptide

loaded with the OT-II peptide $OVA_{323-339}$, the number of cells dividing is 59.8% and up to 4 divisions are observed. This result indicates that the presentation capacity of $CYLD^{ex7/8}$ does not have an effect on the ability to interact and promote the division of antigen specific T cells. $CYLD^{ko}$ BMDCs stimulate OT-II T cells to the same degree whether processing is involved or not. However, the degree of OT-II T cells in the dividing state appears to be lower. Of course, this experiment does not reveal the exact nature of the presentation capability of $CYLD^{ex7/8}$ BMDCs, but its indirect approach indicates that although processing may be altered (Figure 17) the presentation and ability to stimulate Ag-specific T cells is not. The discrepancy between processing and this indirect approach to analyzing presentation may lie in the fact that $CYLD^{ex7/8}$ BMDCs express higher levels of CD86, MHC II and Ox40L which may tilt the balance towards higher activation of T cells regardless of the level of processing and/or presentation capacity.

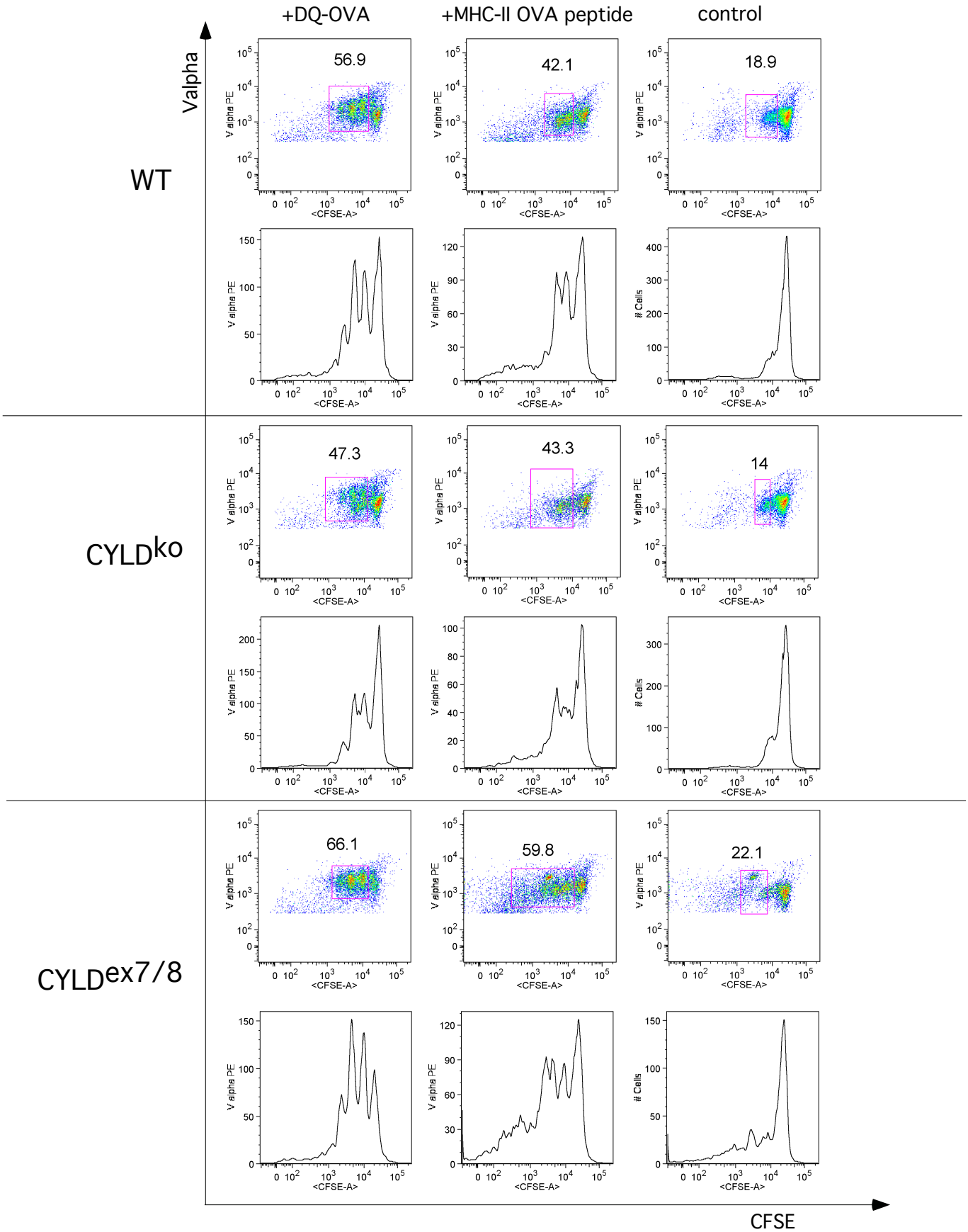

Figure 19. The altered capacity to process antigens in CYLD$^{ex7/8}$ BMDCs does not hinder T cell division

1.0x10^5 unstimulated day06 differentiated WT, CYLD^{ko} or CYLD$^{ex7/8}$ BMDCs were incubated with 100ug DQ-OVA for 60 minutes or peptide loaded with 1ug/mL OVA$_{323-339}$ class II restricted peptide and then co-cultured with 1.0x10^6 CFSE labeled purified OT-II T cells in media containing 100ng/mL IL-2. As a control BMDCs with no DQ-OVA exposure and no peptide loading were also co-cultured with CFSE labeled OT-II T cells. Figure is representative of day 03 timepoint which is the peak of expansion in this experimental setup. Dot plots show gated population which represents the CFSE Valpha positive population (OT-II T cells) dividing. Underneath, histogram plots display the number of divisions per CFSE decrease in relative intensity by half. Figure is representative of 2 independent experiments with triplicates.

3.5. PDL-2 expression in CYLD$^{ex7/8}$ BMDCs

To explore if there may be other factors that contribute to the hyper-reactive phenotype of CYLD$^{ex7/8}$ BMDCs, the molecules responsible for inhibition of immune responses were studied. The candidates in this category include B7H3, B7H4 and PDL-2 (otherwise known as B7DC). There was no direct evidence that either B7H3 or B7H4 are differently expressed in CYLD$^{ex7/8}$ BMDCs. PDL-2 is known to bind to PD-1 on T cell and is a putative negative regulator for immune function [95]. Negative regulation is critical for homeostasis of the immune system and PDL-2 has been previously shown to reduce T cell proliferation. When CYLD$^{ex7/8}$ differentiated BMDCs were stimulated overnight with LPS and stained with PDL-2 antibody, the percentage of BMDCs expressing PDL-2 was significantly lower compared to WT and CYLD^{ko} BMDCs (Figure 20). FACS analysis revealed that only half of the BMDC CD11c+ population expressed high levels of PDL-2. The majority of WT and CYLD^{ko} BMDCs gated on a CD11c+ population expressed high levels of PDL-2 upon LPS stimulation. This result suggests that the lower PDL-2 expression correlates well to the hyper-reactive phenotype already observed in Figure 14.

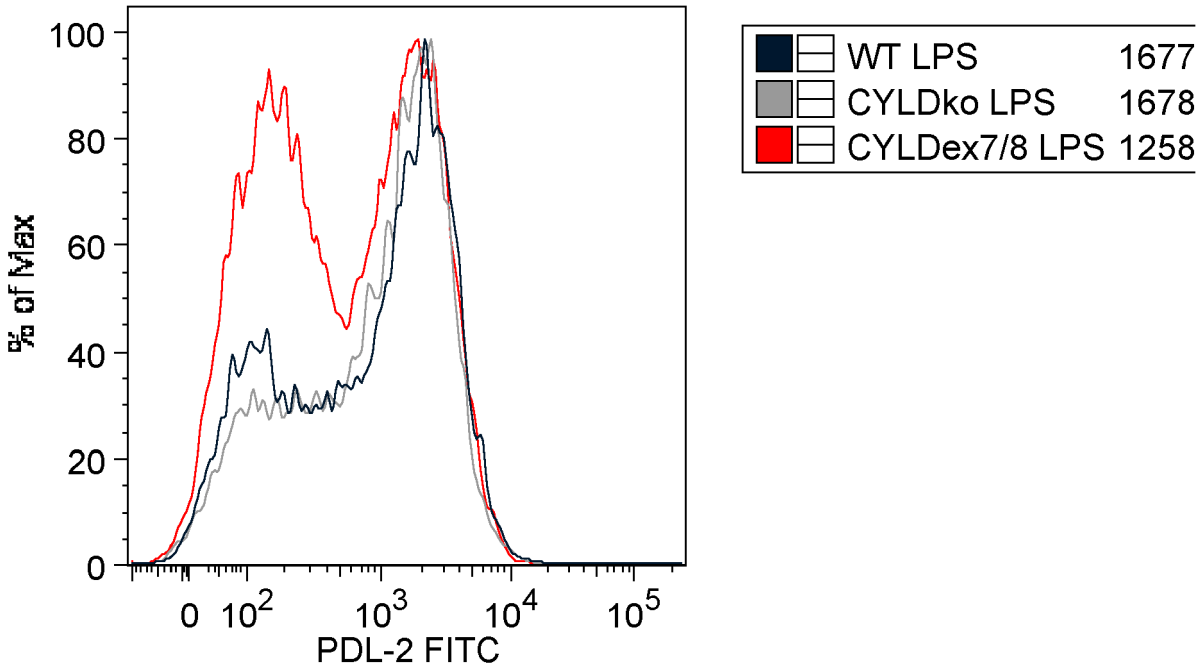

Figure 20. The inhibitory receptor PDL-2 expression is lower in CYLD$^{ex7/8}$ BMDCs
Day06 differentiated BMDCs were stimulated overnight with 100ng/mL LPS. BMDCs were stained with CD11c PE-Cy7 and PDL-2 FITC. FACS analysis was performed. Histogram plot displays the PDL-2 FITC histogram for all 3 BMDC types gated on live (PI negative) CD11c positive population. MFI values of PDL-2 are indicated for each BMDC type. Figure is representative of 2 independent BMDC preparations.

3.6. Treg interaction with CYLD$^{ex7/8}$ BMDCs does not result in suppression

BMDCs cultured from CYLD$^{ex7/8}$ mice display a hyper-reactive phenotype and this beckons the question as to whether CYLD$^{ex7/8}$ BMDCs can be suppressed by T regulatory cells (Treg). DCs display multiple interactions with Tregs including the ability of Tregs to potentially suppress effector T cell responses in part by down-regulating the ability of less mature DCs to effectively present antigen[96]. To explore whether Tregs can suppress the hyper-reactive phenotype of CYLD$^{ex7/8}$ BMDCs, Tregs were co-cultured with day 06 differentiated immature BMDCs (WT or CYLD$^{ex7/8}$) and IL-6 secretion, CD86 and MHC class II expression was assayed. Co-culture with FoxP3+ CD25+ CD4+ Tregs (>95% purity) and BMDCs (WT or CYLD$^{ex7/8}$, >80% CD11c+ purity) with the indicated stimulation conditions (CD3/LPS, LPS, CD3 or media alone) was assayed for the secretion of IL-6 after 24 hours. As indicated in Figure 21A, WT BMDCs co-cultured with Tregs showed relatively lower secretion of IL-6 upon α-CD3 stimulation compared to LPS alone stimulation. This indicates that the suppressive function of Tregs was initiated upon α-CD3 treatment. Simultaneous stimulation with LPS and α-CD3 resulted in IL-6 secretion that was lower than LPS stimulation alone but higher than with α-CD3 which demonstrates the compromise between two opposing stimuli. CYLD$^{ex7/8}$ BMDCs however, were largely ignorant of Treg suppression as evidenced by the persistent secretion of IL-6 even upon exposure to α-CD3. Indeed, there appeared to be a reduction of IL-6 secretion after α-CD3 stimulation of Tregs, however, IL-6 secretion was significantly higher in CYLD$^{ex7/8}$ BMDCs than in the WT BMDC + Treg scenario (Figure 21A). Furthermore, as indicated in previous figures (Figure 15A,B), IL-6 secretion in CYLD$^{ex7/8}$ BMDCs is higher at a basal unstimulated level compared to WT and CYLD^{ko} BMDCs. To understand if the cell surface expression of the B7 family (CD86) and MHC class II receptors can be affected by the introduction of Tregs to the culture we explored the cell surface expression patterns in the FACS. In the DC alone setup, CD86 cell surface expression is higher in CYLD$^{ex7/8}$ BMDCs compared to WT, as expected. Upon introduction of Tregs to the culture, the high CD86 expressing population in WT BMDCs (percentage shown in gate Figure 21B) diminishes substantially (60% decrease in high CD86 expressing population) upon α-CD3 stimulation. CYLD$^{ex7/8}$ BMDCs do not respond equally to the co-presence of Tregs stimulated with α-CD3; the response is half of WT BMDCs. Only a 30% reduction in high CD86 expressing population was observed upon introduction of α-CD3 stimulated

Tregs. Furthermore, a clear distinct high CD86 expressing population is still observed in the $CYLD^{ex7/8}$ BMDCs in all stimulation conditions. Upon investigation of MHC class II receptor expression levels, again, $CYLD^{ex7/8}$ BMDCs had a substantially higher proportion of cells expressing high MHC II (Figure 21C). WT BMDCS, when co-cultured in the presence of Tregs, downregulated their MHC class II receptor, especially when α-CD3 was added to the culture. This resulted in only 39% of the WT BMDCs expressing high MHC class II. On the other hand, $CYLD^{ex7/8}$ BMDCs appeared to be ignorant to the presence of Tregs in the culture, as the high MHC class II population changed little in all stimulation conditions in the co-culture.

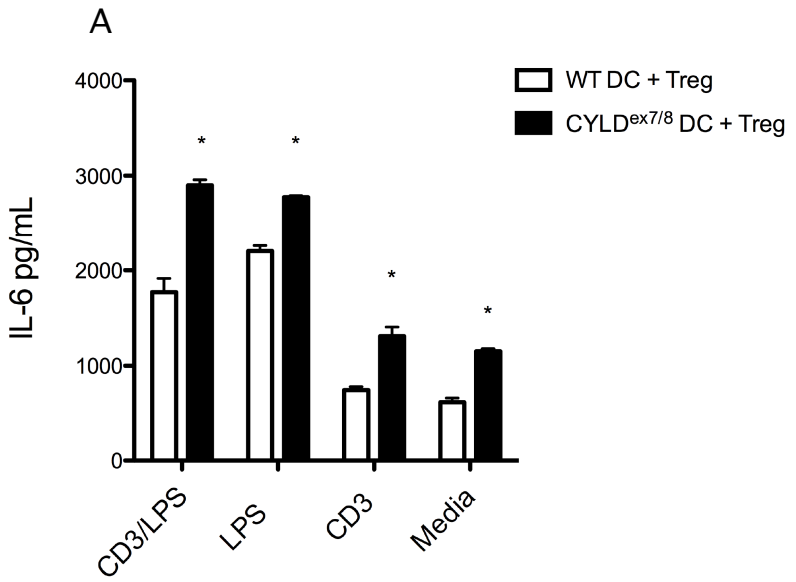

Figure 21. CYLD$^{ex7/8}$ BMDC interaction with Tregs further confirms a hyper-reactive phenotype in vitro BMDC interaction with Tregs assayed by IL-6 cytokine secretion and changes in CD86 and MHC class II cell surface expression on BMDCs

A) IL-6 ELISA from 24hour supernatants of 1.0x10^5 BMDCs (WT or CYLD$^{ex7/8}$) co-cultured with 5.0x10^5 FoxP3+ CD25+ CD4+ Tregs. Stimulation conditions are indicated on the x-axis. * indicates $p<0.05$ using T-test to grouped stimulation condition between WT BMDC versus CYLD$^{ex7/8}$ BMDC co-culture with Tregs. B) FACS histogram plots showing changes in high CD86 expressing population (gated with percentages indicated) in CD11c+ BMDCs. Stimulation conditions are indicated. C) FACS histogram plots showing changes in high MHC class II expressing population (gated with percentages indicated) in CD11c+ BMDCs. Stimulation conditions are indicated. This figure is representative of 2 independent experiments with triplicates. I gratefully acknowledge the co-operation of Sonja Reißig, a PhD. student in the Waisman lab who purified and cultured the Tregs. In addition she was of invaluable help in coordinating this experimental setup.

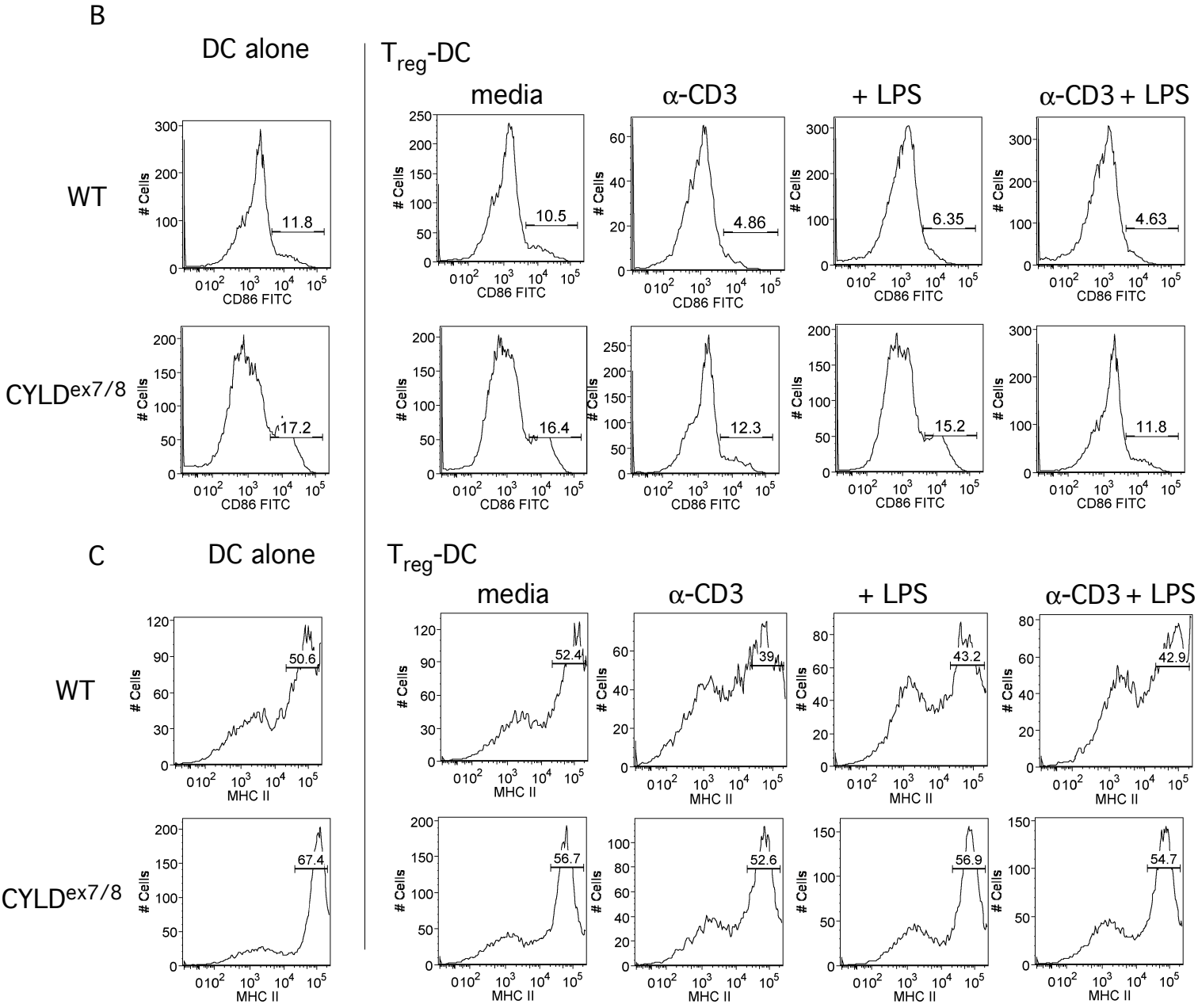

3.7. Ubiquitination and CYLD targets

Protein modification by ubiquitination plays a major role in many biological processes including signaling, cell cycle progression and apoptosis. Ubiquitin (Ub) is a highly conserved protein composed of 76 amino acids (aa) that can be covalently attached to lysine (K) residues of target proteins. CYLD is mainly responsible for deubiquitinating proteins modified by ubiquitin. More specifically, CYLD deubiquitinates proteins which are modified by lysine 63 (K^{63}) linked Ub chains such as mediators involved in the NF-κB pathways including NEMO and TRAF2 (reviewed in [35]).

To explore the impact of ubiquitin levels in CYLD mutated BMDCs, FK2 antibody against Ub was used. FK2 detects mono and polyubiquitin, but not free Ub and is able to detect K^{29}, K^{48} and K^{63} Ub linked chains equally well. In western blot analysis, an increase in ubiquitination in both $CYLD^{ko}$ and $CYLD^{ex7/8}$ BMDC lysates compared to WT control was observed (Figure 22A). The differences in quantity of ubiquitination also corresponded to accumulation of Ub aggregates as visualized by the formation of Dendritic Cell Aggresome Like Induced Structures (DALIS), in this case, however, only in the $CYLD^{ex7/8}$ BMDCs (Figure 22B). These structures, which have been previously related to antigen processing events by incorporating DRiPs (defective ribosomal proteins) and prolonging their half life, are only formed during DC activation[30, 31]. Surprisingly, we observed DALIS formation already in unstimulated $CYLD^{ex7/8}$ BMDCs (Figure 22B) whereas WT and $CYLD^{ko}$ BMDCs displayed DALIS formation after LPS-induced maturation, as expected. This observation suggests once again that $CYLD^{ex7/8}$ BMDCs have an increased tendency towards activation which is further supported by the cell surface expression patterns and cytokine secretion profile in $CYLD^{ex7/8}$ BMDCs (figure14&15) and their ability to activate T cell expansion *in vivo* (figure 16).

The distinct effect of increased protein ubiquitination and the formation of Ub-protein aggregates accompanied by the enhanced maturation lead us to question whether any components of the NF-κB pathway regulated by ubiquitination are affected in $CYLD^{ex7/8}$ BMDCs. Strikingly, an increase in the protein levels of the TNF receptor-associated factor 2 (TRAF2) was found in the $CYLD^{ex7/8}$ BMDC lysates using Western Blot analysis (Figure 22C). This observation is rather interesting as activation of NF-κB is mediated by Ub^{K63} linkage of TRAF2 and it is reversed by the deubiquitinase CYLD which removes K^{63} linked polyUb chains from TRAF2. $CYLD^{ex7/8}$ BMDCs expressed higher levels of TRAF2 compared to WT and $CYLD^{ko}$ both in the unstimulated and LPS stimulated

condition (Figure 22C). The implications of this finding are difficult to interpret without investigating the ubiquitin state of TRAF2. Day 06 differentiated BMDCs were grown in a Lab-TEK Chamber Slide System and stimulated overnight with LPS or left untreated. BMDCs were then stained for FK2 (Ub), TRAF2 and DAPI in an attempt to visualize whether the TRAF2 protein is more or less ubiquitinated in the different BMDCs. There appeared to be not only brighter TRAF2 expression in $CYLD^{ex7/8}$ unstimulated BMDCs but also a slight increase in the occurrence of FK2 and TRAF2 colocalization, indicating ubiquitination of TRAF2 (Figure 22D). Upon stimulation, there was an increase in the colocalization of TRAF2 and FK2 demonstrated by the yellow colourization in some cells, but this observation was present in all 3 BMDC types. Hence, without an immunoprecipitation of TRAF2 from the BMDCS and then the subsequent FK2 blot, it is difficult to interpet this result. However, the results suggest that there are differences in the ubiquitination patterns in $CYLD^{ex7/8}$ BMDCs and innovative techniques need to be employed to discover the targets of ubiquitination in the CYLD mutated BMDCs (see figure 29).

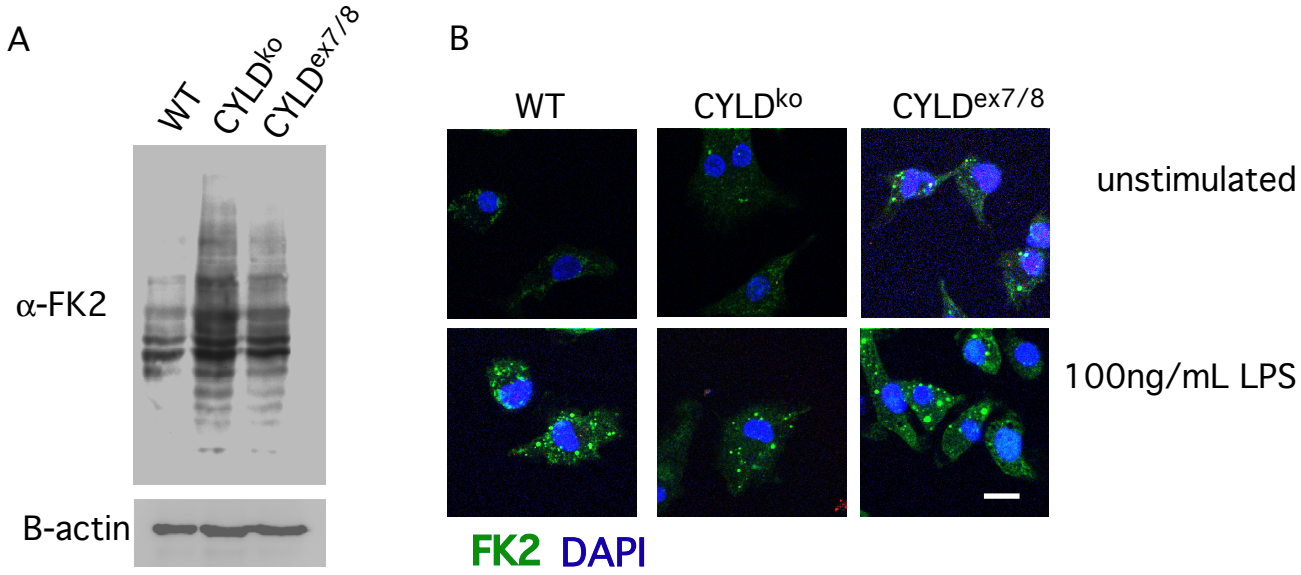

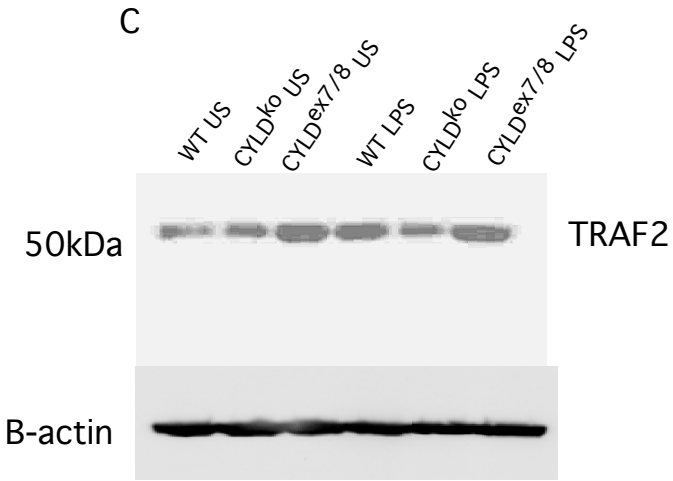

Figure 22. Differences in ubiquitination patterns and protein targets of ubiquitin modification may account for the phenotype observed in CYLD$^{ex7/8}$ BMDCs
Ubiquitination patterns and ubiquitin targets in BMDCs. A) Western blot of LPS stimulated BMDC lysates blotted with FK2 antibody. 25ug of lysate was loaded per lane. B–actin was used as a loading control. B) Microscope images of immunohistochemical staining of BMDCs for FK2 (green) and DAPI (blue) analyzed by confocal microscopy (Zeiss). Bar represents 5uM. C) Western blot of unstimulated and overnight LPS stimulated BMDCs blotted against TRAF2. 25ug of lysate was loaded per lane. B-actin was used as a loading control. D) Microscope images of immunohistochemical staining of BMDCs for FK2 (green), TRAF2 (red) and DAPI (blue) analyzed by confocal microscopy (Zeiss). Bar represents 10uM.
Western blots and microscope images are representative of 2 independent experiments.

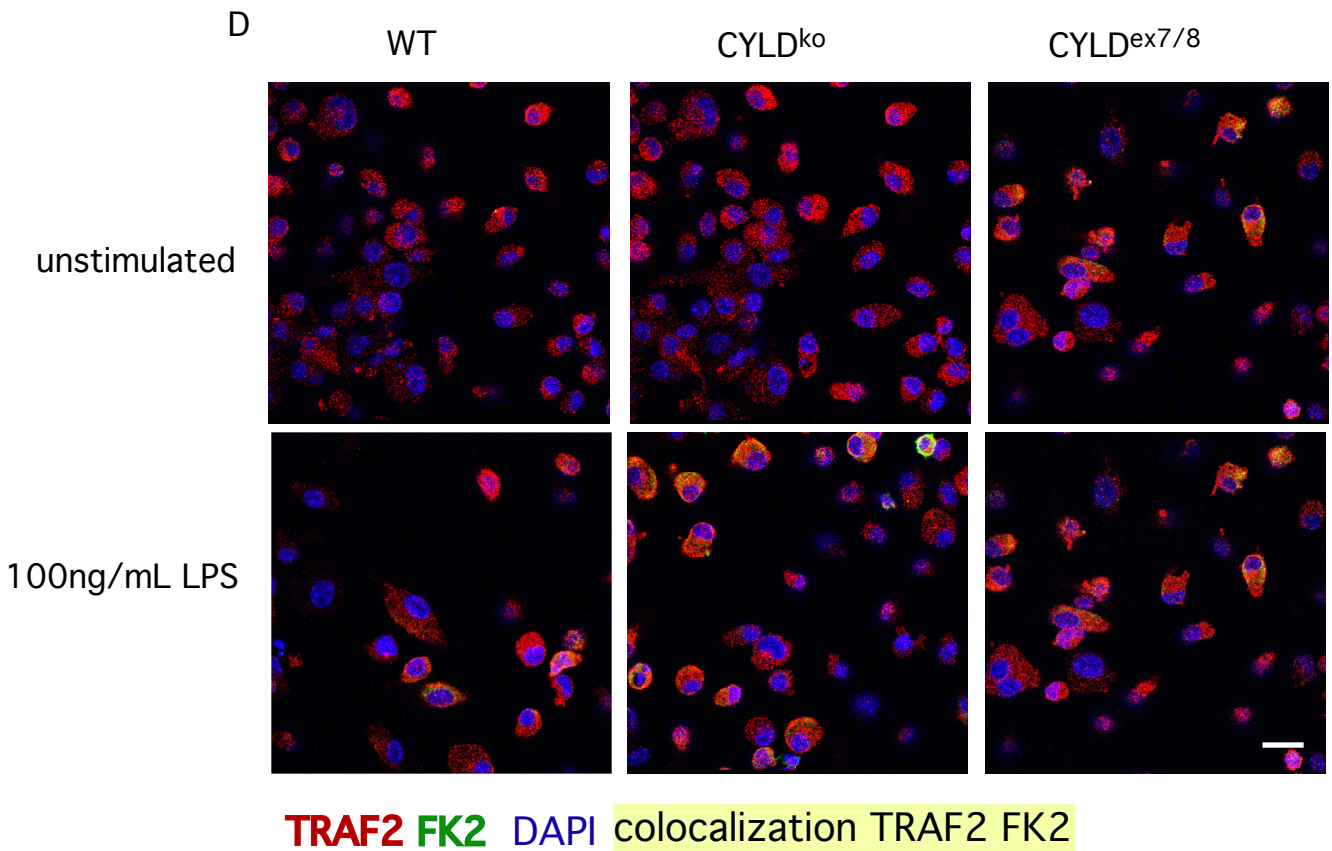

3.8. A20 and CYLD the determinants of disparate phenotype in CYLD mutations?

The NF-κB pathway not only utilizes CYLD but another DUB called A20. A20 is a cytoplasmic protein that inhibits TNF-induced NF-κB activity [76]. It is intriguing to note that both CYLD and A20 interact with TRAF2 and NEMO to deubiquitinate K^{63} linked Ub chains. Their relationship and function whether cooperative, altruisitic or redundant is of great interest in understanding the role of DUBs in NF-κB signaling.

To begin to understand the reason behind the disparate phenotype of the $CYLD^{ko}$ vs. $CYLD^{ex7/8}$ BMDCs I hypothesized that other DUB enzymes may be involved. The **complete** absence of CYLD may signal the upregulation of another DUB to perform the deubiqutinating task of CYLD. In this hypothesis the deubiquitination of a target such as TRAF2 can be taken over by a DUB enzyme that has similar substrate specificity. As DUB enzymes are highly expressed in the brain, we investigated A20 protein levels first from the brain homogenates of WT, $CYLD^{ko}$ and $CYLD^{ex7/8}$ mice. An increase in the DUB A20 protein was found in both $CYLD^{ko}$ and $CYLD^{ex7/8}$ compared to WT (Figure 23A), suggesting the involvement of a compensatory mechanism in a CYLD mutated environment as described above. If one DUB enzyme is unable to deubiquitinate its target then another DUB with similar target specificity as is the case for CYLD and A20 may potentially take over. To assess if the same scenario applies to BMDCS, real-time PCR for A20 was performed (as Western blot analysis in BMDCs is still being optimized, and DUB expression is much lower in DCs than in brain). $CYLD^{ko}$ BMDCs have higher mRNA expression of A20 both in the unstimulated and LPS stimulated state. Compared to unstimulated $CYLD^{ex7/8}$ BMDCs, unstimulated $CYLD^{ko}$ BMDCs have a 5 fold higher A20 mRNA expression and when stimulated, and a 12 fold increase compared to stimulated $CYLD^{ex7/8}$ BMDCs (Figure 23B). This finding suggests that differences in the expression patterns of DUB enzyme with similar target specificity may account for the phenotypes observed in $CYLD^{ko}$ vs $CYLD^{ex7/8}$ mice.

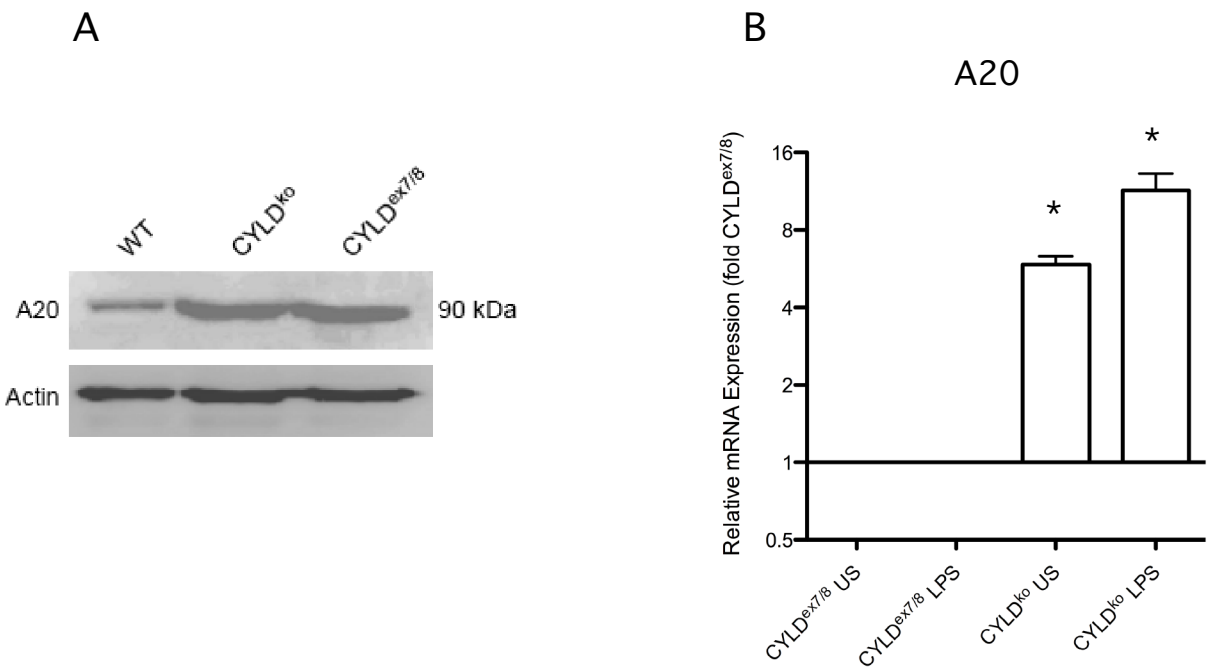

Figure 23. The deubiquitinating enzyme A20 is differentially expressed in CYLD mutated BMDCs
Investigation of A20 DUB. A) Western blot analysis of brain homogenates against A20. 25 ug protein loaded per lane. B-actin was used as a loading control. B) Differentiated day 6 WT BMDCs were exposed to 100ng/mL LPS overnight or left untreated after which qRT-PCR was performed to detect mRNA levels of A20. The mRNA levels were normalized by HPRT levels and expressed as fold change relative to unstimulated and stimulated $CYLD^{ex7/8}$ cells. * indicates $p>0.05$ using T-test between $CYLD^{ex7/8}$ vs. $CYLD^{ko}$ corresponding stimulation condition. Western blot is representative of 2 independent experiments. A20 real time PCR is representative of 3 independent experiments with triplicates.

3.9. Endogenous CD11c+populations in CYLD$^{ex7/8}$ mice

To continue our investigation of the effects of CYLD on dendritic cell function we analyzed the endogenous CD11c+populations so as to extend this inquiry to *in vivo* models dependent on intact endogenous DC performance (see figure 25&26). Endogenous CD11c+were purified from the spleen or bone marrow of WT and CYLD$^{ex7/8}$ mice. Upon investigation of CD11c+ endogenous cells from the spleen using FACS analysis, it was seen that CD86 cell surface expression was higher in CYLD$^{ex7/8}$ vs. WT (Figure 24A). CD86 expression was two fold higher in endogenous CD11c+ CYLD$^{ex7/8}$ cells compared to WT. This correlates to the effect observed in the cultured BMDC preparation and indicates that the hyperreactive phenotype is an inheritant feature of CYLD$^{ex7/8}$ mice and not an effect from culture conditions. Analysis of the common DC population which is defined by CD11c+ CDllb+ population in the bone marrow showed that CYLD$^{ex7/8}$ mice have an increased CD11c^{high} CD11b^{high} population (10.9% vs 8.36% in WT) as well as a higher occurrence of CD11c^{int} CD11b^{int} population (12.5% vs.3.6% in WT) (Figure 24B). This was also true in the bone marrow where the CD11c+CD11b+ double population was almost 2 fold higher in CYLD$^{ex7/8}$ mice compared to WT (5.11% vs. 2.94%) (Figure 24B). Mac1+(CD11b) Gr1+ double positive cells are defined as the myeloid population. Strikingly, both in the spleen and lymph nodes, CYLD$^{ex7/8}$ mice have an increase in this particular population. An increase in a particular cell population, ie. B cells, has already been observed in the CYLD$^{ex7/8}$ mice[81]. Investigations to pinpoint which dendritic cell populations (pDCs/lymphoid DCs,etc) may be increased is ongoing.

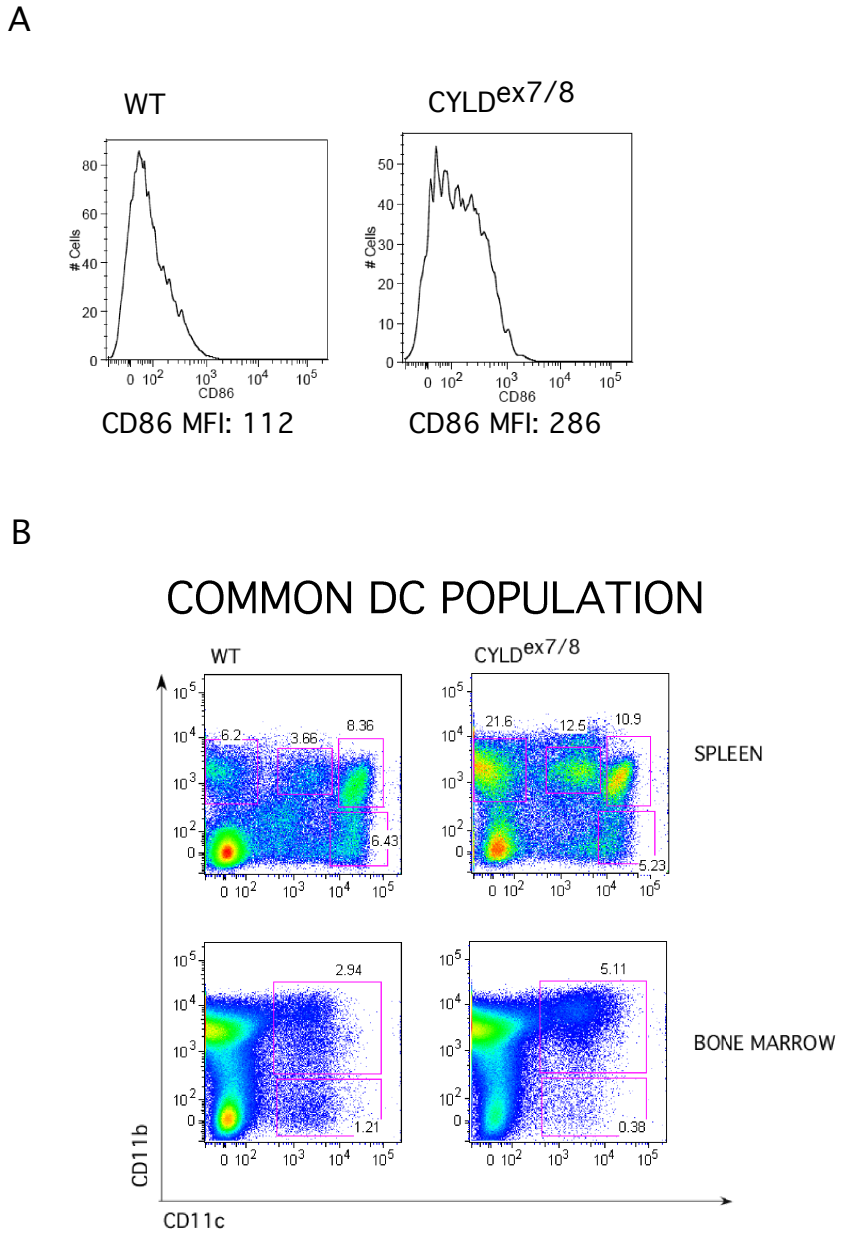

Figure 24. Endogenous CD11c+ populations are affected by the overexpression of sCYLD splice variant

Investigation of endogenous dendritic cell populations. A) FACS analysis of CD3-B220-CD19- CD11c+ endogenous cells from the spleen of mice. Histogram plot of CD86 expression with MFI values indicated. B) Dot plots of CD3-B220-CD19- population investigating the common DC population CD11c+ CD11b+ in WT or CYLD$^{ex7/8}$ spleen and bone marrow. Boxes are drawn to indicate percentage of CD11c+high/int/low and CD11b+high/int/low populations. C) Dot plots of CD3-B220-CD19- population investigating the myeloid population Mac-1(CD11b+) CD11c+ in WT or CYLD$^{ex7/8}$ spleen and lymph nodes. Boxes are drawn to indicate percentage of double positive populations.

Figure is representative of two independent experiments. *PhD. student Joumana Masri from the laboratory of Dr. Ari Waisman collaborated in this experiment.*

Note: *Because the marker CD11c is not only exclusively expressed on dendritic cells, the endogenous populations derived from the various organs cannot be defined as dendritic cells with absolute confidence.*

3.10. CYLD$^{ex7/8}$ mice respond normal to LCMV infection

The ability to respond to LCMV is dependent on many factors, including an intact DC function [97].To assess the impact of sCYLD expression in DC on viral infections, we obtained a mouse from Ari Waisman's lab, in which sCYLD is only soley and excessively expressed in the CD11c+ population while the rest of the cell populations express the full length CYLD (CYLD$^{ex7/8\ fl/fl}$x CD11c-Cre). WT, CYLD^{ko}, CYLD$^{ex7/8}$, CYLD$^{ex7/8\ fl/fl}$x CD11c-Cre and fl/fl (control for CYLD$^{ex7/8fl/fl}$ x CD11c-Cre) were challenged i.v. with 100 Pfu of LCMV-WE and CD8+ tetramer and IFN-γ responses were measured. Figure 25A shows that the responses to two immunodominant epitopes of LCMV, GP33 and NP396. Although variable from mouse group to mouse group, figure 25A indicates that the CD8+ response to LCMV is essentially present in all mouse types. This is more evident when the CD8+ IFN-γ response to three different immunodominant peptides of LCMV is analyzed. CD8+ IFN-γ response to GP33 peptide stimulation is strong in all mouse groups with no apparent significant difference (one way ANOVA revealed no statistical difference) (Figure 25B). Furthermore, the other less potent peptide stimulation with GP276 or NP396, although showing more variability in CD8+ IFN-γ response, displayed essentially no statistical difference. This result indicates that sCYLD expression either in all cells or only in the CD11c+ cell population does not alter the LCMV response and that the ability to prime T cell immunity against viruses is not altered or enhanced in the presence of CYLD mutations.

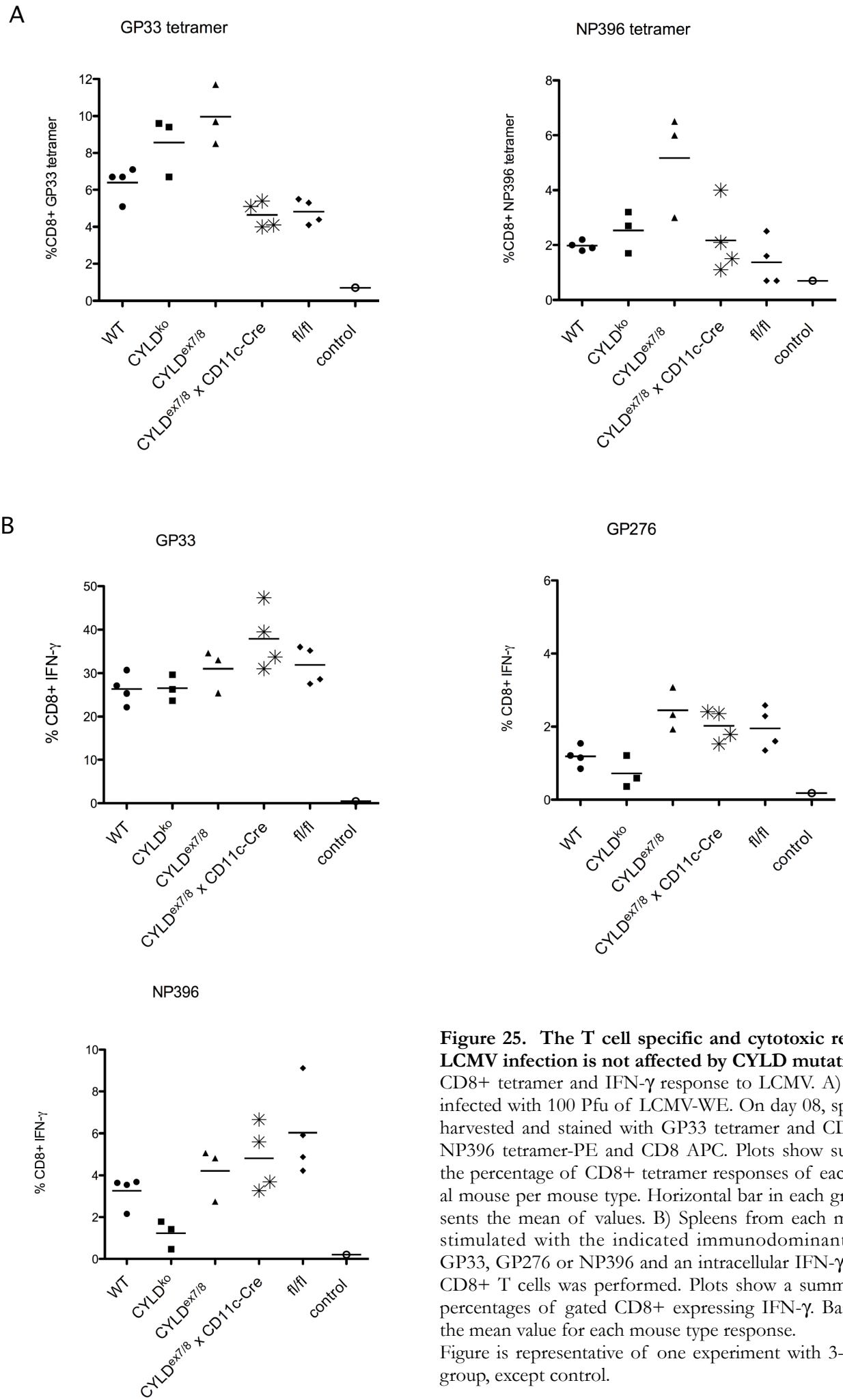

Figure 25. The T cell specific and cytotoxic response to LCMV infection is not affected by CYLD mutation

CD8+ tetramer and IFN-γ response to LCMV. A) Mice were infected with 100 Pfu of LCMV-WE. On day 08, spleens were harvested and stained with GP33 tetramer and CD8 APC or NP396 tetramer-PE and CD8 APC. Plots show summary of the percentage of CD8+ tetramer responses of each individual mouse per mouse type. Horizontal bar in each group represents the mean of values. B) Spleens from each mouse were stimulated with the indicated immunodominant peptides, GP33, GP276 or NP396 and an intracellular IFN-γ staining in CD8+ T cells was performed. Plots show a summary of the percentages of gated CD8+ expressing IFN-γ. Bar represent the mean value for each mouse type response.

Figure is representative of one experiment with 3-4 mice per group, except control.

3.11. DEC-205:OVA mediated peripheral tolerance in CYLD$^{ex7/8}$ mice

DC are essential elements in the induction of immunity and tolerance. As no effect was observed in CYLD$^{ex7/8}$ upon LCMV viral infection (no effect on induction of immunity) we sought another *in vivo* model to test the capacity of DC to tolerize T cells. In the immune system, dendritic cells are involved in peripheral tolerance. This means that DCs in the periphery continuously capture proteins from the airway and intestine since they are anatomically positioned to present these antigens to T cells in lymphoid organs. Tolerance induction by DCs involves suppressing T cell function so that the exposure to everyday foreign non-pathogenic antigens does not initiate a harmful and unnecessary immune response.

DEC205 (CD205) is expressed mainly by CD8α+ DCs in the T-cell areas of the lymphoid organs and mediates the efficient processing and presentation of antigens on MHC class II products *in vivo* [16]. DEC-205:OVA delivers endocytosed protein in the absence of infection to the TAP-dependent pathway for MHC class I peptide loading. Small amounts of injected antigen into mice are able to induce solid peripheral CD8+ T cell tolerance [15]. DEC-205:OVA provides an efficient receptor-based method for DCs to continually capture antigens for presentation on MHC class I products in the steady state and to block the development of CD8+ T cell reactivity. To investigate T cell tolerance mediated by DEC-205 receptor ligation and the role of sCYLD in this effect, CYLD$^{ex7/8}$ mice along with WT and CYLD^{ko} were adoptively transferred with $1.0x10^6$ purified OT-1 CD45.1 T cells on day 0 (for schematic overview of experimental setup see Figure 26A). Next day, 20ug of DEC-205:OVA was subcutaneously injected into recipient mice. On day 12 of the experimental setup, recipients were challenged with 50ug OVA in CFA subcutaneously and the disappearance of the adoptively transferred OT-1 CD45.1 T cells was investigated. *Note: on days 3,5 and 7 of the experimental timeline, OT-1 CD45.1 T cell expansion in the blood was observed through FACS analysis. This indicated that OT-1 T cells have come into contact with DEC-205:OVA stimulated DCs (data not shown).* On day 15, spleens from recipient mice were harvested and the presence of OT-1 CD45.1 T cells was examined. As indicated in Figure 26B, recipient mice which did not receive DEC-205:OVA initially but were challenged with OVA on day 12, showed the persistent presence of OT-1 CD45.1 T cells in the spleen. However, WT and CYLD^{ko}, but not CYLD$^{ex7/8}$ mice appeared to almost completely lose the presence of OT-1 CD45.1 T cells in the spleen. CYLD$^{ex7/8}$ mice still had a lingering population of the adoptively transferred

T cells on day 15. Figure 26C summarizes the fold change in OT-I numbers compared to PBS control in each recipient group. As evidenced by the summarized plot, WT and $CYLD^{ko}$ mice had a significant depletion of the OT-I T cells upon OVA challenge while $CYLD^{ex7/8}$ mice had a persistent presence of OT-I T cells in the spleen. This finding suggests that $CYLD^{ex7/8}$ mice lack the capacity for DC-mediated induction of tolerance towards exogenous antigens either due to their predisposed high activation status or due to an altered interaction with regulatory T cells (Treg).

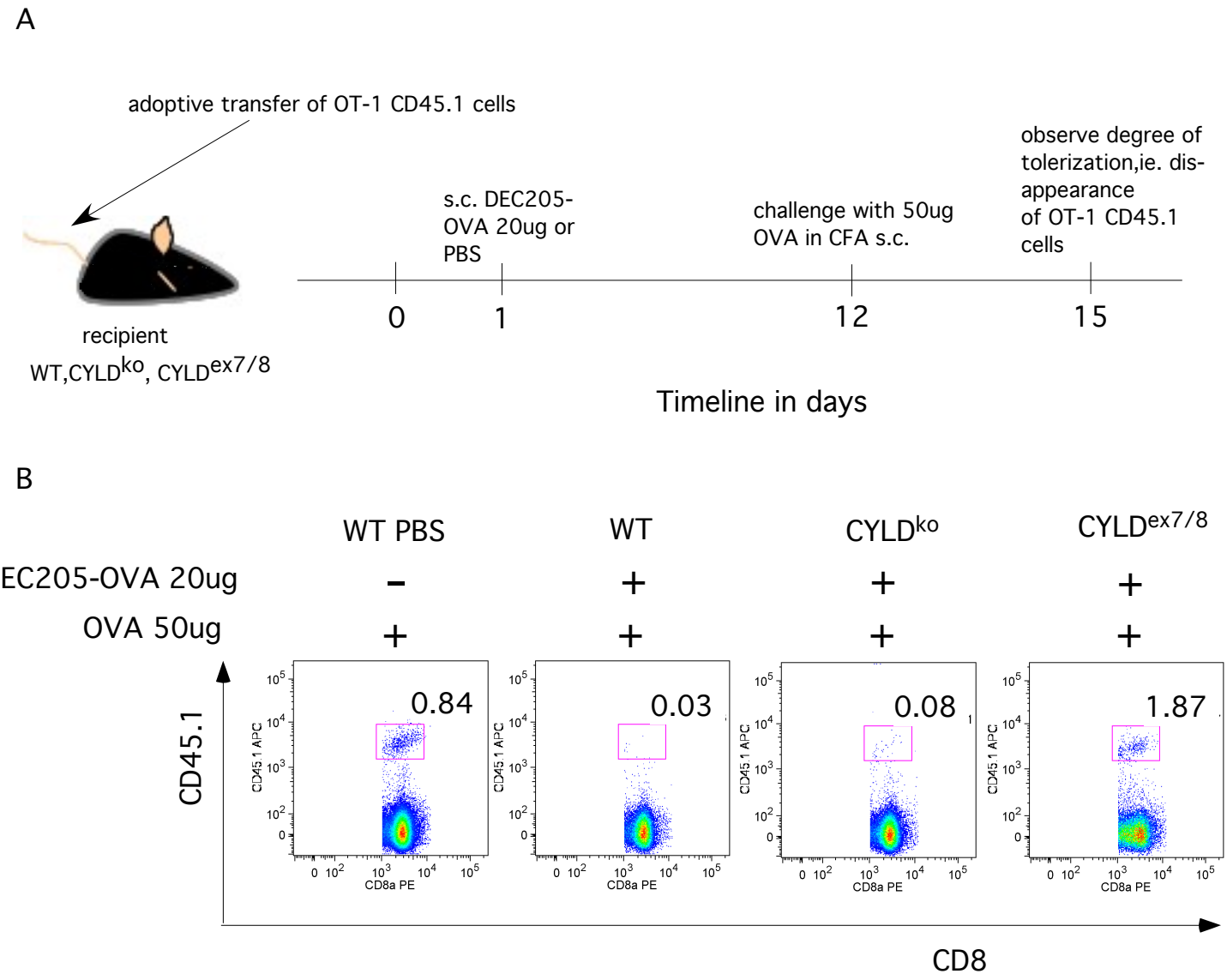

Figure 26. CYLD$^{ex7/8}$ mice are unable to achieve tolerance mediated via DEC-205:OVA
A) Schematic representation of experimental set-up. B) FACS plots of splenocytes from recipient mice on day15, gated on the percentage of CD8+ cells expressing CD45.1. Treatments are indicated above FACS dot plots. C) Fold change in OT-I T cell numbers compared to PBS control in the spleen of recipient mice adoptively transferred with OT-I cells, given 20ug DEC-205:OVA in footpad and challenged with 50ug OVA protein in CFA subcutaneously. Cell detection analyzed by FACS using CD45.1 and CD8 antibodies to detect OT-I CD45.1 cells gated on CD8. Values represent n>4 mice per group, with mean values and SEM. * indicates $p<0.05$ using one-way ANOVA Figure is representative of one independent experiment with n>4 per group.

3.12. The effect of sCYLD on NF-κB family members

The involvement of CYLD in the NF-κB signaling prompted us to investigate the effect of sCYLD in this cascade. To understand the cause for the hyper-reactive phenotype of the CYLD$^{ex7/8}$ BMDCs, the expression of Bcl-3, an IκB family member implicated as a target of CYLD was investigated[84]. QRT-PCR revealed an increase in Bcl-3 in stimulated CYLD$^{ex7/8}$ BMDCs (Figure 27A). The increase in Bcl-3 mRNA levels was 3 fold higher compared to WT LPS stimulated BMDCs and 1.4 fold higher than CYLD^{ko} BMDCs. Strikingly, confocal microscopy images show a strong increase of Bcl-3 expression already in non-stimulated CYLD$^{ex7/8}$ BMDCs (Figure 27B) and a detectable increase of Bcl-3 in CYLD^{ko} BMDCs but only upon stimulation (Figure 27A&B). Western blot analysis confirmed that protein levels of Bcl-3 are already upregulated in unstimulated CYLD$^{ex7/8}$ BMDC whole cell lysates with a further increase upon overnight LPS stimulation (Figure 27C).

The role of Bcl-3 in NF-κB activity is dependent on which factors are associated with Bcl-3. As Bcl-3 Tg mice display altered germinal centers and increased B cell survival[65] we believe that the increased Bcl-3 expression in BMDCs of CYLD$^{ex7/8}$ mice reflects a BMDC state of increased NF-κB activity. Figure 27D shows the NF-κB luciferase reporter assay conducted with transfected BMDCs. This reporter construct comprises three copies of NF-κB binding sites from the murine c-Myb intronic enhancer. Upon transfection of this reporter construct, the NF-κB activity was measured in unstimulated and overnight LPS stimulated BMDCs. The NF-κB activity was 2 fold higher in unstimulated CYLD$^{ex7/8}$ BMDCs compared to control unstimulated counterparts (Figure 27D). In addition, this was also the case for overnight LPS stimulated CYLD$^{ex7/8}$ BMDCs (Figure 27D). In order to ascertain which NF-κB dimers of NF-κB may be involved, we chose to look at p105 and p65. The CYLD$^{ex7/8}$ BMDC state of increased NF-κB activity is supported by the enhanced degradation of cytoplasmic p105 (Figure 27E) and increased nuclear accumulation of p65 (Figure 27F).

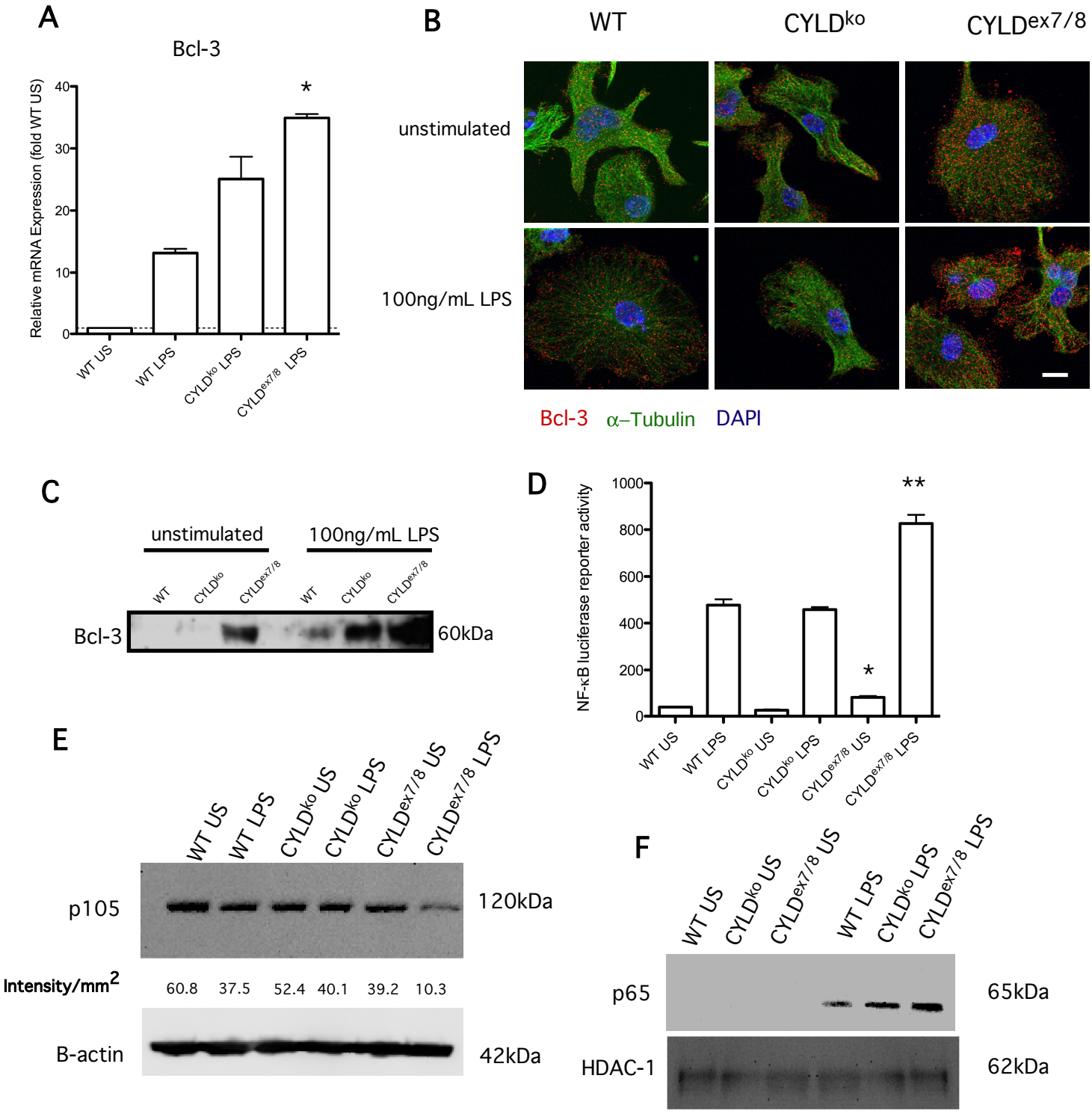

Figure 27. NF-KB family members account for the hyper-reactive phenotype of CYLD$^{ex7/8}$ BMDCs
A) Differentiated day 6 WT BMDCs were exposed to 100ng/mL LPS overnight or left untreated after which qRT-PCR was performed to detect mRNA levels of Bcl-3.The mRNA levels were normalized by HPRT levels and expressed as fold change relative to unstimulated WT cells. B) Immunohistochemical staining of GM-CSF-differentiated BMDCs for Bcl-3 (red), tubulin (green) and DAPI (blue) analyzed by confocal microscopy (Zeiss). Bar represents 10uM. C) Western blot analysis of BMDC whole cell lysates unstimulated or stimulated overnight with 100ng/mL LPS stained with Bcl-3 antibody. Protein loading was normalized using Roti-Nanoquant D) NF-**K**B luciferase reporter activity in BMDCs untreated or stimulated with 100ng/mL LPS overnight. Luciferase values are standardized to control renillin luciferase activity and normalized to WT unstimulated luciferase value. E) Western blot of cytoplasmic extracts from unstimulated or overnight LPS -stimulated BMDCs blotted with p105 antibody and B-actin for loading control. Numbers indicate relative intensity/mm^2 measured on ChemiDoc XRS(Bio-Rad) between samples. F) Western blot analysis of nuclear extracts from unstimulated and overnight LPS stimulated BMDCs using p65 antibody and HDAC1 as loading control.

3.13. sCYLD expression correlates with stimulation in WT BMDCs

It has previously been shown that sCYLD is expressed also in WT mice and might positively regulate NF-κB signaling [81]. This hypothesis is strongly supported by our observation that sCYLD is also expressed and strongly upregulated during DC activation (Figure 28). With the help of PCR primers that discriminate between sCYLD and FL-CYLD we detected more than a 10-fold increase in the expression of the sCYLD splice variant after 6 hours of LPS activation whereas FL-CYLD mRNA levels only double (Figure 28A). Western blot analysis showed an increase of sCYLD in WT overnight LPS stimulated BMDCs (Figure 28B) which supports the increase observed in sCYLD mRNA levels to protein levels. Overall, these findings link sCYLD expression to DCs activation. In addition, this suggests that in contrast to FL-CYLD, sCYLD is a positive regulator of NF-κB activity and its over-expression induces a hyper-reactive phenotype in DCs.

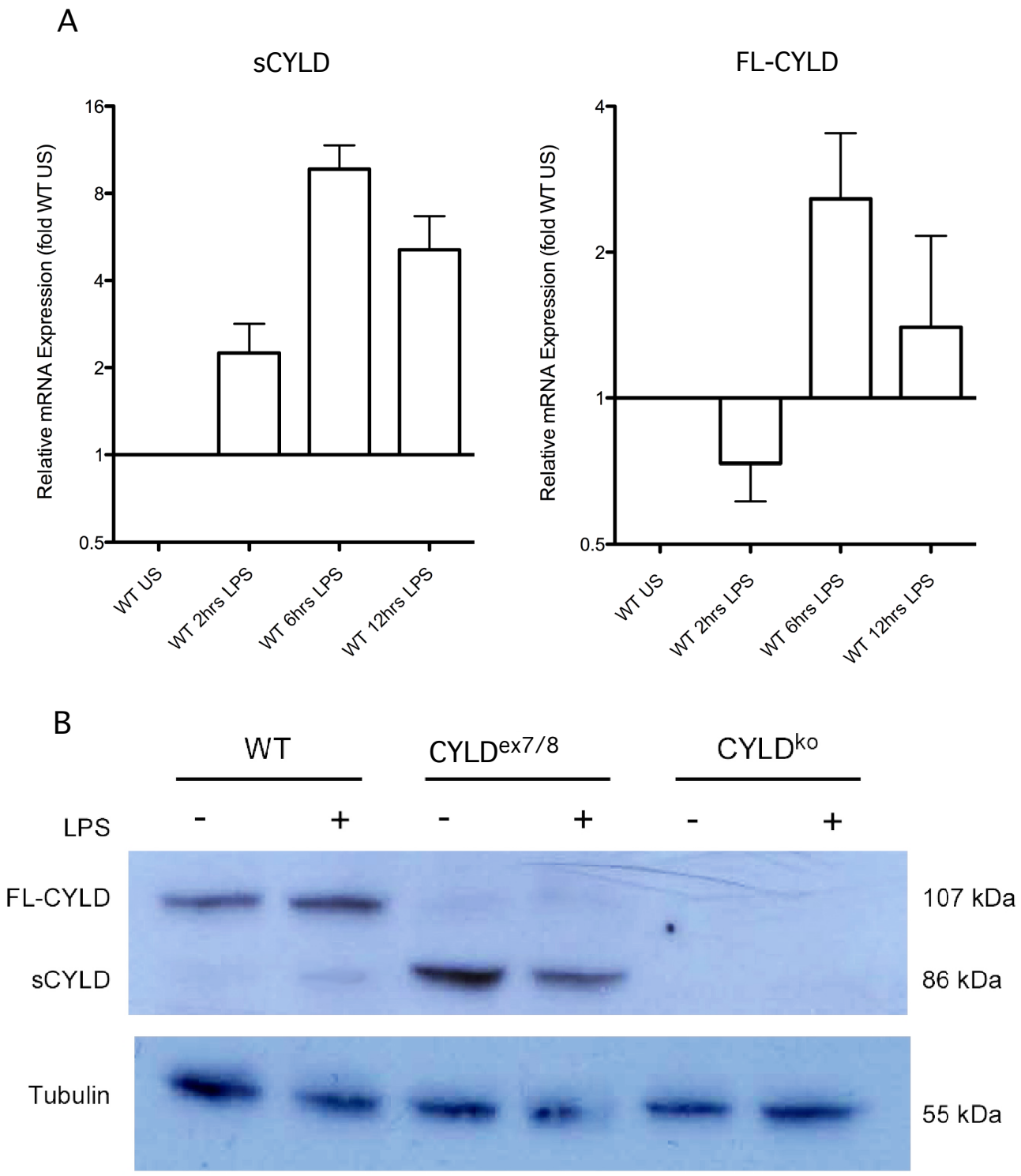

Figure 28. Dramatic upregulation of sCYLD mRNA levels in WT stimulated BMDCs
A) Differentiated day 6 WT BMDCs were exposed to 100ng/mL LPS at the indicated time points or left untreated, after which qRT-PCR was performed to detect mRNA levels of sCYLD or FL-CYLD. The mRNA levels were normalized by HPRT levels and expressed as fold change relative to unstimulated WT cells. B) Western blot analysis of whole cell lysates from unstimulated and overnight LPS stimulated BMDCs using anti-CYLD antibody and tubulin as loading control. *Western blot analysis was performed by PhD. student Joumana Masri, from the laboratory of Dr. Ari Waisman as a collaborative effort.*

3.14. Searching for ubiquitin targets of FL-CYLD and sCYLD

Since the expression of FL-CYLD and sCYLD differs in WT BMDCs upon stimulation, we hypothesized that they have unique ubiquitinated targets. To undertake the complex task of identifying ubiquitin targets of CYLD and sCYLD, the proteasomal subunit S5a was employed for the isolation and purification of polyubiquitinated proteins. The proteasomal subunit S5a has been shown to bind both K^{48} as well as K^{63}-linked polyubiquitin and hence it was used in this experiment as a bait for polyubiquitinated proteins. pGEX-2TK N-terminal glutathione-S-transferase (GST) fusion prokaryotic expression vector into which the full length human S5a cDNA (obtained from Martin Scheffner) has been cloned. This vector was used for the recombinant expression of S5a in E.coli. GST-S5a was subsequently purified by affinity chromatography using GSTrap (Glutathione immobilized on Sepharose 4B) columns using an AKTA HPLC system. For use as a negative control, recombinant GST protein (with no S5a) was purified using the same methodology. For the purification of polyubiquitinated proteins from WT brain homogenates, purified GST-S5a or GST (as a negative control) was bound to GSTrap sepharose beads and incubated together with WT brain homogenates overnight at 4˚C with the addition of complete protease inhibitors. (see schematic diagram figure 29A). After washes that removed unspecifically bound proteins, polyubiquitinated proteins were eluted either with the protease thrombin for which there is a unique cutting site between the GST tag and the S5a, the application of a denaturing elution buffer (SDS buffer) or the competitive addition of excess GSH to compete for the binding in the GST trap column and subsequently to elute the bound polyUb proteins. As seen in Figure 29B, the elution with thrombin and GSH competition was successful in producing a smear on the western blot using anti-FK2 antibody. The SDS elution was the least successful, perhaps because it was the harshest of all elutions. Control GST did not appear to elute the degree of ubiquitinated proteins seen in S5a-GST and hence the first of many steps to find polyUb targets was optimized. At the moment, the next steps are being optimized by the research group of Dr. Stefan Tenzer. The polyUb proteins eluted from the S5a-GST trap column will need to be exised from the SDS page gel, trypsinized and subjected to mass spectrometry. In the mass spectrometer, we hope to identify different ubiquitinated targets and also to assess the different polyUb linkages using the ubiquitin AQUA method. The AQUA method supplements the trypsin digests with isotope-labelled internal standard peptides representing each polyUb linkages and

unbranched Ub and then the standards plus their corresponding native analytes are detected in high resolution precursor ion scans using narrow range-extracted ion chromatograms.

A

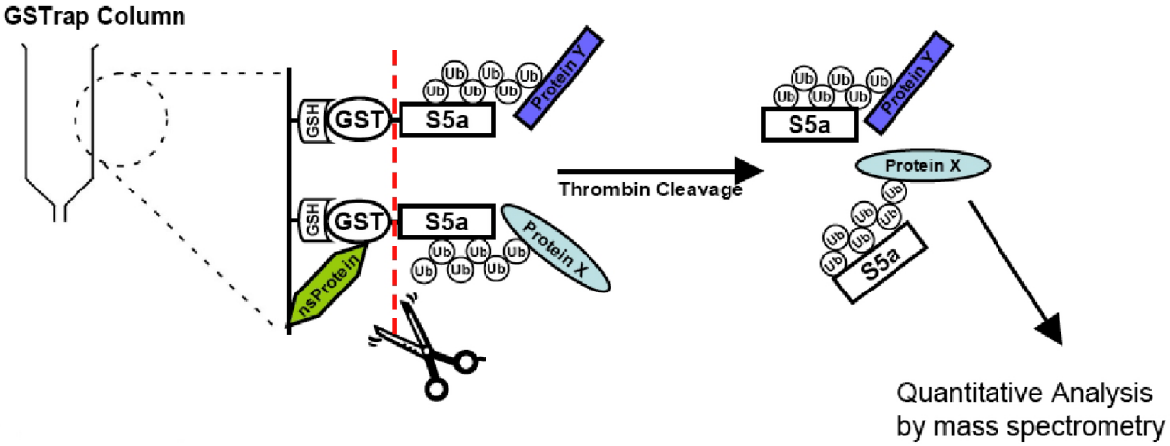

B

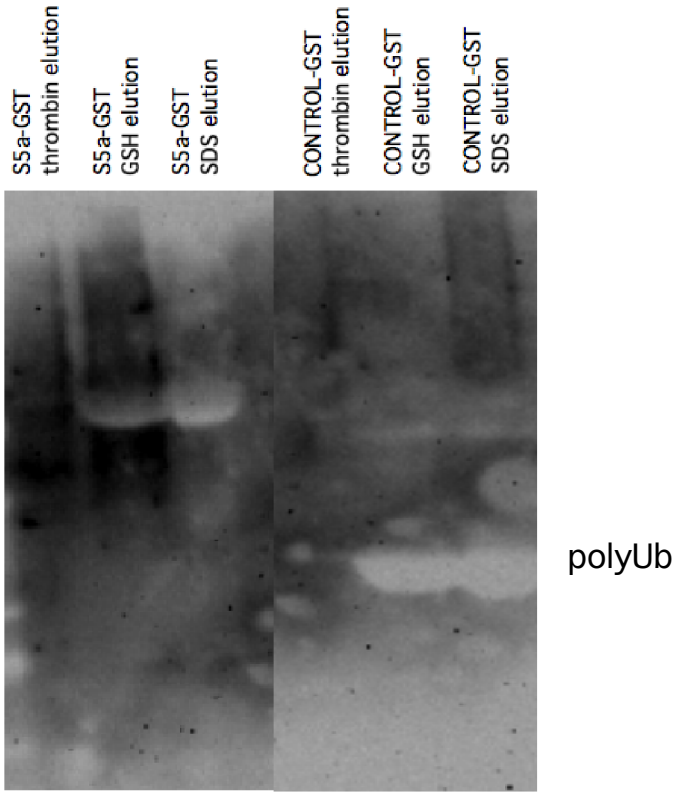

Figure 29. The search for ubiquitin targets of CYLD
A) Schematic diagram of the intended protocol to elute and analyze ubiquitinated proteins. B)WT brain homogenates (30mg) were bound to either S5a-GST or GST alone (500ug) and rotated overnight at 4C and eluted either with thrombin, 10mM GSH, or SDS buffer. Eluates from S5a-GST and GST control were run on a SDS gradient gel (12%-4%) and blotted with anti-FK2 antibody. Smear in S5a eluates indicates polyUb proteins.*This experiment is part of a large ongoing collaborative effort to identify ubiquitinated proteins with Dr. Stefan Tenzer and PhD. student Joumana Masri who were involved in the planning and performing of the experiments.*

4. Discussion

Comparisons can be drawn between the hyper-reactive phenotype of CYLD$^{ex7/8}$ BMDCs (Figures 14-16) to the APCs of the DUB A20-/- mice. Like CYLD$^{ex7/8}$ BMDCs, A20-/- macrophages have an increased sensitivity to LPS stimulation [76]. This finding implies that DUB activity is an important regulator of APC function. Indeed, in our experiments, investigating the effect of DUB CYLD on BMDCs certainly showed a prominent phenotype. As observed in Figure 14A, CYLD$^{ex7/8}$ BMDCs have elevated CD86 expression upon exposure to TLR ligands, LPS, P_3Cys and PolyI:C and TNFR ligand, agonistic anti-CD40. In all stimulation conditions and interestingly, also in the unstimulated condition, CYLD$^{ex7/8}$ BMDCs had increased expression of CD86 receptor. As expression of the co-stimulatory CD86 molecule is essential for the stimulatory capacity of DCs, the higher mean fluorescence intensity of CD86 in CYLD$^{ex7/8}$ BMDCs suggests the capacity for an enhanced magnitude of activation. Furthermore, the expression of other important cell surface receptors such as Ox40L and MHC class II receptor was significantly increased in CYLD$^{ex7/8}$ BMDCs (Figure 14B&C). This finding demonstrates that the exclusive expression of the sCYLD had a stronger influence on BMDC phenotype than the lack of CYLD. Along with the higher expression of cell surface markers, CYLD$^{ex7/8}$ BMDCs secreted higher levels of pro-inflammatory cytokines, IL-6 and TNF-α while secreting less anti-inflammatory IL-10 cytokine (Figure 15A&B). This finding is consistent with the notion that CYLD$^{ex7/8}$ mice have populations of cells that are altered in their function. For example, B cells in CYLD$^{ex7/8}$ mice display prolonged survival and manifest a variety of signalling disarrangements that do not occur in CYLD^{ko} B cells[81]. The *in vivo* ability of CYLD$^{ex7/8}$ BMDCs to stimulate antigen specific T cells reflected their high expression of co-stimulatory and B7 family members along with increased pro-inflammatory cytokine secretion. The consequence of this hyper-reactive phenotype resulted in the enhanced capacity of CYLD$^{ex7/8}$ BMDCs to initiate T cell mediated immunity (Figure 16). Elevated T cell proliferation as well as the procurement of increased cytotoxic capacity (increased IFN-γ secretion) resulted when recipient mice adoptively transferred with TCR transgenic cells were immunized with peptide loaded CYLD$^{ex7/8}$ BMDCs. These findings are reminiscent of another study with the DUB A20, where A20 silenced DCs showed spontaneous and enhanced expression of co-stimulatory molecules and proinflammatory cytokines in addition to hyper-activating cytotoxic T lymphocytes [98]. Intriguingly, these two DUBs, CYLD and A20 have similar substrate specificity for K^{63} polyubiquitinated targets and the similar

phenotype observed in sCYLD over-expressing mice suggests that DUBs are capable of regulating DC activity. The discrepancy in $CYLD^{ko}$ BMDCs phenotype in comparison to both $CYLD^{ex7/8}$ and A20-/- BMDCs could be a matter of compensation with another DUB and/or the allocation to sCYLD vs FL-CYLD to perform the positive regulatory functions in DC activity (discussed below).

How DCs ingest, process and present Ags is dependent on many factors including its differentiation and maturation state [4, 99]. Maturation of DCs is characterized by a decreased antigen processing capacity and an increased cell surface expression of MHC and co-stimulatory molecules. $CYLD^{ex7/8}$ BMDCs which possess an increased cell surface expression of MHC and co-stimulatory molecules are unable to process DQ-OVA as efficiently as $CYLD^{ko}$ and WT BMDCs (Figure 17C). This is in agreement to the principle of activation status decreasing the antigen processing capacity of BMDCs since $CYLD^{ex7/8}$ BMDCs which have a predetermined high activation phenotype were inefficient at antigen processing. In addition, when WT and $CYLD^{ko}$ BMDCs were stimulated with LPS, they too followed the principle of activation affecting antigen processing and displayed significant decrease in antigen processing capacity. Surprisingly, $CYLD^{ex7/8}$ BMDCs were capable of ingesting antigens equally well compared to counterparts despite their highly activated status; which is in disagreement with the principle stated above. However, because the reagent used to assess ingestion, TMR-dextran, is a completely different reagent compared to DQ-OVA and ingested through a different manner, the comparisons or conclusions as to the ingestion property of $CYLD^{ex7/8}$ cannot be conclusively stated. The DQ-OVA processing is supposedly dependent on an intact lysosomal processing function as addition of NH_4Cl and chloroquine markedly inhibited the processing and presentation of DQ-OVA in BMDCs (Figure 18). Upon NH_4Cl + chloroquine administration, DQ-OVA processing is further restrained in $CYLD^{ex7/8}$ BMDCs. This phenomenon is also observed in $CYLD^{ko}$ BMDCs which signifies that changes in CYLD expression or its absence in DCs attenuates antigen processing. WT BMDCs when incubated prior with inhibitors, process DQ-OVA to almost the same extent as $CYLD^{ko}$ and $CYLD^{ex7/8}$ BMDCs that have not been exposed to any inhibitor. Nonetheless, the altered capacity to process the DQ-OVA antigen does not hinder the ability of $CYLD^{ex7/8}$ BMDCs, which ingested, processed and subsequently presented class II OVA peptides from DQ-OVA, to promote OT-II cell division equally well compared to control counterparts (Figure 19). Furthermore, it appears that the increased expression of MHC class II molecules and co-stimulatory

receptors nullifies the inefficiency in DQ-OVA presentation capacity in CYLD$^{ex7/8}$ BMDCs. What is interesting to point out, is that when no antigen processing is required to present peptides to OT-II T cells, as in the condition where BMDCs are peptide-loaded prior to co-culture with OT-II T cells, the CYLD$^{ex7/8}$ BMDCs are 20% better at achieving OT-II T cell division compared to CYLD^{ko} and WT peptide loaded BMDCs. Again, we postulate that this is a result of the cell surface and cytokine expression observed in CYLD$^{ex7/8}$ BMDCs which qualifies them with superior stimulatory abilities. Uniform with the above results that a DUB enzyme can regulate antigen presentation, the A20 DUB has also been postulated as an antigen presentation attenuator [98].

T cell activation and tolerance are critically regulated by co-stimulatory molecules, especially those from the B7 and CD28 superfamilies. Two ligands from the B7 family, B7-H1/PDL1 and PDL2/B7DC are expressed on APCs and bind to PDL-1 on T cells. APCs from PDL2-/- mice have an enhanced ability to activate T cells compared with WT cells[100]. Therefore, we also considered the possibility that not only do CYLD$^{ex7/8}$ BMDCs express high levels of receptors essential for priming and eliciting immune responses, but they may also express lower amounts of inhibitory receptors. PDL-2 expressed on APCs is a negative regulator of T cell activation and is essential for regulation of T cell tolerance[100]. BMDCs from CYLD$^{ex7/8}$ displayed a lower fraction of PDL-2^{high} expression (Figure 20), suggesting that not only is the co-stimulatory properties of CYLD$^{ex7/8}$ BMDCs augmented but also the inhibitory capacity is impeded.

The above findings prompted us to investigate the interaction of CYLD$^{ex7/8}$ BMDCs with Tregs to test if the activated status of CYLD$^{ex7/8}$ BMDCs can be manipulated. Based on our above mentioned results, the ability of CYLD$^{ex7/8}$ BMDCs to react to Treg mediated suppression was of paramount interest as Treg-DC interactions are one of the main contributing factors in the establishment of peripheral tolerance. *In vitro* co-culture of CYLD$^{ex7/8}$ BMDCs with WT Tregs stimulated with α-CD3, LPS or a combination of the two, resulted in a persistent secretion of IL-6 cytokine, presumably from the BMDCs (Figure 21A). WT BMDCs were suppressed by Tregs as exemplified by the decreased secretion of IL-6 upon α-CD3 stimulation. Although CYLD$^{ex7/8}$ BMDCs were also suppressed in terms of IL-6 secretion by Tregs, they still secreted significantly more IL-6 compared to WT BMDCs. Additionally, the co-stimulatory receptor CD86 expression was resistant to down-modulation by Treg suppression in CYLD$^{ex7/8}$ BMDCs (Figure 21B). CYLD$^{ex7/8}$ BMDCs perpetually expressed CD86 even upon α-CD3 stimulation. The same was true for MHC class II expression on CYLD$^{ex7/8}$ BMDCs which also did

not succumb to Treg mediated suppression (Figure 21C). This was in sharp contrast to WT BMDCs which were sensitive to the presence of Tregs and downregulated their CD86 and MHC class II cell surface expression. The opposition to Treg mediated suppression has also been observed in A20 silenced DCs[98]. This study by Song et al. points to the DUB A20-/- hyper-activated DCs being capable of overriding Treg cell-mediated immune suppression. In our studies, the $CYLD^{ex7/8}$ BMDCs were also capable of revoking Treg mediated suppression and all together, our studies together with A20 published reports highlight the importance of a functional intact DUB activity (most likely the presence of a DUB with negative downregulating functions) in maintaining control over Treg mediated DC activity.

To begin to understand the underlying causes of $CYLD^{ex7/8}$ BMDC hyper-reactivity we turned to investigate the ubiquitination status in these cells. As CYLD is a DUB enzyme and in $CYLD^{ex7/8}$ and $CYLD^{ko}$ mice the ability to deubiquitinate targets may be altered, we were not surprised to see increased polyubiquitination in the western blot analysis (Figure 22A) of LPS stimulated BMDC whole cell lysates. This result displays the effect of DUB CYLD mutation on real cells without transfection of over-expressed tagged targets and that in general, there is an increase in polyubiquitinated proteins in CYLD mutated cells. In addition, Figure 22B suggests that different DUB CYLD mutations can have distinct effects on cell types. $CYLD^{ex7/8}$ BMDCs appeared to generate ubiquitin aggregates called DALIS already in the unstimulated state, contrary to WT and $CYLD^{ko}$ unstimulated BMDCs. This finding was actually anticipated as DALIS formation is synchronous with DC activation and the acquirement of co-stimulatory and MHC class II expression[29-31]. This observation suggests once again that $CYLD^{ex7/8}$ BMDCs have an increased tendency towards activation which is further supported by the cell surface expression patterns and cytokine secretion profile in $CYLD^{ex7/8}$ BMDCs (figure14&15) and their ability to activate T cell expansion *in vivo* (Figure 16).

It is of course not enough to ascertain that there is an increased polyubiquitination state of proteins in $CYLD^{ko}$ and $CYLD^{ex7/8}$ BMDCs. The BMDCs phenotypes differ in these mice and a logical explanation may lie in the differential polyubiquitination state of FL-CYLD vs. sCYLD targets. The first target of focus was TRAF2. TRAF2 is an adapter protein which contains a RING finger domain and acts as an E3 ligase capable of synthesizing Ub K^{63} chains on itself through an auto-ubiquitination step[101] and then acts to further potentiate NF-κB signaling. Inhibitory DUBs such as A20 and CYLD, which can degrade Ub K^{63} chains from TRAF2, counteract this activation process.

$CYLD^{ex7/8}$ mice over-express the sCYLD splice variant which is lacking a TRAF2 binding site. Therefore, we hypothesized that TRAF2 expression and ubiquitination may be altered in these mice. Upon analysis of BMDC cell lysates, TRAF2 expression was significantly upregulated in unstimulated $CYLD^{ex7/8}$ BMDCs compared to WT and $CYLD^{ko}$ BMDCs (Figure 22C) which is in agreement with the elevated levels of TRAF2 in $CYLD^{ex7/8}$ B cells[81]. Surprisingly, $CYLD^{ko}$ BMDCs did not show the elevated TRAF2 expression levels in either the unstimulated or stimulated condition. We speculated that TRAF2 levels should have increased upon stimulation to help propogate the further downstream signaling cascades and this should have been also evident in $CYLD^{ko}$ BMDCs. However, the ubiquitination status needs to be considered when discussing TRAF2 as TRAF2 can be polyubiquitinated through lysine 63 or lysine 48 linked chains which means it could be acting as an activating platform for other signaling adaptors or signaling its own degradation through the proteasomal pathway, respectively. Analysis of the ubiquitination status of TRAF2 in the different cell types revealed that $CYLD^{ex7/8}$ unstimulated BMDCs had a slightly elevated TRAF2 ubiquitination state and upon stimulation, both $CYLD^{ko}$ and $CYLD^{ex7/8}$ BMDCs had elevated ubiquitinated TRAF2 compared to WT (Figure 22D). It is possible that even though TRAF2 appears equally polyubiquitinated between $CYLD^{ko}$ and $CYLD^{ex7/8}$ BMDC microscope images, it is in fact, polyubiquitinated with different lysine linkages. As FK2 antibody recognizes both K^{63} and K^{48} polyubiquitinated linkages equally well, this hypothesis cannot be ruled out. This postulation could also provide a clearer reason as to why A20 DUB mRNA levels are increased in the $CYLD^{ko}$ BMDCs (Figure 23B). Perhaps A20 is able to compensate for the complete lack of FL-CYLD and deubiquitinate K^{63} linked polyubiquitin and subsequently add K^{48} linked polyubiquitin to signal TRAF2 for proteasomal degradation. In the future, we will use the polyubiquitin linkage specific antibodies [39] that have just recently been made available to study this very interesting proposal. Moreover, the regulation of and mechanisms of DUBs and their relationship with one another -especially A20 and CYLD, which possess same substrate specificities needs further investigation. CYLD for example is controlled through phosphorylation and is unable to deubiquitinate when phosphorylated[102] and A20 mechanisms of action require that it removes Ub K^{63} chains before conjugating substrates with Ub K^{48} chains[103]. Further insights will only help us to begin to understand this complex DUB system and to understand the implications and possible functional redundancies with CYLD and other DUBs.

To begin to advance our knowledge of the DC properties in CYLD$^{ex7/8}$ mice, we chose to inspect the endogenous DC population and subsequently apply *in vivo* models of experimentation which are dependent on an intact DC function. Endogenously derived CD11c+ cells from CYLD$^{ex7/8}$ have an increased CD86 cell surface expression (Figure 24A) which indicates that our previous BMDCs cultures were not biased in their findings. Furthermore, upon inspection of endogenous DC populations-common and myeloid, it was established that the common and myeloid populations are different in CYLD$^{ex7/8}$ mice compared to WT. The CD11c+ CD11b+ population was increased in the spleen and bone marrow of CYLD$^{ex7/8}$ mice in addition to the Gr-1+ Mac-1+ population in the spleen and lymph node (Figure 24B&C). The apparent increase in a cell population in CYLD$^{ex7/8}$ organs has previously been reported with B cells. The increase in CD11c+CD11b+ and Gr-1+ Mac-1+ cell populations indicates that B cells are not the only cells to expand in the presence of over-expressed sCYLD. Therefore, the splenomegaly and lymphomegaly observed in CYLD$^{ex7/8}$ mice [81] may also be due to the increased presence of common and myeloid DC populations. Additionally, the influence of DUBs in establishing the repertoire of APCs has already been observed in the spleens of A20-/- mice which display a substantial increase in the myeloid population, Gr-1+ Mac-1+ [76]. To test the *in vivo* capacity of CYLD$^{ex7/8}$ DCs to perform their functions, we employed two strategies, one to test induction of viral immunity and the other to assess tolerance induction. LCMV infection, which is dependent on an intact DC function [97] did not induce different T cell responses in the CYLD mutated mice (Figure 25). Based on the previously described phenotype, we expected the mice over-expressing sCYLD in either all cells or only in CD11c+ to have heightened responses to LCMV. However, the nature of the LCMV virus is such that unless severely immunocompromised, most mouse models react strongly to the virus infection[104]. Therefore, we investigated the other end of the scale in DC function, that is, the induction of tolerance. As expected, WT and CYLD^{ko} mice displayed a strong reduction in OT-I T cell numbers whereas in CYLD$^{ex7/8}$ mice the OT-I cells expanded more than 10-fold (Figure 26B&C). This finding suggests that CYLD$^{ex7/8}$ mice lack the capacity for DC-mediated induction of tolerance towards exogenous antigens either due to their predisposed high activation status or due to an altered interaction with regulatory T cells (Treg) which we already observed in *in vitro* cultures with CYLD$^{ex7/8}$ BMDCs and Tregs (Figure 21).

The increase in mRNA expression and nuclear localization of IκB family member Bcl-3 (Figure 27 A&B), was not so surprising given that previous reports with B cells from

CYLD$^{ex7/8}$ confirmed an increase in its nuclear localization[81]. However, the *degree* of increase in expression compared to WT and CYLD^{ko} BMDCs was impressive. In CYLD$^{ex7/8}$ BMDCs, unlike B cells, the Bcl-3 gene expression levels were significantly higher upon stimulation with LPS when compared to WT US, WT LPS and CYLD^{ko} LPS conditions. Furthermore, what is noteworthy to mention is the Bcl-3 expression both on the mRNA and protein level between CYLD^{ko} versus CYLD$^{ex7/8}$ BMDCs. Although CYLD^{ko} keratinocytes have elevated cyclin D1 levels which are upregulated by the increased Bcl-3 nuclear localization[67], the increase in CYLD^{ko} BMDCs was nowhere near as profound as that of CYLD$^{ex7/8}$ BMDCs. Already in the unstimulated, confocal images show an overall increased expression of Bcl-3 in CYLD$^{ex7/8}$ BMDCs, especially in the cytoplasm and upon stimulation - a significant increased localization in the nucleus (Figure 27B). Western blot analysis of Bcl-3 with whole cell lysates from BMDCs confirms the observations seen in the confocal microscope. Bcl-3 expression is highly upregulated in unstimulated CYLD$^{ex7/8}$ BMDCs and as WT and CYLD^{ko} BMDCs upregulate Bcl-3 upon LPS stimulation, the upregulation of CYLD$^{ex7/8}$ supercedes that of these other cell types (Figure 27C). Fundamentally, it was important to investigate how this Bcl-3 upregulation influences NF-κB activity. After performing a transfection of BMDCs with the NF-κB luciferase reporter, it could be clearly seen that NF-κB activity is amplified in both the unstimulated and LPS stimulated state of CYLD$^{ex7/8}$ BMDCs (Figure 27D). We observed an increase in NF-κB reporter activity after LPS stimulation both in the WT and CYLD^{ko} BMDCS, but it was significantly lower compared to the CYLD$^{ex7/8}$ BMDCs. Once again, this suggests that the phenotype of CYLD$^{ex7/8}$ investigated in previous experiments in this thesis, which all showed a disregulated and hyper-reactive BMDC as well as the *in vivo* DC phenotype , coincide with an elevated NF-κB activity. As to which NF-κB members are directly affected by the over-expression of sCYLD, we turned to the degradation of p105 since it is well known that Bcl-3 interacts with the p105 (NF-κB1) breakdown product p50[51, 105-108]. Unlike IκBα and IκBβ which associate with active NF-κB dimers in the cytosol, Bcl-3 specifically associates with the transcriptionally inactive p50-p50 or p52-p52 homodimers in the nucleus [50, 107, 109]. However, the precise role of Bcl-3 is controversial, with extensive literature examining this complex relationship, often times disputing whether Bcl-3 is a transcriptional activator or inhibitor upon interaction with p50. For instance, recent reports for the inhibitory role for Bcl-3 claim the following: Bcl-3 and p50 attenuate LPS-induced inflammatory responses in macrophages[110], Bcl-3 is an essential

negative regulator of TLR signaling by blocking the ubiquitination (and supposedly then the degradation) of a p50 complex that inhibits transcription[53] and that Bcl-3 and p50-p50 homodimers act as transcriptional repressors in tolerant CD4+ T cells[111]. In spite of the aforementioned convincing data, the positive role for Bcl-3 as a transactivator of NF-κB transcription is also credible. The reports include the involvement of Bcl-3 in NF-κB activity in breast cancer tissues[54, 112] and Bcl-3 as an activator of NF-κB activity which transcends to cellular proliferation and tumorogenesis[112]. These effects are of course without mention to the Bcl-3 transgenic[65] or knockout[66] mouse models, which suggest a positive role for Bcl-3 in NF-κB in what is arguably a more physiologically-relevant *in vivo* setting. In our experimental circumstances, the increase in Bcl-3 expression (Figure 27A-C), not only showed an increased NF-κB activity (Figure 27D) but p105 degradation was more pronounced in $CYLD^{ex7/8}$ BMDCs suggesting the generation into p50. The supposed generation of p50 together with the observed increased expression of nuclear p65/RelA (a NF-κB member with a TAD domain) (Figure 27E) translates into a heterodimer which activates NF-κB activity [113]. Therefore, in our particular experimental setting, sCYLD expression in BMDCs results in an increased Bcl-3 expression which translates to increased NF-κB activity. Surprisingly, this Bcl-3 increase is observed in the keratinocytes of $CYLD^{ko}$ and coinciding with these results, also in the B cells of $CYLD^{ex7/8}$ mice. Clearly these two conflicting findings cause much confusion. The model proposed from the $CYLD^{ko}$ study argues that CYLD deubiquitinates Bcl-3 to control its localization[67]. That is, only when ubiquitinated can Bcl-3 enter the nucleus with p50 dimers and perform its transactivation function on NF-κB activity. Hence, the complete absence of CYLD in the $CYLD^{ko}$ keratinocytes allows for Bcl-3 translocation to the nucleus to promote NF-κB transcriptional activity. Nuclear Bcl-3 is known to recruit the histone acetyltransferase Tip60 to p50 or p52 homodimers and to activate the gene for cyclin D1, which is responsible for cell cycle progression [56]. By reversing Bcl-3 ubiquitination, CYLD prevents nuclear accumulation of Bcl-3, stimulation of cyclin D1 expression and proliferation[67]. However, sCYLD has been shown to still possess the ability to deubiquitinate Bcl-3[81] and therefore from the results in this thesis and those from $CYLD^{ex7/8}$ B cells, the translocation of Bcl-3 must not be absolutely dependent on ubiquitination alone or Bcl-3 deubiquitination by sCYLD is somehow resistant/refractive in the *in vivo* physiological setting because Bcl-3 can obviously translocate to the nucleus in the $CYLD^{ex7/8}$ setting, and all the more; at an improved efficiency or a greater extent

than in a CYLD^{ko} background. What also needs to be taken into consideration is that another protein modification process is involved in Bcl-3 besides ubiquitination, namely phosphorylation; recently discovered to be mediated by the kinase GSK3 [114], which regulates the ability of Bcl-3 to bind to p50 to confer its transactivating activity[107, 115, 116]. Therefore, the increased Bcl-3 expression in the nucleus of B cells and BMDCs is not contradictory, but emphasizes the need to investigate further how Bcl-3 and CYLD with its splice variants interact with one another.

The next important question to ask is if the increased Bcl-3 expression actually *correlates* with increased NF-κB activity and whether sCYLD over-expression actually drives this event. We have begun experiments that target the silencing of Bcl-3 in CYLD$^{ex7/8}$ BMDCs, however they are confounded by the increased sensitivity of BMDCs to transfection and the difficulty in assessing the quality of siRNA silencing. Ultimately, a Bcl3-/- x CYLD$^{ex7/8}$ mouse cross could provide some more insights into this compelling question as well as the Bcl-3 over-expressing mouse model which is being currently investigated by PhD. student Joumana Masri.

Even more intriguing is the possibility that increased Bcl-3 expression concomitant with increased NF- κB activity points to sCYLD as a positive regulator in NF-κB activity. This is in stark contrast to FL-CYLD which functions to inhibit NF-κB activity and deubiquitinates Bcl-3 to retain it in the cytoplasm and away from NF-κB dimers. The implications that sCYLD could be a positive regulator are substantiated by our observations that mRNA sCYLD expression relative to mRNA FL-CYLD expression increases over 10 fold in WT BMDCs after LPS stimulation (Figure 28A), while mRNA FL-CYLD expression changes little compared to mRNA sCYLD. Western blot analysis using anti-CYLD antibodies in BMDCs stimulated with LPS overnight show a very slight increase of the sCYLD protein in WT BMDCs upon stimulation (Figure 28B). Because of the poor availability of good anti-CYLD antibodies, the search for CYLD and sCYLD at the protein level is a bit confounded and until good antibodies are made available it will be difficult to access the situation. However, the over-expressed sCYLD in the CYLD$^{ex7/8}$ BMDCs is clearly visible and therefore suggests that the slight increase observed in the WT setting corresponds to the increase in sCYLD mRNA levels in WT BMDCs. It can be postulated that the increase in sCYLD aids to drive the positive regulation of NF-κB activity, perhaps by mediating the nuclear translocation of Bcl-3 and thereby transactivating genes responsible for LPS- induced activation. FL-CYLD on the other hand, performs its inhibitory effect after sCYLD expression starts to decline

(which can be seen in Figure 28A to slightly decline after 12 hour stimulation) in possibly an auto-regulatory loop to inhibit NF-κB activation. How the expression of sCYLD and FL-CYLD is regulated is still unknown and is an area that needs to be further investigated.

Ultimately, identification of polyubiquitinated targets of sCYLD and FL-CYLD could provide a clearer explanation as to why such a disparate phenotype exists between $CYLD^{ko}$ and $CYLD^{ex7/8}$ mice, not only in DCs but also in B cells and other cell types. We have begun to establish a method in our laboratory to purify polyubiquitinated proteins (see schematic in Figure 29A) which has led to a positive ubiquitin smear in the SDS gel (Figure 29B). This is the first of many steps required to establish and optimize this protocol. However, I believe this approach holds the key to discovering answers to the many pertinent and pressing questions regarding the role of CYLD and its naturally short splice variant in the immune system.

4.1. Incorporation of results in thesis to a model hypothesis:

I would like to take this opportunity to address a hypothetical model based on the results of this thesis. The key to understanding the differences in $CYLD^{ko}$ and $CYLD^{ex7/8}$ mice is most likely based on the interaction of Bcl-3 with NF-κB dimers which are affected differently in the absence of FL-CYLD and in the presence of sCYLD. I hypothesize that in the presence of sCYLD, Bcl-3 is positively regulated through sCYLD perhaps because sCYLD has a tendency to be more phosphorylated and as a result deubiquitination efficiency is lowered. Furthermore, due to sCYLD's inability to interact with TRAF2 and NEMO, the deubiquitination of these key targets is of course hampered and NF-κB signaling cannot be downregulated efficiently (Figure 30A). Furthermore, although sCYLD possesses the capacity to deubiquitinate Bcl-3 so that theoretically it cannot transcend into the nucleus, it is also possible that not only ubiquitination but also phosphorylation regulate Bcl-3. Perhaps in the over-expressed sCYLD environment the phosphorylation of Bcl-3 is so that it can nevertheless translocate into the nucleus. On the other hand, in the $CYLD^{ko}$ background, the lack of CYLD signals for the upregulation of another DUB with similar substrate specificity – A20. As shown in this thesis A20 is upregulated in the $CYLD^{ko}$ environment to a greater degree than in the $CYLD^{ex7/8}$ or WT background. With a functioning negative regulator of NF-κB, the phenotype of $CYLD^{ko}$ is not as profound as that of $CYLD^{ex7/8.}$ (Figure 30B).

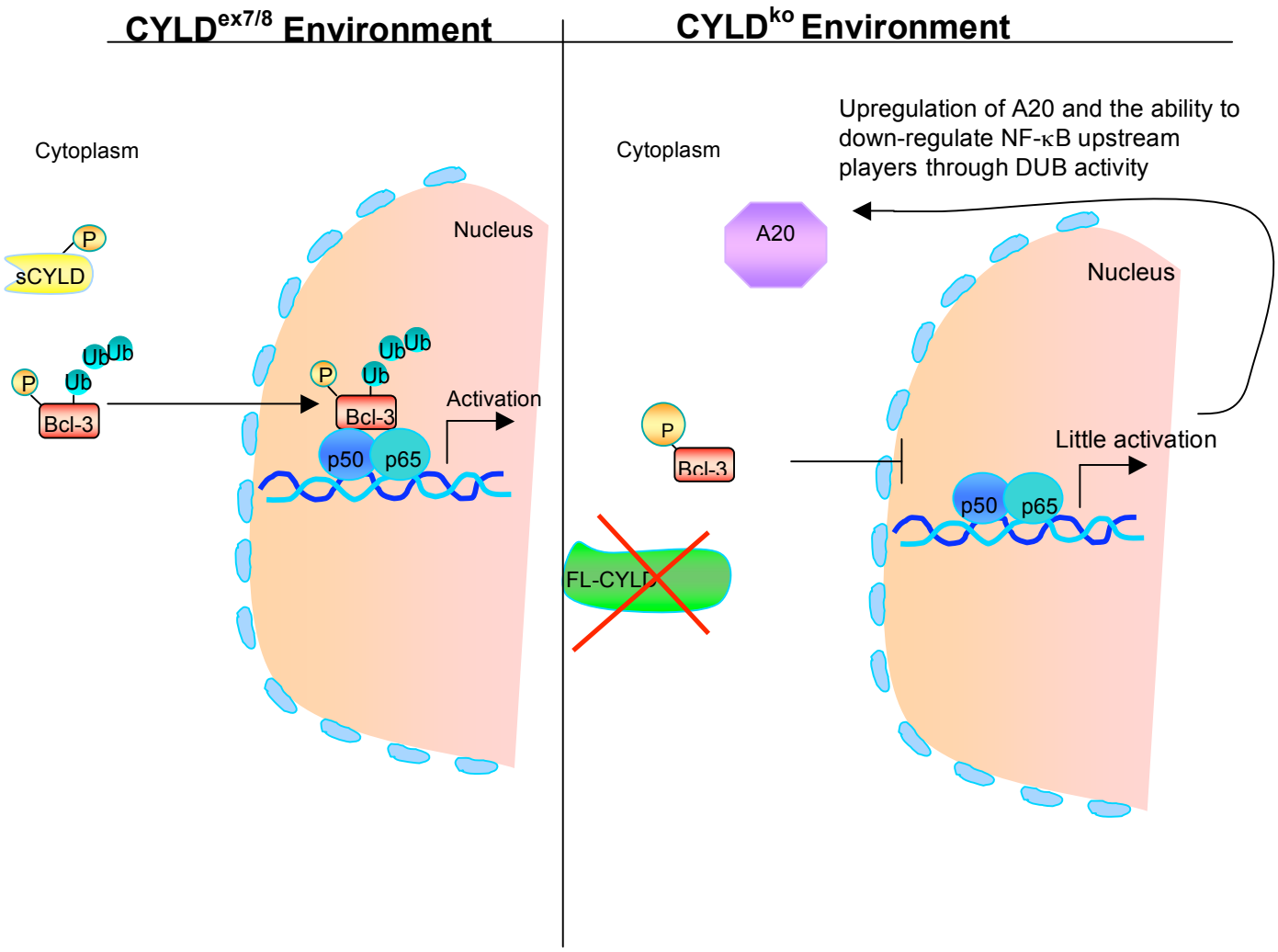

Figure 30. Hypothetical models incorporating Bcl-3 and A20 results from this thesis to explain the disparate phenotype between CYLD$^{ex7/8}$ and CYLD^{ko} dendritic cells. Figure created in PowerPoint together with Canvas software.

5. Future Directions

I. Purification of polyubiquitinated proteins from CYLD$^{ex7/8}$ and CYLD^{ko} BMDCs

This future direction is already in progress in our laboratory. PhD. student Joumana Masri and I have successfully established a protocol to purify polyubiquitinated proteins. The next step is analyze the polyubiquitinated proteins in the mass spectrometer to identify possible candidates that are differentially ubiquitinated in the two mice. With the aid of linkage specific polyubiquitin antibodies [39] and the AQUA Ubiquitin Method that is established in our laboratory, we will be able to not only identify potential new ubiquitinated targets of FL-CYLD and sCYLD but also reveal which ubiqutin linkage chains are involved (K^{48} vs K^{63}).

II. Understand the relationship between Bcl-3 and sCYLD

To understand the relationship between Bcl-3 and sCYLD, a knockdown of Bcl-3 with siRNA would help to understand if the over-expression of Bcl-3 is the determinant factor in the increased NF-κB activity observed in CYLD$^{ex7/8}$ BMDCs. Furthermore, analyzing exactly which NF-κB dimers are associated with Bcl-3 in the nucleus through confocal microscopy could provide insights into the mechanisms behind increased Bcl-3 translocation to the nucleus in CYLD$^{ex7/8}$ BMDCs. Additionally, a cross between Bcl-3-/- x CYLD$^{ex7/8}$ could provide answers to questions on a more physiologically relevant level. Additionally, how sCYLD actually allows Bcl-3 translocation even though it can still deubiquitinate Bcl-3 is of great importance. Analyzing the phosphorylation state of sCYLD and Bcl-3 as well as the ubiquitination status of Bcl-3 in CYLD$^{ex7/8}$ BMDCs may provide clues as to how these 2 proteins are regulated.

III. Relationship between sCYLD vs. FL-CYLD

The naturally occurring splice variant obviously has a role in the immune system, but how exactly sCYLD and FL-CYLD exert their effects is unknown and how they are regulated is not evident. For example, is sCYLD a breakdown product of FL-CYLD or is it expressed initially to promote the positive role of CYLD and then FL-CYLD is expressed so that it functions to downregulate and inhibit the NF-κB pathway? Development of improved anti-CYLD antibodies would aid in this pressing questions so that one could analyze the expression of these two proteins under many different settings.

IV. Rescuing sCYLD targets through the expression of another DUB A20

The relationship between CYLD and A20 would be an intringuing research project to pursue. To understand if the sCYLD phenotype is a result of the inability to deubiquitinate K63 tagged substrates, the expression of A20 might rescue the hyper-active phenotype observed, that is, downmodulate NF-KB activity through deubiquitination of target substrates. This can be simply performed in CYLDex7/8 MEFs by transfecting an A20 plasmid. Furthermore, it would be optimal to look at the expression of A20 in different stimulus conditions over different timepoints in $CYLD^{ko}$ and $CYLD^{ex7/8}$ cells.

6. References

1. Hart, D.N., *Dendritic cells: unique leukocyte populations which control the primary immune response*. Blood, 1997. **90**(9): p. 3245-87.
2. Matzinger, P., *Tolerance, danger, and the extended family*. Annu Rev Immunol, 1994. **12**: p. 991-1045.
3. Steinman, R.M., *The dendritic cell system and its role in immunogenicity*. Annu Rev Immunol, 1991. **9**: p. 271-96.
4. Villadangos, J.A. and P. Schnorrer, *Intrinsic and cooperative antigen-presenting functions of dendritic-cell subsets in vivo*. Nat Rev Immunol, 2007. **7**(7): p. 543-55.
5. Shortman, K. and S. Naik, *Steady-state and inflammatory dendritic-cell development*. Nat Rev Immunol, 2007. **7**(1): p. 19-30.
6. Tacke, F. and G.J. Randolph, *Migratory fate and differentiation of blood monocyte subsets*. Immunobiology, 2006. **211**(6-8): p. 609-18.
7. Kopp, E., *Recognition of microbial infection by Toll-like receptors*. Curr Opin Immunol, 2003. **15**(4): p. 396-401.
8. Akira, S., K. Takeda, and T. Kaisho, *Toll-like receptors: critical proteins linking innate and acquired immunity*. Nat Immunol, 2001. **2**(8): p. 675-80.
9. Inaba, K., et al., *High levels of a major histocompatibility complex II-self peptide complex on dendritic cells from the T cell areas of lymph nodes*. J Exp Med, 1997. **186**(5): p. 665-72.
10. Caux, C., et al., *B70/B7-2 is identical to CD86 and is the major functional ligand for CD28 expressed on human dendritic cells*. J Exp Med, 1994. **180**(5): p. 1841-7.
11. Izawa, T., et al., *Crosstalk between RANKL and Fas signaling in dendritic cells controls immune tolerance*. Blood, 2007. **110**(1): p. 242-50.
12. Redmond, W.L. and L.A. Sherman, *Peripheral tolerance of CD8 T lymphocytes*. Immunity, 2005. **22**(3): p. 275-84.
13. Jiang, W., et al., *The receptor DEC-205 expressed by dendritic cells and thymic epithelial cells is involved in antigen processing*. Nature, 1995. **375**(6527): p. 151-5.
14. Mahnke, K., et al., *Induction of CD4+/CD25+ regulatory T cells by targeting of antigens to immature dendritic cells*. Blood, 2003. **101**(12): p. 4862-9.
15. Bonifaz, L., et al., *Efficient targeting of protein antigen to the dendritic cell receptor DEC-205 in the steady state leads to antigen presentation on major histocompatibility complex class I products and peripheral CD8+ T cell tolerance*. J Exp Med, 2002. **196**(12): p. 1627-38.
16. Hawiger, D., et al., *Dendritic cells induce peripheral T cell unresponsiveness under steady state conditions in vivo*. J Exp Med, 2001. **194**(6): p. 769-79.
17. Wilson, N.S. and J.A. Villadangos, *Regulation of antigen presentation and cross-presentation in the dendritic cell network: facts, hypothesis, and immunological implications*. Adv Immunol, 2005. **86**: p. 241-305.
18. Heath, W.R. and F. Carbone, *Cross-presentation in viral immunity and self-tolerance*. Nat Rev Immunol, 2001.
19. Heath, W.R., et al., *Cross-presentation, dendritic cell subsets, and the generation of immunity to cellular antigens*. Immunol Rev, 2004. **199**: p. 9-26.
20. Huang, A.Y., et al., *In vivo cross-priming of MHC class I-restricted antigens requires the TAP transporter*. Immunity, 1996. **4**(4): p. 349-55.
21. Schnare, M., et al., *Toll-like receptors control activation of adaptive immune responses*. Nature Immunology, 2001. **2**(10): p. 947-50.
22. Medzhitov, R., *Toll-like receptors and innate immunity*. Nat Rev Immunol, 2001. **1**(2): p. 135-45.
23. Iwasaki, A. and R. Medzhitov, *Toll-like receptor control of the adaptive immune responses*. Nat Immunol, 2004. **5**(10): p. 987-95.

24. Wright, S.D., et al., *Lipopolysaccharide (LPS) binding protein opsonizes LPS-bearing particles for recognition by a novel receptor on macrophages.* J Exp Med, 1989. **170**(4): p. 1231-41.
25. Schromm, A.B., et al., *Molecular genetic analysis of an endotoxin nonresponder mutant cell line: a point mutation in a conserved region of MD-2 abolishes endotoxin-induced signaling.* J Exp Med, 2001. **194**(1): p. 79-88.
26. Kawai, T., et al., *Unresponsiveness of MyD88-deficient mice to endotoxin.* Immunity, 1999. **11**(1): p. 115-22.
27. Fitzgerald, K.A., et al., *Mal (MyD88-adapter-like) is required for Toll-like receptor-4 signal transduction.* Nature, 2001. **413**(6851): p. 78-83.
28. Cao, Z., W.J. Henzel, and X. Gao, *IRAK: a kinase associated with the interleukin-1 receptor.* Science, 1996. **271**(5252): p. 1128-31.
29. Pierre, P., *Dendritic cells, DRiPs, and DALIS in the control of antigen processing.* Immunol Rev, 2005.
30. Lelouard, H., et al., *Transient aggregation of ubiquitinated proteins during dendritic cell maturation.* Nature, 2002. **417**(6885): p. 177-82.
31. Herter, S., et al., *Dendritic cell aggresome-like-induced structure formation and delayed antigen presentation coincide in influenza virus-infected dendritic cells.* J Immunol, 2005. **175**(2): p. 891-8.
32. Robinson, P.A. and H.C. Ardley, *Ubiquitin-protein ligases.* J Cell Sci, 2004. **117**(Pt 22): p. 5191-4.
33. Hershko, A. and A. Ciechanover, *The ubiquitin system for protein degradation.* Annu Rev Biochem, 1992. **61**: p. 761-807.
34. Pickart, C.M. and D. Fushman, *Polyubiquitin chains: polymeric protein signals.* Curr Opin Chem Biol, 2004. **8**(6): p. 610-6.
35. Sun, S.C., *Deubiquitylation and regulation of the immune response.* Nat Rev Immunol, 2008. **8**(7): p. 501-11.
36. Varadan, R., et al., *Structural properties of polyubiquitin chains in solution.* J Mol Biol, 2002. **324**(4): p. 637-47.
37. Varadan, R., et al., *Solution conformation of Lys63-linked di-ubiquitin chain provides clues to functional diversity of polyubiquitin signaling.* J Biol Chem, 2004. **279**(8): p. 7055-63.
38. Varadan, R., et al., *Structural determinants for selective recognition of a Lys48-linked polyubiquitin chain by a UBA domain.* Mol Cell, 2005. **18**(6): p. 687-98.
39. Newton, K., et al., *Ubiquitin chain editing revealed by polyubiquitin linkage-specific antibodies.* Cell, 2008. **134**(4): p. 668-78.
40. Gilmore, T.D., *Introduction to NF-kappaB: players, pathways, perspectives.* Oncogene, 2006. **25**(51): p. 6680-4.
41. Scheidereit, C., *I kappa B kinase complexes: gateways to NF-kappa B activation and transcription.* Oncogene, 2006.
42. Ben-Neriah, Y., *Regulatory functions of ubiquitination in the immune system.* Nat Immunol, 2002. **3**(1): p. 20-6.
43. Li, Q. and I.M. Verma, *NF-kappaB regulation in the immune system.* Nat Rev Immunol, 2002. **2**(10): p. 725-34.
44. Deng, L., et al., *Activation of the IkappaB kinase complex by TRAF6 requires a dimeric ubiquitin-conjugating enzyme complex and a unique polyubiquitin chain.* Cell, 2000. **103**(2): p. 351-61.
45. Hayden, M.S. and S. Ghosh, *Shared principles in NF-kappaB signaling.* Cell, 2008. **132**(3): p. 344-62.
46. Hayden, M., A.P. West, and S. Ghosh, *NF-kappa B and the immune response.* Oncogene, 2006.

47. Hacker, H. and M. Karin, *Regulation and function of IKK and IKK-related kinases.* Sci STKE, 2006. **2006**(357): p. re13.
48. Fujita, T., et al., *The candidate proto-oncogene bcl-3 encodes a transcriptional coactivator that activates through NF-kappa B p50 homodimers.* Genes Dev, 1993. **7**(7B): p. 1354-63.
49. Franzoso, G., et al., *The candidate oncoprotein Bcl-3 is an antagonist of p50/NF-kappa B-mediated inhibition.* Nature, 1992. **359**(6393): p. 339-42.
50. Bours, V., et al., *The oncoprotein Bcl-3 directly transactivates through kappa B motifs via association with DNA-binding p50B homodimers.* Cell, 1993. **72**(5): p. 729-39.
51. Watanabe, N., et al., *Regulation of NFKB1 proteins by the candidate oncoprotein BCL-3: generation of NF-kappaB homodimers from the cytoplasmic pool of p50-p105 and nuclear translocation.* Embo J, 1997. **16**(12): p. 3609-20.
52. Heissmeyer, V., et al., *NF-kappaB p105 is a target of IkappaB kinases and controls signal induction of Bcl-3-p50 complexes.* Embo J, 1999. **18**(17): p. 4766-78.
53. Carmody, R.J., et al., *Negative regulation of toll-like receptor signaling by NF-kappaB p50 ubiquitination blockade.* Science, 2007. **317**(5838): p. 675-8.
54. Cogswell, P.C., et al., *Selective activation of NF-kappa B subunits in human breast cancer: potential roles for NF-kappa B2/p52 and for Bcl-3.* Oncogene, 2000. **19**(9): p. 1123-31.
55. McKeithan, T.W., et al., *BCL3 rearrangements and t(14;19) in chronic lymphocytic leukemia and other B-cell malignancies: a molecular and cytogenetic study.* Genes Chromosomes Cancer, 1997. **20**(1): p. 64-72.
56. Westerheide, S.D., et al., *The putative oncoprotein Bcl-3 induces cyclin D1 to stimulate G(1) transition.* Mol Cell Biol, 2001. **21**(24): p. 8428-36.
57. Ohno, H., G. Takimoto, and T.W. McKeithan, *The candidate proto-oncogene bcl-3 is related to genes implicated in cell lineage determination and cell cycle control.* Cell, 1990. **60**(6): p. 991-7.
58. Bauer, A., et al., *The NF-kappaB regulator Bcl-3 and the BH3-only proteins Bim and Puma control the death of activated T cells.* Proc Natl Acad Sci U S A, 2006. **103**(29): p. 10979-84.
59. Rebollo, A., et al., *Bcl-3 expression promotes cell survival following interleukin-4 deprivation and is controlled by AP1 and AP1-like transcription factors.* Mol Cell Biol, 2000. **20**(10): p. 3407-16.
60. Mitchell, T.C., et al., *Stronger correlation of bcl-3 than bcl-2, bcl-xL, co-stimulation, or antioxidants with adjuvant-induced T cell survival.* Ann N Y Acad Sci, 2002. **975**: p. 114-31.
61. Mitchell, T.C., et al., *A short domain within Bcl-3 is responsible for its lymphocyte survival activity.* Ann N Y Acad Sci, 2002. **975**: p. 132-47.
62. Valenzuela, J.O., C.D. Hammerbeck, and M.F. Mescher, *Cutting edge: Bcl-3 up-regulation by signal 3 cytokine (IL-12) prolongs survival of antigen-activated CD8 T cells.* J Immunol, 2005. **174**(2): p. 600-4.
63. Rangelova, S., et al., *FADD and the NF-kappaB family member Bcl-3 regulate complementary pathways to control T-cell survival and proliferation.* Immunology, 2008.
64. Chilton, P.M. and T.C. Mitchell, *CD8 T cells require Bcl-3 for maximal gamma interferon production upon secondary exposure to antigen.* Infect Immun, 2006. **74**(7): p. 4180-9.
65. Ong, S.T., et al., *Lymphadenopathy, splenomegaly, and altered immunoglobulin production in BCL3 transgenic mice.* Oncogene, 1998. **16**(18): p. 2333-43.
66. Franzoso, G., et al., *Critical roles for the Bcl-3 oncoprotein in T cell-mediated immunity, splenic microarchitecture, and germinal center reactions.* Immunity, 1997. **6**(4): p. 479-90.
67. Massoumi, R., et al., *Cyld inhibits tumor cell proliferation by blocking Bcl-3-dependent NF-kappaB signaling.* Cell, 2006. **125**(4): p. 665-77.

68. Nijman, S.M., et al., *A genomic and functional inventory of deubiquitinating enzymes*. Cell, 2005. **123**(5): p. 773-86.
69. Welchman, R.L., C. Gordon, and R.J. Mayer, *Ubiquitin and ubiquitin-like proteins as multifunctional signals*. Nat Rev Mol Cell Biol, 2005. **6**(8): p. 599-609.
70. Kee, Y., N. Lyon, and J.M. Huibregtse, *The Rsp5 ubiquitin ligase is coupled to and antagonized by the Ubp2 deubiquitinating enzyme*. Embo J, 2005. **24**(13): p. 2414-24.
71. Hu, M., et al., *Structure and mechanisms of the proteasome-associated deubiquitinating enzyme USP14*. Embo J, 2005. **24**(21): p. 3747-56.
72. Kovalenko, A., et al., *The tumour suppressor CYLD negatively regulates NF-kappaB signalling by deubiquitination*. Nature, 2003. **424**(6950): p. 801-5.
73. Brummelkamp, T.R., et al., *Loss of the cylindromatosis tumour suppressor inhibits apoptosis by activating NF-kappaB*. Nature, 2003. **424**(6950): p. 797-801.
74. Trompouki, E., et al., *CYLD is a deubiquitinating enzyme that negatively regulates NF-kappaB activation by TNFR family members*. Nature, 2003. **424**(6950): p. 793-6.
75. Reiley, W.W., et al., *Regulation of T cell development by the deubiquitinating enzyme CYLD*. Nat Immunol, 2006. **7**(4): p. 411-7.
76. Boone, D.L., et al., *The ubiquitin-modifying enzyme A20 is required for termination of Toll-like receptor responses*. Nat Immunol, 2004. **5**(10): p. 1052-60.
77. Bignell, G.R., et al., *Identification of the familial cylindromatosis tumour-suppressor gene*. Nat Genet, 2000. **25**(2): p. 160-5.
78. Wilkinson, K.D., *Regulation of ubiquitin-dependent processes by deubiquitinating enzymes*. Faseb J, 1997. **11**(14): p. 1245-56.
79. D'Andrea, A. and D. Pellman, *Deubiquitinating enzymes: a new class of biological regulators*. Crit Rev Biochem Mol Biol, 1998. **33**(5): p. 337-52.
80. Almeida, S., et al., *Five New CYLD Mutations in Skin Appendage Tumors and Evidence that Aspartic Acid 681 in CYLD Is Essential for Deubiquitinase Activity*. J Invest Dermatol, 2007.
81. Hovelmeyer, N., et al., *Regulation of B cell homeostasis and activation by the tumor suppressor gene CYLD*. J Exp Med, 2007.
82. Reiley, W., et al., *Regulation of T cell development by the deubiquitinating enzyme CYLD*. Nat Immunol, 2006. **7**(4): p. 411-7.
83. Lim, J.H., et al., *Tumor suppressor CYLD regulates acute lung injury in lethal Streptococcus pneumoniae infections*. Immunity, 2007. **27**(2): p. 349-60.
84. Massoumi, R., et al., *Cyld inhibits tumor cell proliferation by blocking Bcl-3-dependent NF-kappaB signaling*. Cell, 2006. **125**(4): p. 665-77.
85. Hövelmeyer, N., et al., *Regulation of B cell homeostasis and activation by the tumor suppressor gene CYLD*. J Exp Med, 2007.
86. Jin, W., et al., *Deubiquitinating enzyme CYLD regulates the peripheral development and naive phenotype maintenance of B cells*. J Biol Chem, 2007. **282**(21): p. 15884-93.
87. Lee, E.G., et al., *Failure to regulate TNF-induced NF-kappaB and cell death responses in A20-deficient mice*. Science, 2000. **289**(5488): p. 2350-4.
88. Evans, P.C., et al., *Zinc-finger protein A20, a regulator of inflammation and cell survival, has de-ubiquitinating activity*. Biochem J, 2004. **378**(Pt 3): p. 727-34.
89. Mauro, C., et al., *ABIN-1 binds to NEMO/IKKgamma and co-operates with A20 in inhibiting NF-kappaB*. J Biol Chem, 2006. **281**(27): p. 18482-8.
90. Hitotsumatsu, O., et al., *The Ubiquitin-Editing Enzyme A20 Restricts Nucleotide-Binding Oligomerization Domain Containing 2-* …. Immunity, 2008.
91. Wertz, I.E., et al., *De-ubiquitination and ubiquitin ligase domains of A20 downregulate NF-kappaB signalling*. Nature, 2004. **430**(7000): p. 694-9.

92. Suhasini, M., et al., *cAMP-induced NF-kappaB (p50/relB) binding to a c-myb intronic enhancer correlates with c-myb up-regulation and inhibition of erythroleukemia cell differentiation.* Oncogene, 1997. **15**(15): p. 1859-70.
93. Jones, S.A., *Directing transition from innate to acquired immunity: defining a role for IL-6.* J Immunol, 2005. **175**(6): p. 3463-8.
94. Hart, P.D. and M.R. Young, *Ammonium chloride, an inhibitor of phagosome-lysosome fusion in macrophages, concurrently induces phagosome-endosome fusion, and opens a novel pathway: studies of a pathogenic mycobacterium and a nonpathogenic yeast.* J Exp Med, 1991. **174**(4): p. 881-9.
95. Nishimura, H. and T. Honjo, *PD-1: an inhibitory immunoreceptor involved in peripheral tolerance.* Trends Immunol, 2001. **22**(5): p. 265-8.
96. Tarbell, K.V., S. Yamazaki, and R.M. Steinman, *The interactions of dendritic cells with antigen-specific, regulatory T cells that suppress autoimmunity.* Semin Immunol, 2006. **18**(2): p. 93-102.
97. Probst, H.C. and M. van den Broek, *Priming of CTLs by lymphocytic choriomeningitis virus depends on dendritic cells.* J Immunol, 2005. **174**(7): p. 3920-4.
98. Song, X.T., et al., *A20 is an antigen presentation attenuator, and its inhibition overcomes regulatory T cell–mediated* …. Nat Med, 2008.
99. Banchereau, J. and R.M. Steinman, *Dendritic cells and the control of immunity.* Nature, 1998. **392**(6673): p. 245-52.
100. Zhang, Y., et al., *Regulation of T cell activation and tolerance by PDL2.* Proc Natl Acad Sci U S A, 2006. **103**(31): p. 11695-700.
101. Dempsey, P.W., et al., *The signaling adaptors and pathways activated by TNF superfamily.* Cytokine Growth Factor Rev, 2003. **14**(3-4): p. 193-209.
102. Reiley, W., et al., *Regulation of the deubiquitinating enzyme CYLD by IkappaB kinase gamma-dependent phosphorylation.* Mol Cell Biol, 2005. **25**(10): p. 3886-95.
103. Wertz, I.E., et al., *De-ubiquitination and ubiquitin ligase domains of A 20 downregulate NF-κB signalling.* Nature(London), 2004.
104. Andreasen, S.O., et al., *Role of CD40 ligand and CD28 in induction and maintenance of antiviral CD8+ effector T cell responses.* J Immunol, 2000. **164**(7): p. 3689-97.
105. Inoue, J., et al., *Bcl-3, a member of the I kappa B proteins, has distinct specificity towards the Rel family of proteins.* Oncogene, 1993. **8**(8): p. 2067-73.
106. Naumann, M., F.G. Wulczyn, and C. Scheidereit, *The NF-kappa B precursor p105 and the proto-oncogene product Bcl-3 are I kappa B molecules and control nuclear translocation of NF-kappa B.* Embo J, 1993. **12**(1): p. 213-22.
107. Nolan, G.P., et al., *The bcl-3 proto-oncogene encodes a nuclear I kappa B-like molecule that preferentially interacts with NF-kappa B p50 and p52 in a phosphorylation-dependent manner.* Mol Cell Biol, 1993. **13**(6): p. 3557-66.
108. Wulczyn, F.G., M. Naumann, and C. Scheidereit, *Candidate proto-oncogene bcl-3 encodes a subunit-specific inhibitor of transcription factor NF-kappa B.* Nature, 1992. **358**(6387): p. 597-9.
109. Franzoso, G., et al., *The oncoprotein Bcl-3 can facilitate NF-kappa B-mediated transactivation by removing inhibiting p50 homodimers from select kappa B sites.* Embo J, 1993. **12**(10): p. 3893-901.
110. Wessells, J., et al., *BCL-3 and NF-kappaB p50 attenuate lipopolysaccharide-induced inflammatory responses in macrophages.* J Biol Chem, 2004. **279**(48): p. 49995-50003.
111. Grundstrom, S., et al., *Bcl-3 and NFkappaB p50-p50 homodimers act as transcriptional repressors in tolerant CD4+ T cells.* J Biol Chem, 2004. **279**(9): p. 8460-8.
112. Na, S.Y., et al., *Bcl3, an IkappaB protein, stimulates activating protein-1 transactivation and cellular proliferation.* J Biol Chem, 1999. **274**(40): p. 28491-6.

113. Ghosh, S. and M.S. Hayden, *New regulators of NF-kappaB in inflammation*. Nat Rev Immunol, 2008. **8**(11): p. 837-48.
114. Viatour, P., et al., *GSK3-mediated BCL-3 phosphorylation modulates its degradation and its oncogenicity*. Mol Cell, 2004. **16**(1): p. 35-45.
115. Bundy, D.L. and T.W. McKeithan, *Diverse effects of BCL3 phosphorylation on its modulation of NF-kappaB p52 homodimer binding to DNA*. J Biol Chem, 1997. **272**(52): p. 33132-9.
116. Caamano, J.H., et al., *Constitutive expression of Bc1-3 in thymocytes increases the DNA binding of NF-kappaB1 (p50) homodimers in vivo*. Mol Cell Biol, 1996. **16**(4): p. 1342-8.